Multiscale Computational Modeling of High-Pressure Phase Stability, Structure, and Thermophysical Properties of Compressible Polyolefin Solutions

Moeed Shahamat

Doctor of Philosophy

Department of Chemical Engineering
McGill University, Montréal
April 2014

A thesis submitted to McGill University in partial fulfillment of
the requirements of the degree of Doctor of Philosophy

Dedication

This thesis is dedicated to my family who has supported me all the way in my career. A special feeling of gratitude to my loving mother, whose words of encouragement and endless patience throughout my life made all this possible. I am also grateful to my father who ensured that I have progressed successfully towards personal and professional fulfillment.

Contributions of the Author

The present author chooses the manuscript-based thesis option according to the guidelines for thesis preparation given by the Faculty of Graduate and Post-doctoral Studies of McGill University. Contents of chapters 2 to 7 of the present thesis are adopted or revised from the articles published in or to be submitted to scientific journals under the normal supervision of the author's research supervisor, Prof. Alejandro Rey, who is also co-author. All the computations and also the articles included in chapters 2-7 are the work of the author.

Acknowledgements

First and foremost, I would like to express my sincere gratitude to my thesis supervisor, Professor Alejandro Rey for his invaluable support and contributions of time, brilliant ideas, and funding to make my Ph.D. experience productive and stimulating. Professor Rey has been a tremendous mentor whilst allowing me room to work in my own way which enabled me to grow as a research scientist and an independent thinker throughout the course of this process.

Financial support provided by McGill International Doctoral Awards, the Natural Sciences and Engineering Research Council of Canada, the Eugenie Lamothe Fellowship and the Graduate Excellence Fellowship in Chemical Engineering is greatly appreciated. Special thanks go to my former and current labmates for many useful discussions and their friendship.

Last but not the least, I wish to acknowledge the role of my parents, for your faith in me, unconditional love and care. Words fail to express how grateful I am to you for all of the sacrifices that you have made on my behalf which has enabled me to make it this far.

Abstract

The knowledge of high-pressure phase behavior and phase equilibria of polyethylene (PE) in hydrocarbon solutions is an integral part of the process design and manufacturing of PE via solution polymerization. This thesis focuses on the study of fundamental polymer thermodynamics and key mechanisms that govern phase stability in polyolefin solutions via combined thermodynamics-molecular modeling algorithms.

Force field-molecular dynamics simulations are utilized to bridge the gap between experimentally observed macro-scale phase separation phenomena and molecular-level details of fundamental studies of macromolecular thermodynamics in polymer-solvent systems. In this context, the main contributions of the present thesis work focus on molecular thermodynamic characterization of the pressure-induced phase separation (PIPS) mechanism and lower critical solution temperature (LCST) fluid phase behavior of PE solution; high-pressure thermodynamic and structural properties of binary and ternary solutions of PE + hexane and PE + hexane + ethylene, respectively; improvement of the computational efficiency and accuracy of the isobaric-isothermal and canonical ensemble simulations; overcoming the practical challenges involved in the implementation of equation of state theories.

A fully-atomistic molecular mechanics force field combined with molecular dynamics is implemented to compute solubility parameter, liquid phase density, structure, and internal pressure of HDPE and hexane over a broad range of pressures. Based upon the knowledge of pressure and temperature dependence of solubility parameters the binary interaction parameter is computed to shed light on phase stability predictions in PIPS mechanism and LCST phase behavior. A molecular-level explanation for the change in cohesive properties and structure of PE and hexane upon raising the external pressure is provided. Additionally, a relation is established between cohesive energy density and internal pressure for the solvent and polymer as a function of pressure. The molecular mechanics model that incorporates the usually neglected electrostatic energy contribution is found to predict more accurately the PE in hexane miscibility as a result of a larger chemical potential factor. A comparison is reported between electrostatic algorithms of switch function and the particle mesh Ewald method, and also the effect of grid spacing on the computational accuracy of electrostatic energy contribution is revealed.

This thesis also implements the state of the art molecular modeling methods and equation of state modeling to report on the pressure dependence of binary PE solution density for various polymer compositions, required to solve the phase equilibria and kinetics of compressible polymer solutions. A detailed insight into the polymer-polymer, polymer-solvent, and solvent-solvent interactions is provided by analyzing the breakdown of the total system energy. The effect of the cut-off radius of intermolecular potentials on the non-bonded forces and densities of the polymer-solvent mixture with the objective of improving the computational efficiency of molecular dynamics simulations is investigated and an optimized cut-off distance is suggested for high-pressure molecular mechanics modeling of compressible polyolefin solutions. An atomistic-level analysis of the impact of pressure on the structure of PE-solvent mixture is also provided.

The isobaric-isothermal molecular dynamics methodology together with the equation of state model is further extended to incorporate ethylene as unreacted monomer in the solution polymerization process for PE production. The inclusion of supercritical ethylene lays the foundation for the analysis of the effect of adding co-solvent on the density of PE + hydrocarbon solvent system and also to elucidate the impact of pressure and temperature upon the ternary PE solution density. Additionally, a significant insight into the exact nature of intermolecular interactions in the binary subsystems of polymer/solvent/co-solvent is presented. Ultimately, an integrated equation of state-molecular simulation algorithm is presented to compute the characteristic parameters involved in the equation of state theory, which eliminates the need for rigorous experimental phase equilibrium data and tedious non-linear fitting of thermodynamic data.

The findings of this simulation-based thesis are verified with the experimental and theoretical observations. The modeling and simulation approach undertaken in this thesis work provide a substantial basis for molecular thermodynamic characterization of PE in hydrocarbon solvents at conditions of technological interest.

Resumé

La connaissance du comportement des phases à haute pression et des équilibres de phase du polyéthylène (PE) dans les solutions d'hydrocarbures est une partie intégrante de la conception du procédé et de la fabrication du PE par l'intermédiaire d'une polymérisation en solution. Cette thèse porte sur l'étude de la thermodynamique fondamentale des polymères et des mécanismes clés qui en régissent la stabilité de phase dans les solutions de polyoléfines par des algorithmes combinées de thermodynamique et modélisation moléculaire.

Les simulations de champ de force-dynamique moléculaire sont utilisées pour combler le fossé entre les observations expérimentales des phénomènes de séparation de phase à l'échelle macro et des détails au niveau moléculaire des études fondamentales de la thermodynamique macromoléculaire dans les systèmes de polymère-solvant. Dans ce contexte, les contributions principales de la présente thèse se concentrent sur la caractérisation thermodynamique moléculaire du mécanisme de la séparation de phase induite par la pression (PIPS) et le comportement de la température inférieure critique de solution (LCST) de phase liquide de solution PE; les propriétés thermodynamiques et structurelles à haute pression des solutions binaires et ternaires de PE + hexane et PE + hexane + éthylène, respectivement; l'amélioration de l'efficacité de calcul et la précision des simulations dans l'ensemble isobare-isotherme et canonique; surmonter les difficultés pratiques liées à la mise en œuvre des théories de l'équation d'état.

Un champ de force mécanique moléculaire complètement atomistique combinée avec la dynamique moléculaire est mis en œuvre pour calculer le paramètre de solubilité, la densité de la phase liquide, la structure, et la pression interne du HDPE et de l'hexane sur une large plage de pressions. Basé sur la connaissance de la dépendance en pression et température des paramètres de solubilité, le paramètre d'interaction binaire est calculé pour faire la lumière sur les prévisions de stabilité de phase dans le mécanisme PIPS et le comportement de phase de LCST. Une explication au niveau moléculaire pour le changement des propriétés de cohésion et de la structure du PE et de l'hexane lors de l'augmentation de la pression externe est fournie. En outre, une relation est établie entre la densité d'énergie cohésive et la pression interne pour le solvant et le polymère en fonction de la pression. Le modèle de la mécanique moléculaire qui comprend l'apport d'énergie

électrostatique habituellement négligée prévoit plus précisément la miscibilité du PE dans l'hexane à la suite d'un plus grand facteur potentiel chimique. Une comparaison est rapportée entre les algorithmes électrostatiques de la switch function et la méthode de PME, et aussi l'effet de l'espacement de la grille sur la précision de calcul de la contribution de l'énergie électrostatique est révélé.

Cette thèse implémente également des méthodes de modélisation moléculaire et d'équation d'état dans l'état de l'art afin de rendre compte de la dépendance de la densité des solutions binaires de PE en fonction de la pression pour diverses compositions de polymères, afin de résoudre les équilibres de phase et la cinétique des solutions de polymères compressibles. Un aperçu détaillé des interactions polymère-polymère, polymère-solvant, et solvant-solvant est fournie par l'analyse de la répartition de l'énergie totale du système. L'effet du rayon de coupure des potentiels intermoléculaires sur les forces non liées et les densités du mélange polymère-solvant avec l'objectif d'améliorer l'efficacité de calcul des simulations de dynamique moléculaire est étudiée et une distance de coupure optimisée est suggérée pour la modélisation mécanique moléculaire à haute pression des solutions de polyoléfine compressibles. Une analyse au niveau atomistique de l'impact de la pression sur la structure du mélange de PE-solvant est également fournie.

La méthode de la dynamique moléculaire isobare-isotherme avec le modèle de l'équation d'état est en outre étendue pour incorporer de l'éthylène en tant que monomère n'ayant pas réagi dans le procédé de polymérisation en solution pour la production de PE. L'inclusion de l'éthylène supercritique pose les bases de l'analyse de l'effet de l'ajout d'un co-solvant sur la densité du PE + système solvant hydrocarbure et également pour élucider l'impact de la pression et de la température sur la densité de la solution de PE ternaire. En outre, un aperçu significatif de la nature exacte des interactions intermoléculaires dans les sous-systèmes binaires de polymère/solvant/co-solvant est présenté. En fin de compte, un algorithme qui intègre l'équation d'état et la simulation moléculaire est présenté pour calculer les paramètres caractéristiques impliqués dans la théorie de l'équation d'état, ce qui élimine le besoin de données expérimentales rigoureuses d'équilibre de phase et la régression fastidieuse non-linéaire des données thermodynamiques.

Les résultats de cette thèse basée sur la simulation sont vérifiés avec des observations expérimentales et théoriques. L'approche de modélisation et de simulation entreprise dans

ce travail de thèse constituent une base importante pour la caractérisation thermodynamique moléculaire du PE dans les solvants hydrocarbonés à des conditions d'intérêt technologique.

Table of Contents

List of Figures

List of Tables

1 Introduction and Literature Review

1.1 General Introduction

There are innumerable applications for commercially produced polymers of both synthetic and biological origin (natural polymers). The spread of polymers of biological origin such as proteins and carbohydrates as well as synthetic polymers into every conceivable aspect of everyday life is undeniable. Synthetic polymers are used in a wide array of applications. Some examples include synthetic fibers, films, resins, plastics, and synthetic rubber. Due to the numerous applications of synthetic polymers, such as polyethylene (or polythene) and nylon, the industrial production of these polymers has increased significantly over the past decades. Polyethylene (often shortened to PE) is widely used in the consumer packaged goods industry to produce plastic shopping bags, bottles, and food containers. Other applications include film making, coating, and pipe manufacturing.

A significant portion of current commodity polymers as PE is produced at high pressure and temperature. Linear low-density polyethylene (LLDPE) is one of the widely used plastic materials which is produced at high pressure and temperature (around 20 MPa and 430 K) by a solution polymerization process. This manufacturing process requires characterizing the fluid phase behavior and physical properties of PE solutions. The present thesis focuses on combined thermodynamic-molecular modeling algorithms to understand the phase behavior of PE in hydrocarbon solutions at elevated pressures relevant to current industrial process.

This introductory chapter is organized as follows. First, the solution polymerization process will be explained and then polymer chain models as well as PE classifications will be highlighted in terms of density, molecular architecture, and potential uses. Second, an

overview of thermodynamics and phase behavior of polymer solutions is provided with a review of the different efforts in modeling the phase behavior of polymer-solvent systems. Third, the experimental and theoretical investigations related to the phase equilibria of PE solutions are summarized. The chapter concludes with an identification of the areas that need further investigation.

Based on this introductory information, section 1.7 defines the objectives of the thesis and section 1.8 discusses the overall scope, implemented methodology, and organization.

1.2 Solution Polymerization Process for Producing PE

Solution polymerization is an industrial process in which a monomer is dissolved in a non-reactive solvent that contains a catalyst. This process is frequently applied in PE production due to the ease of adding many olefin co-monomers. In the PE production process, the polymerization reaction of ethylene along with a co-monomer in an inert hydrocarbon solvent (e.g. *n*-hexane) takes place. Before entering the reactor, the monomer ethylene is compressed in the inert solvent to allow the reactor to operate at lower pressures. This additionally reduces the viscosity of the solution leaving the reactor, allowing for continuous process operation. As in solution polymerization the viscosity of the solution increases with increasing the molar mass of PE, this process is widely applicable to PE production with relatively low-molecular weight as LLDPE, a co-polymer of ethylene and an alkene co-monomer. Such alkene co-monomers can include octene-1 within a mixture of single or multi-component alkanes.[1]

As illustrated in Figure 1.1 the polymerization process involves two reactors that are fed catalysts (or activators). The operating conditions in the first reactor are 415-435 K and 14-20 MPa approximately. The second reactor has a larger volume operating at higher temperature under similar pressure. The feed mixture entering the first reactor containing 12-20 wt% ethylene yields 80-95% overall ethylene conversion at the outlet of the second reactor. The effluent leaving the second reactor consists of a polymer solution of 10-20 wt% PE, 1-3% ethylene, the unreacted monomer and the remainder an inert hydrocarbon solvent. The reactor effluent mixture leaving the reactors is heated upstream of a depressurizing valve to produce multiple fluid phases and then undergoes high and low-pressure separators. The hydrocarbon solvent, unreacted monomer and co-monomers are

recovered from the top of the separators and go to a distillation unit for further purification and reuse. The liquid effluent coming out of the low-pressure separator, consisting mainly of PE, goes to an extruder where thin PE strands are generated. The strands are cut into small PE pellets, which are the final product of the solution polymerization process.[2]

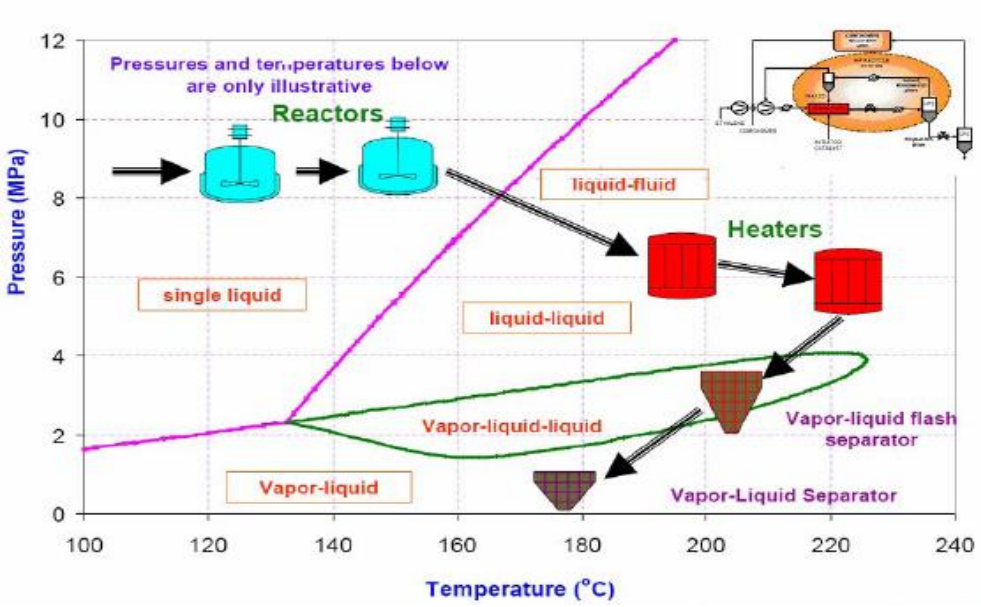

Figure 1.1. Schematic diagram of the solution polymerization process (source: NOVA Chemicals).

1.3 PE Classifications

The structure of PE is simple compared to all other commercial polymers. This polymer consists of long chains of the monomer ethylene (i.e. a chain of carbon atoms, with two hydrogen atoms connected to each carbon). The scientific name for PE originates from that of the monomer. PE is classified into several categories based on its density, branching, and molecular weight. Three of the most common classes of PE are high-density polyethylene (HDPE), low-density polyethylene (LDPE), and linear low-density polyethylene (LLDPE).

HDPE is defined by a density between 0.941 and 0.969 g/cm^3.[3] Since the macromolecules that fall in this category have a linear structure with only a few short branches, they are also called linear polyethylene (LPE). Because of the low degree of branching, HDPE has stronger intermolecular forces and tensile strength. Therefore, it is used in rigid objects as pipes.

LDPE, also called branched polyethylene (BPE), is defined by a density range of 0.910–0.925 g/cm^3. It has a high degree of branching resulting in less strong intermolecular forces. This molecular configuration (longer branches) lowers the density. LDPE is used in flexible products such as plastic shopping bags and coatings. LLDPE, a linear polymer with a number of short branches, has the same density as LDPE. It is made by using special catalysts during co-polymerization of ethylene with short-chain alpha-olefins such as 1-butene, 1-hexene, or 1-octene. LLDPE has higher tensile strength than LDPE and is commonly used in packaging as well as in film applications due to its flexibility and transparency.

1.4 Polymer Chain Architecture and Models

Three major architectures of a polymer molecule include a linear chain, a branched chain, and a cross-linked polymer (see Figure 1.2). Models of a linear polymer chain, can be divided into two classes.[4] a) *Models in a continuous space*, in which the chain conformation, defined as an instantaneous shape of a polymer chain, can be represented by removing all atoms other than those on the backbone (main-chain model), connected bonds (e.g. links of C-C bonds in case of PE), or a flexible thread (thread model). The distance between the two ends of a linear chain in its fully extended conformation is called the contour length which is proportional to degree of polymerization or molecular weight; however, a realistic polymer chain is crumpled and takes the conformation of a random coil. b) *Models in a discrete space*, wherein a linear chain is constructed on a discrete space, are commonly referred to as lattice models. In the lattice model, monomers of a polymer chain occupy the grid points (sites). The lattice coordinate *z* refers to the number of neighbors of each monomer in the grid. These models are widely used in theories and computer simulations, as discussed further in detail below. A cross-linked polymer forms a network and cannot be dissolved in a solvent.

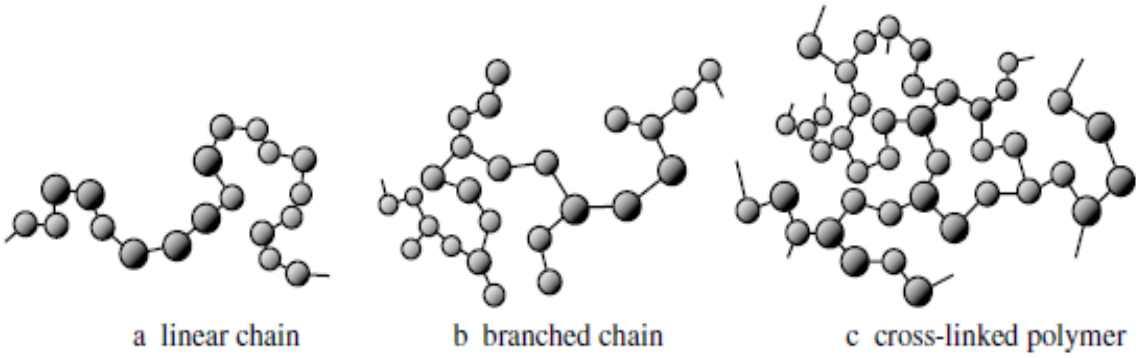

Figure 1.2. Architecture of polymer chain:[4] a linear chain (a), a branched chain (b), and a cross-linked polymer (c).

In the lattice model, monomers of a polymer chain can occupy the same site (ideal chain); however, in any real polymer chain, monomers do not overlap which results in a reduction in the conformational possibilities of the chain. This effect is known as excluded volume and a real chain is referred to as an excluded volume chain. Although, an ideal chain model allows the polymer to cross itself, an effect that does not exist in reality, it is commonly applied to various theories in polymer physics concerned with characterization of polymers in the liquid state. As an example, the concept of random walk for an ideal chain is developed and used to express the polymer size. Two such measures used to characterize linear flexible polymer chains are end-to-end distance and radius of gyration, R_g, where the latter provides a measure of the molecular size and compactness of the polymer structure. R_g, defined as the root-mean-square distance between the center of gravity of the molecule and other atoms at a given time, is formulated as:

$$R_g = \left(\frac{\sum_i m_i |r_i|^2}{\sum_i m_i} \right)^{1/2} \qquad (1.1)$$

where m_i is the mass and r_i is the position of atom *i* with respect to the molecular center of mass.

1.5 Thermodynamics of Polymer-Solvent Miscibility

1.5.1 Dissolution of a Polymer into a Solvent

This section briefly reviews some fundamental polymer solution thermodynamics and theories. Qualitatively, solubility may be defined as "like dissolves like" but quantitatively, solubility is governed by the Gibbs free energy of mixing. When solvation of a polymer in a solvent lowers the Gibbs free energy of the polymer-solvent system, a polymer dissolves in a solvent. The solvent that dissolves well a certain polymer is called a good solvent (non-solvents do not dissolve a polymer). A good solvent, therefore, lowers the free energy while a non-solvent increases it. The good solvents and non-solvents are known for many polymers.[5] From the thermodynamic point of view, the miscibility condition can be expressed as:

$$\Delta G_{mix} = \Delta H_{mix} - T\Delta S_{mix} < 0 \qquad (1.2)$$

where ΔG_{mix} is the Gibbs free energy of mixing, ΔH_{mix} the enthalpy of mixing, and ΔS_{mix} is the entropy of mixing (entropy of mixing is always positive since entropy increases upon mixing). Since the product of temperature and entropy change is always positive, the magnitude of enthalpy of mixing determines the sign of Gibbs free change. It should be noted that a negative Gibbs free energy change is essential but not sufficient for miscibility.

1.5.2 Thermodynamics of Phase Separation

There are a number of industrially important polymer processing operations involving phase separation that render the phase behavior in polymeric systems a topic of technological interest. The phase behavior of polymer solutions is arguably more complex than that of polymer blends because of the large disparity in the size of polymer and solvent molecules. For a polymer-solvent system to form a homogenous mixture, the Gibbs free energy of mixing ΔG_{mix} must be negative. However, a negative Gibbs free energy change is not a sufficient condition for miscibility. The upper part of Figure 1.3 shows a schematic diagram of ΔG_{mix} as a function of polymer concentration at different temperatures or pressures. The lower part of the figure illustrates a temperature (or pressure)-polymer

concentration phase diagram (a phase diagram is a graphic representation of thermodynamic equilibrium state of the system). At T_1, ΔG_{mix} exhibits only one minimum over the entire range of polymer concentration. Thus, at this temperature the polymer-solvent system is completely miscible over the whole range of polymer concentration (stable region in the phase diagram). At T_2 and T_3, ΔG_{mix} is negative for the whole range of polymer concentration but the system is only partially miscible since the curve shows two local minima. Being at the lowest possible Gibbs free energy is essential for a solution to be stable, in addition to satisfying the condition for equality of chemical potentials. If a system can achieve a lower value for Gibbs free energy of mixing by splitting into two phases, then the system forms two phases rather than one phase. At T_2 and T_3, in order to achieve the overall minimum of free energy change, the system will have to separate into two phases, wherein the concentration of the resulting phases is determined by tangent points on the curve. These two points are called binodal points and the curve resulting from connecting all binodal points at different temperatures (or pressures) is called binodal curve. The inflection points (or spinodes) of curves are called spinodal points and the curve resulting from connecting all spinodal points at different temperatures (or pressures) is called spinodal curve. The binodal and spinodal curves meet at the critical point. The mathematical condition for the critical point is $\partial^2(\Delta G_{mix})/\partial x^2 = \partial^3(\Delta G_{mix})/\partial x^3 = 0$. In the phase diagram, the region on the outside of the binodal curve is referred to as the stable region, while the region enclosed by the spinodal curve is the unstable region corresponding to $\partial^2(\Delta G_{mix})/\partial x^2 < 0$, where the system spontaneously separates into two continuous phases. In the region between binodal and spinodal curves the system may be one phase but is metastable corresponding to $\partial^2(\Delta G_{mix})/\partial x^2 > 0$. At T_4, as the Gibbs free energy of mixing is positive, the system is completely immiscible for all polymer concentrations.

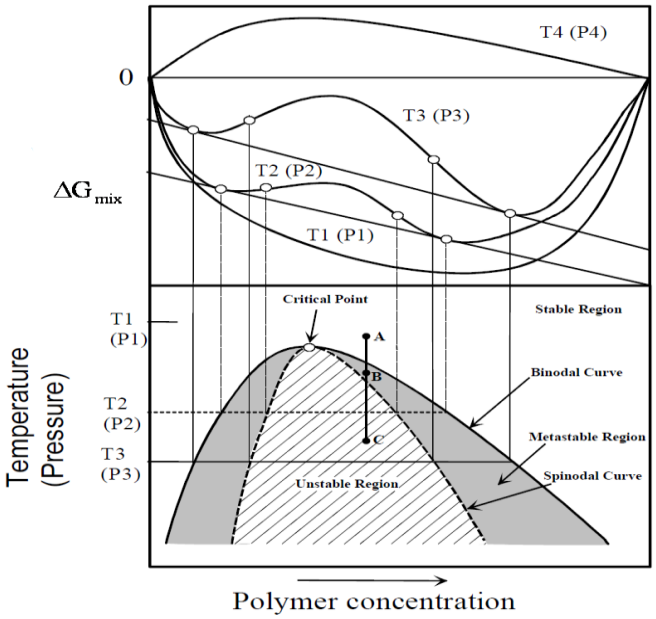

Figure 1.3. Construction of phase diagram from the Gibbs free energy of mixing as a function of polymer concentration (adapted figure[6] from source document[7]).

It may be concluded that the sign of the second derivative of Gibbs free energy of mixing with respect to concentration determines the thermodynamic stability of the system. A negative second derivative, corresponding to the points around the apex of the downward concave on the free energy curve, definitely implies a polymer-solvent mixture is unstable while in the case of a positive sign the system may be either thermodynamically stable or metastable. The lower part of Figure 1.3 illustrates a phase diagram showing the so-called upper critical solution behavior. The critical temperature on this curve (apex of the curve) is called the upper critical solution temperature (UCST). In this type of phase behavior, the system enters the stable region by increasing the temperature from point *C* to *A*. Lower critical solution behavior with a lower critical solution temperature (LCST) corresponds to systems where increasing the temperature brings the system from miscible to immiscible region (i.e. phase separation occurs upon raising the temperature). Figure 1.4 represents various types of phase behavior in polymer solutions. For solutions that exhibit both LCST and UCST behavior, the system is miscible for temperatures between LCST and UCST,

whereas at higher or lower temperatures it is not thermodynamically stable. The phase behavior becomes more complex for a three-component system.

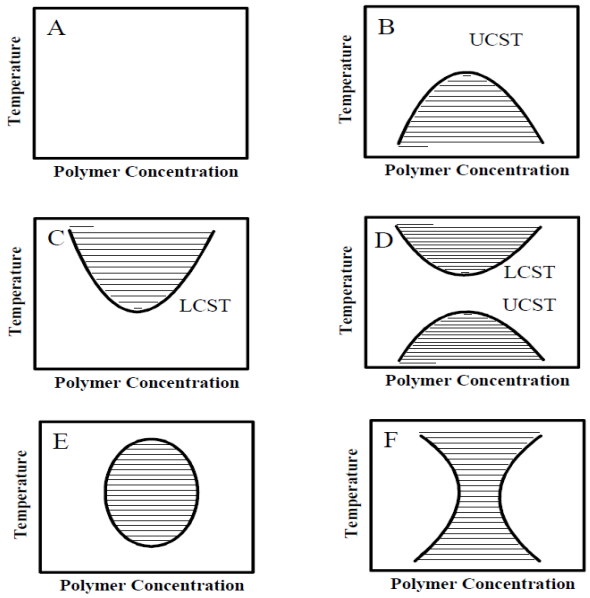

Figure 1.4. Schematic of phase behavior in polymer solutions. Shaded areas represent the two-phase regions and the un-shaded areas represent one-phase regions (adapted figure[6] from source document[8]).

1.5.3 Phase Separation Kinetics

Besides the thermodynamics of polymer solutions, dynamic aspects are also of great importance in processes that are relevant to the synthesis and characterization of polymer solution-based materials. In this section, the fundamental theories of phase separation kinetics will be briefly reviewed. Depending upon the region where the system is brought to starting from the stable region, the solution may experience two distinguishable phase separation mechanisms. The polymer solution may be quenched to metastable or unstable region. Two major mechanisms by which the initial process of phase separation occurs include nucleation and growth, and spinodal decomposition. Nucleation and growth mechanism is associated with metastability, i.e. when a polymer solution is brought from the stable region into the metastable region the system may be stable to small concentration, temperature, or pressure fluctuations, yet it is unstable against large

fluctuations. In the latter case, the system will phase separate into two co-existing phases, namely, polymer-rich and solvent-rich phases. When a system is brought from the stable region to unstable region, phase separation occurs through spinodal decomposition mechanism. This is because unlike nucleation and growth, spinodal decomposition mechanism involves a negligible energy barrier. Therefore, even small concentration fluctuations results in phase separation.

1.5.4 Early Development of the Flory–Huggins Mean-Field Theory

Non-ideal behaviors arise in polymeric systems, as demonstrated by deviations in experimental data with Raoult's law predictions. In an ideal solution the partial vapor pressure equals the mole fraction in the liquid multiplied by the vapor pressure of the pure component. In addition, as ideal solubility precludes volume change on mixing and enthalpy of mixing, the free energy change is completely determined by the entropy change. To understand non-ideal polymer solutions Flory[9] and Huggins[10] independently developed a lattice model, commonly known as the Flory-Huggins (FH) theory. This theory is based on occupations of a lattice by low-molecular weight solvent and solute where solvent and solute molecules are of the same size. The number of possible ways that low-molecular weight components can be arranged in the lattice determines the mixing entropy. The next thought experiment was to extend the original model to describe the mixing of low-molecular weight solvent and high-molecular weight polymer where each segment (the repeating units of polymer placed on lattice sites are called segment) of the polymer occupies a lattice site which is as large as the solvent molecules (see Figure 1.5). Here, the entropy of mixing will be far lower since it is restricted by the segments of the polymer. The well-known FH expression for the entropy of mixing in a polymer solution is given by:

$$\frac{\Delta S_{mix}}{N} = -R\left(\phi_1 \ln \phi_1 + \frac{\phi_2}{r} \ln \phi_2 \right) \tag{1.3}$$

in which ϕ_1 and ϕ_2 denote the volume fractions of solvent and polymer, respectively, r is the number of segments each polymer chain occupies, and N is the number of moles of two components. To treat more accurately the thermodynamic properties of polymer-solvent

systems based on the FH model several modifications were suggested to account for the interaction between lattice sites. The model provides an expression for non-zero enthalpy of mixing of non-ideal polymer-solvent mixture in terms of an energy parameter called the interaction parameter χ_{12}, which is a function of intermolecular forces. The enthalpy of mixing can be calculated by considering the interaction energies between solvent and polymer molecules as:

$$\frac{\Delta H_{mix}}{N} = RT\chi_{12}\phi_1\phi_2 \tag{1.4}$$

where $\chi_{12} = \frac{z\Delta\varepsilon_{12}}{RT}$ is the interaction parameter, z is the coordination number, and $\Delta\varepsilon_{12}$, the energy of formation, is defined in terms of ε_{ij}, the interaction energy of *i-j* pair, given as:

$$\Delta\varepsilon_{12} = \varepsilon_{12} - \frac{1}{2}\left(\varepsilon_{11} + \varepsilon_{22}\right) \tag{1.5}$$

This parameter is a measure of change in the internal energy of the mixture as a result of change in the contacts between nearest neighbors when a polymer chain mixes with solvent molecules. Combination of equations for mixing entropy and enthalpy gives the Gibbs energy of mixing:

$$\frac{\Delta G_{mix}}{N} = RT\left(\phi_1 \ln\phi_1 + \frac{\phi_2}{r}\ln\phi_2 + \chi_{12}\phi_1\phi_2\right) \tag{1.6}$$

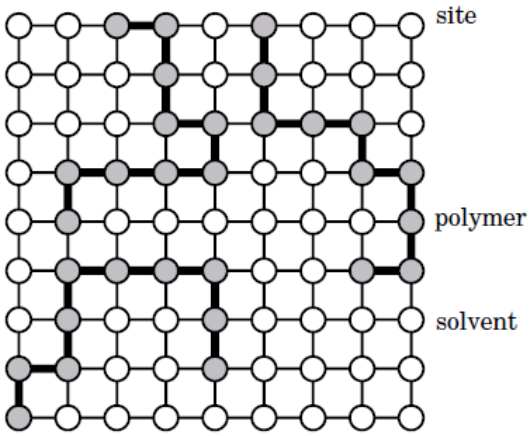

Figure 1.5. Lattice model for polymer solution. Gray sites are occupied by polymer chains, and white sites are occupied by low-molar mass solvent molecules.[4]

1.5.5 Cohesive Energy and Solubility Parameter

The solubility parameter δ (also Hildebrand solubility parameter) can be used to estimate the interaction parameter from which the solubility can be estimated. The solubility parameter approach has been found to be useful for the characterization of the strength of interactions (cohesion of the material) in a liquid. This quantity is defined as the square root of the cohesive energy density (CED) representing the energy needed to separate all molecules in a unit volume of liquid. Thus, CED is an estimate of the energy amount that needs to be supplied to a fluid in the liquid state to vaporize it. The solubility parameter can be calculated from the knowledge of component chemical structure:[11]

$$\delta = \frac{\rho \sum G}{M_w} \tag{1.7}$$

where ρ is the density, $\sum G$ is the sum of group molar attraction constants of the repeating unit and M_w is the molar mass of the repeating unit. Nevertheless, for polymers δ cannot be obtained by identifying the heat of vaporization due to low volatility of polymers. One approach to circumvent this issue is to calculate δ through the internal pressure. Solubility parameter, which is a measure of intermolecular energies (interaction energies) between molecules, can be used to estimate the binary interaction parameter. The solubility parameter concept is used in the paints and coatings industry to understand the miscibility

of pigments and polymers in solvents. In the present thesis characterization of pressure and temperature effects on solubility parameter of PE and hexane has been investigated which provides a rational basis to understand miscibility of PE in hexane solutions at conditions of industrial interest.

1.5.6 Further Developments to Lattice Models

Although the FH theory has been largely successful in describing thermodynamics of polymer solutions, there are a number of limitations to the original formulation, which leads to weakness in predictions of phase equilibrium. Some assumptions/limitations include:

- Interchangeability of solute segments in the lattice, i.e. the polymer segments in the cell are not necessarily identical to the polymer structural units.
- Monodisperse polymer chains, i.e. polymer molecules are of the same size.
- Applicability to solutions with uniform segment density.
- Volume change upon mixing is neglected, while favorable interactions between solute and solvent are expected to result in a negative volume change.
- Concentration dependence of interaction parameter is neglected.
- The model does not consider the polymer chain conformation, chain stiffness (flexible chains), and free volume.

Accordingly, numerous developments to the original FH theory were made to eliminate the deficiencies of this approach to model reality. For example experimental data were used to empirically modify χ to describe the concentration dependence of interaction parameter and equation of state (EOS) approaches were adopted to account for the volume change of mixing, discussed below. Further developments to the theory are the different varieties of the lattice-fluid and hole theories,[12] the mean-field lattice gas model,[13] perturbation theories,[14] the UNIQUAC and UNIFAC models,[15] the Sanchez-Lacombe (SL) theory,[16] the cell theory,[17] the statistical associating fluid theory[18] (SAFT), and the perturbed hard-sphere chain theory.[19]

1.5.6.1 Equation of State Theories

The lattice model precludes volume changes on mixing and the model can thus be applied to liquids which exhibit no volume change on mixing. In addition, due to volume independency of the free energy the model is not applicable in high pressure-related processes. Such flaws in the FH mean-field theory underline the requirement of a suitable form of free energy function that enables the prediction of *PVT* behavior of polymer solutions. The EOS theories are based on the expression $A = f(T,V)$ where A is the Helmholtz free energy. An EOS, which relates the thermodynamic variables of pressure, volume, and temperature can be derived since $P = \left(\frac{\partial A}{\partial V}\right)_T$. The solution of EOS corresponds to a surface in three-dimensional space (each point describes an equilibrium state of the system). The projections of solution points onto *P*-*V*/*T*-*V* planes are called the phase diagrams. The pressure and chemical potential equations derived from the free energy model describe thermodynamic equilibrium (e.g. binodals) of binary or multi-component mixture. Of particular note is the SL lattice-fluid model that includes holes in the lattice allowing it to be compressed. This model which is the foundation for a number of lattice-fluid approaches is discussed further in detail below.

1.5.6.2 SL and Modified SL Equation of State

As already indicated, in response to deficiencies of lattice model theories, Sanchez and Lacombe developed an EOS for pure fluids as well as mixtures based upon a hole theory.[16] The EOS uses a random mixing expression (i.e. solution composition everywhere is equal to overall composition) for lattice energy (the attractive energy term). The major difference between the hole theory and the lattice model (used in FH theory) is that here, the mixture density can vary by increasing the fraction of holes in lattice (vacant lattice sites). The model permits compressibility and presence of free volume in the polymer-penetrant mixture because of the vacant segments between the molecules in the lattice. The lattice-fluid theory provides information on thermodynamic properties of polymers, polymer mixtures, and solutions.

The modified Sanchez–Lacombe (MSL) EOS[20] is a compressible lattice-fluid model which is applied to calculate cloud points in polydisperse polymer solutions. To obtain the

MSL equation, the Helmholtz free energy expression of the original SL is modified to ensure properties are consistent with the ideal gas behavior in the low-pressure limit.[20] MSL EOS essentially uses this free energy modification and incorporates the volume translation term[21] which is applied to the original SL equation to improve liquid densities. The MSL equation is an empirical equation that contains four parameters for each pure component and two parameters for each component pair (interaction parameter), wherein conventional linear and quadratic mixing rules are used for the parameters. The core equations and parameters of the MSL equation, the calculation algorithm, and the correlation procedure are presented elsewhere in more detail.[2]

1.6 Experimental and Theoretical Investigations on Phase Equilibria

This section discusses some of the key experimental and theoretical investigations in the area of phase equilibria of PE solutions. Effects of temperature, polymer composition, average molecular weight and molecular weight distribution on phase separation pressures of PE solutions have been widely investigated.[22-25] Among them, the SL model was selected to correlate the measured cloud points for various LLDPE + *n*-hexane + ethylene mixtures and to investigate the effect of adding supercritical ethylene in the 373.2 to 473.2 K temperature range and at pressures up to 20 MPa. Also it was found that the cloud point pressure increases with increasing PE molecular weight.[23] The phase behavior for the hexane + LLDPE and the ethylene + hexane + LLDPE systems at temperatures from 400 to 500 K was studied using the MSL EOS, wherein ranges of weight fractions of LLDPE were up to 0.3 and 0.15 for the binary and the ternary systems, respectively. In addition, the system LLDPE + *n*-hexane showed LCST and upper critical solution pressures. The MSL EOS was used to describe the phase behavior of the binary subsystems of ethylene + *n*-hexane + LLDPE and to predict the phase behavior of the ternary systems using parameters obtained from the fit of the binary subsystems to the experimental cloud point data. It also was found that the addition of ethylene to *n*-hexane + LLDPE shifts the cloud point curve to lower temperatures and higher pressures with approximately 10 K or 3 MPa per wt% ethylene.[24] Liquid-liquid, liquid-vapor and liquid-liquid-vapor phase boundaries for the hexane + PE binary and the ethylene + hexane + PE ternary systems were measured at temperatures from 373 to 473 K and PE weight fractions from 0.009 to 0.12. The

measurements revealed that the phase separation pressures increase with increasing temperature and PE molecular weight. Moreover, the effect of ethylene compositions on phase boundaries was investigated in the ethylene weight fraction range from 0 to 0.1.[25] For LLDPE with *n*-hexane, *n*-heptane, *n*-octane, cyclohexane, and 2-methyl-pentane the LCST-type phase behavior has been observed and it was revealed that the addition of ethylene to a solution of 10 wt% poly(ethylene-co-1-octene) in *n*-heptane at 50 bar lowers the lower solution temperature (cloud point) by 14 K per wt% ethylene added. Furthermore, cloud points of *n*-hexane + LLDPE mixtures were measured and it was observed that in the solubility of PE, the structure of LLDPE itself is of minor importance in comparison to the solvent type and the presence of ethylene.[26] Liquid-liquid equilibrium using SL EOS for PE/hexane and PE/ethylene systems has been calculated and it was found that the calculated results are extremely sensitive to the value of interaction parameters, even at the third decimal place.[27] The experimental data for LLDPE and ethylene were modeled with the SL EOS in which the parameters for LLDPE were found by performing a sequence of non-linear regressions on the experimental cloud point data and *PVT* reference data for molten PE.[28] Phase behavior of binary, ternary, and quaternary systems of ethylene, cyclohexane, hexane, and PE was investigated and the experimental liquid-liquid phase separation pressures for the binary and ternary systems were correlated with the SL EOS by adjusting the binary interaction parameters.[29] The phase behaviors of the hexane + polydispersed PE systems were measured at high temperatures to clarify the effect of the polydispersity of PE on the phase equilibria of PE solutions together with the correlation of experimental liquid-liquid phase boundaries using the SL EOS.[1]

It can be noted that though all the above mentioned investigations describe phase equilibria of PE in hydrocarbon mixtures, experimental data is essential in the development of phase behavior models. The following section identifies the specific needs for further research.

1.7 Motivation and Objectives

PE is produced at a commercial scale at very high pressure and temperature by solution polymerization process. In the solution polymerization process of PE production the mixture exiting the reactor needs to remain in a single homogenous phase to avoid additional downtime to remove solid polymer. The polymer-rich phase has very high viscosity which can accumulate and plug off the exit of reactor. Moreover, multiple fluid phases produce multiple polymer compositions which is conducive to different reaction rates and poor product quality control. In the subsequent processing steps, the pressure of the mixture is reduced to induce phase separation of the hydrocarbon solvent and residual ethylene from the PE product. Consequently, data on thermodynamics and phase behavior are an integral part of the design and operation of this process. To this end, much experimental work has been conducted on the phase behavior of PE solutions at high temperature and pressure;[1, 29] however, experimental investigations are time-consuming and costly to perform.

In addition to experimental research, EOS methods such as the SL model[20, 24, 28, 30] and SAFT[18] have been frequently applied in correlating and predicting the phase behavior of PE solutions. The functional form of the SL EOS is simpler than that of the SAFT-type EOSs which involve intermolecular interactions. Although the SL EOS has a simple functional form, it accounts for large differences in molecular chain lengths and the model can reproduce the experimental results quantitatively. The model contains three pure-component parameters which are typically obtained by a least-square fitting of density and vapor pressure data. A procedure has been recently proposed to obtain pure solvent parameters from the critical temperature, critical pressure, and the acentric factor.[21] Polymer parameters may be found by performing a regression on pressure-volume-temperature reference data.[28] As an example, it has been recently shown that the polymer parameters can be adjusted to fit both polymer/solvent cloud point data and the polymer *PVT* behavior simultaneously.[27]

Although EOS models are accurate and easy to implement tools to predict and correlate phase equilibria, application of these models requires accurate value of model parameters. In principle, the determination of the parameters appearing in a thermodynamic model is carried out by fitting the model to a series of phase equilibrium data. In addition,

to avoid tedious non-linear parameter estimation methods there is demand for alternative methods to obtain model parameters.

Based on the above discussed literature review and challenges faced in the development and implementation of EOS theories, alternative methods that describe polymer-solvent phase equilibria at high pressure and temperature are of great practical and fundamental value. It also has to be noted that though a large number of investigations have been performed in this area, none of them sheds light on the molecular-level information of phase behavior. Hence, future research needs to concentrate on miscibility-related thermodynamic properties of polyolefins and hydrocarbon solvents directed towards understanding the molecular-level details. To alleviate the problem, molecular modeling techniques have been found to be helpful tools. There exists a number of molecular simulation algorithms to model the thermodynamics of polymeric systems. However, there are few systematic studies on atomistic-level understanding of thermodynamic properties in polyolefin mixtures; it is also important to note that the very few investigations are mostly conducted at low pressures.

The unifying theme of the present thesis is to implement appropriate molecular modeling and simulations to address fundamental issues related to miscibility, structure, and thermophysical properties of polyolefins in hydrocarbon mixtures at elevated pressure and temperature, consistent with industrial processes. The fundamental knowledge obtained using fully-atomistic simulations complements experimental and EOS findings, and lays a foundation towards addressing phenomena related to phase separation mechanism with extreme detail. The following list summarizes specific objectives of this thesis:

- Identify and validate an appropriate molecular modeling methodology to develop a molecular-level understanding of thermodynamic properties that play a significant role in pressure-induced phase separation (PIPS) mechanism. Implement the tool and quantitatively understand the atomistic-level details of pressure effects upon the individual energy terms contributing to the total system energy, density, and the intrinsic structural properties that provide a rational basis for high-pressure miscibility predictions.

- Identify and validate an appropriate molecular modeling methodology to investigate the thermodynamic properties related to solubility at high pressures to shed light on the molecular-level information of LCST phase behavior of PE in hydrocarbons.
- Investigate and implement the most appropriate computational algorithms that provide more efficient atomistic calculations for these polymer systems, an investigation that is useful to increase the efficiency of future molecular dynamics simulations.
- Investigate and validate force field-based modeling of compressible polymer solutions, which can without experimental efforts achieve a detailed insight into the phenomena that directly govern the fundamental aspects of macromolecular science and technology, as in the high-pressure production process of PE.
- Develop a molecular mechanics model directed towards understanding the underlying aspects of polymer physics and polyolefin solution properties, essential to thermodynamic processes and transport phenomena.
- Implement the developed and tested force field to overcome the practical challenges involved in the implementation of EOS approaches.
- Demonstrate the potential and applicability of the above modeling approaches to macromolecular systems at elevated pressures.

1.8 Thesis Scope, Methodology, and Organization

The present thesis uses theory and simulation to elucidate the fundamental thermodynamics of PE in hydrocarbon solvents. The scope of the thesis is defined based on a systematic approach to develop a computational platform and to address the phenomenon under investigation. The scope and a brief summary of this thesis are described in the following subsections to prepare the reader for more detailed discussions in chapters 2 through 7. A flowchart containing a detailed description and organization of this thesis is presented in Figure 1.6.

1.8.1 Chapter 2-3: Molecular Thermodynamic Characterization of PIPS Mechanism

The objective of characterizing the pressure effects on miscibility of binary PE in hexane solution is dealt in chapters 2 and 3. The chosen molecular modeling method which enables simulating phenomena at a modest computational cost is molecular mechanics.

Here, efforts are focused on developing a classical force field molecular dynamics calculation platform under the isobaric-isothermal (NPT) ensemble to compute the effect of pressure on densities, structure, and cohesive energies of PE and hexane over a wide range of pressures, by quantifying specific contributions of intra- and intermolecular interactions, to gain a fundamental understanding of phase behavior in PE solutions at high pressures. In this regard, the FH binary interaction parameter, volume change upon mixing, and the chemical potential factor as functions of pressure are investigated to characterize a significant aspect of pressure-driven phase instability and thus contribute to the evolving understanding of the PIPS process. The necessary details of the model and simulation method are also provided.

1.8.2 Chapter 4: Molecular Thermodynamic Characterization of LCST Fluid Phase Behavior

Chapter 4 extends the efforts, focused on PIPS mechanism, to include the effect of temperature with the objective of contributing to fundamental understanding of LCST-type polymer solution. The undertaken methodology is based on a rigorous and correct implementation of a by now well-established force field OPLS-AA (optimized potentials for liquid simulations all-atom), which is widely applicable to hydrocarbon systems. This work seeks to contribute to the characterization of temperature effects on the solubility parameters of PE and hexane, which ultimately allows us to achieve detailed insight on high pressure and high temperature phenomena in polymer solutions. It should be remarked that the implemented molecular mechanics model incorporates the atomic particle charges, despite the fact that electrostatic calculations are computationally expensive. The secondary objective of this study, therefore, is to identify the simplest, most accurate, and efficient computational schemes, of relevance to molecular-level understanding of polyolefin-solvent phase behavior. One approach to improve the calculation time would be to optimize the non-bonded interactions which dominate simulations. This study is a significant computational work that focuses on accelerating electrostatic calculations, as detailed in chapter 4. The simulation details of the NVT-MD approach are also discussed.

1.8.3 Chapter 5: Molecular Mechanics and EOS Modeling of Compressible PE Solutions

Chapter 5 reports new and significant information on thermophysical and structural properties of binary solutions of PE in hexane at elevated pressures for varied polymer concentrations, essential to thermodynamic processes and transport phenomena, based upon a fully-atomistic model under the NPT ensemble. This chapter also recalls the main features of the MSL EOS and the associated parameters. Because of the scarcity of experimental data, the density of binary mixture is modeled with the MSL EOS to verify the simulated densities. Additionally, two mixing rules for the *b* parameter of the MSL equation are employed to calculate densities. To the best of author's knowledge, the simulation results shed light, for the first time, on the exact nature of interactions and changes in intra- and intermolecular potential energies with pressure variations to characterize the thermodynamic and structural properties of PE in hydrocarbon solutions. To be able to perform accurate MD calculations, it is of utmost importance to have a tested molecular mechanics model. Chapter 5, hereby, reports the results of testing the effect of different cut-off radii on the intermolecular potentials and densities of the polymer-solvent mixture. The modeling effort suggests an optimized minimum value for cut-off distance to produce accurate mixture properties depending upon the pressure regime. This work sets the basis for further simulation study of polyolefins at high pressures and extension of the existing model to account for the influence of co-solvent, a topic of significant interest from the viewpoint of industrial applications. All the necessary details of the molecular and EOS modeling methods are also included.

1.8.4 Chapter 6: Multiscale Modeling of Supercritical PE + Hexane + Ethylene System

It is known that supercritical ethylene, which is a monomer in the polymerization reaction for PE, can dramatically change the phase equilibria for the PE/hexane system because it acts as a poor solvent for polymer. Chapter 6, therefore, extends the scope of previous investigation on binary solutions to incorporate ethylene as unreacted monomer in the solution polymerization process for PE production by rigorous implementation of MD computations and EOS modeling. The motivation for the determination of the thermophysical properties of polymer solutions based on atomistic simulations stems from

the need to comprehend the exact nature of interactions and the potential energy contributions that are essentially influenced by pressure variations. This computational work presents a solution technique based on a molecular mechanics and the MSL model to explore the impact of pressure and temperature on the solution density of ternary PE + hexane + ethylene system and also to understand the effect of ethylene composition on the binary PE in hydrocarbon solution. The necessary details of the molecular modeling and simulation methods, and ternary EOS model are also provided.

1.8.5 Chapter 7: Calculating the EOS Characteristic Parameters via the OPLS-AA Force Field

Chapter 7 presents a molecular modeling and simulation effort aimed at computing the SL EOS model parameters, which are difficult to experimentally determine. The essential features of the SL equation are discussed. In addition, the effectiveness of the optimized potentials for liquid simulations all-atom (OPLS-AA) force field in predicting the thermodynamic and physical properties relating to polyolefin solution processes is evaluated. The characteristic variables can be further used in the SL lattice-fluid theory to describe the respective thermophysical properties and to reproduce the experimental results quantitatively. The details of the molecular mechanics model and simulation method are also included.

1.8.6 Chapter 8: Main Conclusions and Accomplishments

Chapter 8 summarizes the main conclusions of the present thesis, and reports the main accomplishments and contributions to knowledge. Recommendations for future work are then suggested.

1.8.7 Appendix

The background and specific details of molecular modeling techniques used in this thesis are provided in the Appendix. Emphasis is given on empirical force field and molecular dynamics.

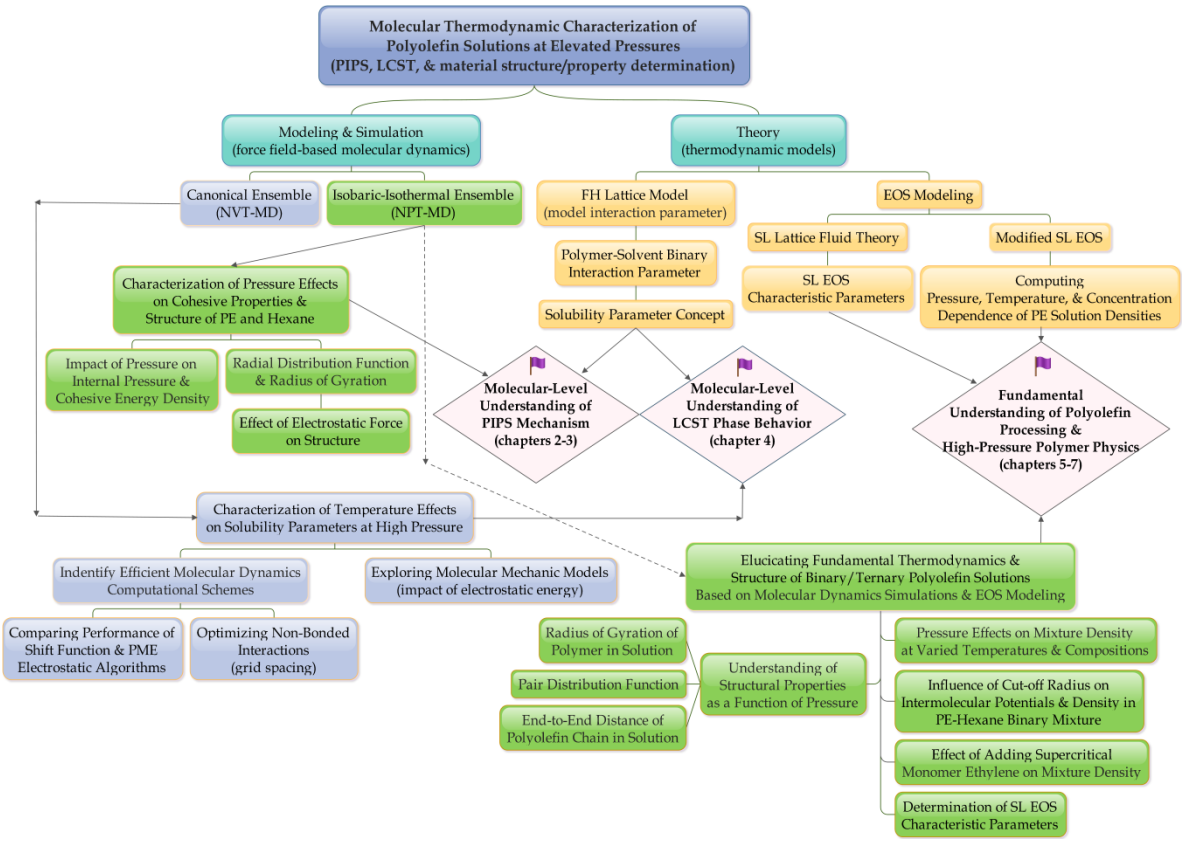

Figure 1.6. Thesis summary and organization.

1.9 References

1. Haruki, M.; Nakanishi, K.; Mano, S.; Kihara, S.; Takishima, S., Effect of molecular weight distribution on the liquid-liquid phase separation behavior of polydispersed polyethylene solutions at high temperatures. *Fluid Phase Equilibria* **2011,** *305* (2), 152-160.
2. Krenz, R. A. Correlating the fluid phase behaviour of polydisperse polyethylene solutions using the Modified Sanchez-Lacombe equation of state. Ph.D. Thesis, University of Calgary, Calgary, 2005.
3. Utracki, L. A., *Polymer blends handbook*. Kluwer Academic Publishers: Dordrecht; Boston, 2002.
4. Teraoka, I., *Polymer solutions: An introduction to physical properties*. Wiley: New York, 2002.
5. Brandrup, J.; Immergut, E. H., *Polymer handbook*. Wiley: New York, 1989.
6. Zhang, W. Phase behavior and phase separation kinetics in polymer solutions under high pressure. Ph.D. Thesis, Virginia Polytechnic Institute and State University, Blacksburg, VA, 2005.
7. Utracki, L. A., Thermodynamics and kinetics of phase separation. In *Interpenetrating polymer networks*, Klempner, D.; Sperling, L. H.; Utracki, L. A., Eds. American Chemical Society: Washington, DC, 1994.
8. Olabisi, O.; Robeson, L. M.; Shaw, M. T., *Polymer-polymer miscibility*. Academic Press: New York, 1979.
9. Flory, P. I., Thermodynamics of high polymer solutions. *Journal of Chemical Physics* **1942,** *10* (1), 51-61.
10. Huggins, M. L., Solutions of long chain compounds. *Journal of Chemical Physics* **1941,** *9* (5), 440-440.
11. Small, P. A., Some factors affecting the solubility of polymers. *Journal of Applied Chemistry* **1953,** *3* (2), 71-80.
12. Simha, R.; Somcynsk.T, On statistical thermodynamics of spherical and chain molecule fluids. *Macromolecules* **1969,** *2* (4), 342-350.
13. Trappeniers, N. J.; Schouten, J. A.; Ten Seldam, C. A., Gas-gas equilibrium and the two-component lattice-gas model. *Chemical Physics Letters* **1970,** *5* (9), 541-545.
14. Beret, S.; Prausnitz, J. M., Perturbed hard-chain theory: An equation of state for fluids containing small or large molecules. *AIChE Journal* **1975,** *21* (6), 1123-1132.
15. Fredenslund, A.; Jones, R. L.; Prausnitz, J. M., Group-contribution estimation of activity coefficients in nonideal liquid mixtures. *AIChE Journal* **1975,** *21* (6), 1086-1099.
16. Sanchez, I. C.; Lacombe, R. H., An elementary molecular theory of classical fluids. Pure fluids. *Journal of Physical Chemistry* **1976,** *80* (21), 2352-2362.
17. Dee, G. T.; Walsh, D. J., A modified cell model equation of state for polymer liquids. *Macromolecules* **1988,** *21* (3), 815-817.
18. Chapman, W. G.; Gubbins, K. E.; Jackson, G.; Radosz, M., SAFT: Equation-of-state solution model for associating fluids. *Fluid Phase Equilibria* **1989,** *52*, 31-38.
19. Hino, T.; Song, Y. H.; Prausnitz, J. M., Liquid-liquid equilibria for copolymer mixtures from a perturbed hard-sphere-chain equation of state. *Macromolecules* **1994,** *27* (20), 5681-5690.
20. Neau, E., A consistent method for phase equilibrium calculation using the Sanchez-Lacombe lattice-fluid equation-of-state. *Fluid Phase Equilibria* **2002,** *203* (1-2), 133-140.

21. Gauter, K.; Heidemann, R. A., A proposal for parametrizing the Sanchez-Lacombe equation of state. *Industrial & Engineering Chemistry Research* **2000,** *39* (4), 1115-1117.
22. Kiran, E.; Xiong, Y.; Zhuang, W. H., Modeling polyethylene solutions in near and supercritical fluids using the Sanchez-Lacombe model. *Journal of Supercritical Fluids* **1993,** *6* (4), 193-203.
23. Chen, X. N.; Yasuda, K.; Sato, Y.; Takishima, S.; Masuoka, H., Measurement and correlation of phase equilibria of ethylene + n-hexane + metallocene polyethylene at temperatures between 373 and 473 K and at pressures up to 20 MPa. *Fluid Phase Equilibria* **2004,** *215* (1), 105-115.
24. Nagy, I.; de Loos, T. W.; Krenz, R. A.; Heidemann, R. A., High pressure phase equilibria in the systems linear low density polyethylene + n-hexane and linear low density polyethylene + n-hexane + ethylene: Experimental results and modelling with the Sanchez-Lacombe equation of state. *Journal of Supercritical Fluids* **2006,** *37* (1), 115-124.
25. Haruki, M.; Takakura, Y.; Sugiura, H.; Kihara, S.; Takishima, S., Phase behavior for the supercritical ethylene + hexane + polyethylene systems. *Journal of Supercritical Fluids* **2008,** *44* (3), 284-293.
26. de Loos, T. W.; de Graaf, L. J.; de Swaan Arons, J., Liquid-liquid phase separation in linear low density polyethylene-solvent systems. *Fluid Phase Equilibria* **1996,** *117* (1-2), 40-47.
27. Gauter, K.; Heidemann, R. A., Modeling polyethylene-solvent mixtures with the Sanchez-Lacombe equation. *Fluid Phase Equilibria* **2001,** *183*, 87-97.
28. Trumpi, H.; de Loos, T. W.; Krenz, R. A.; Heidemann, R. A., High pressure phase equilibria in the system linear low density polyethylene + ethylene: Experimental results and modelling. *Journal of Supercritical Fluids* **2003,** *27* (2), 205-214.
29. Haruki, M.; Sato, K.; Kihara, S.; Takishima, S., High pressure phase behavior for the supercritical ethylene + cyclohexane + hexane + polyethylene systems. *Journal of Supercritical Fluids* **2009,** *49* (2), 125-134.
30. Nagy, I.; Krenz, R. A.; Heidemann, R. A.; de Loos, T. W., High-pressure phase equilibria in the system linear low density polyethylene + isohexane: Experimental results and modelling. *Journal of Supercritical Fluids* **2007,** *40* (1), 125-133.

2 Characterization of Pressure Effects on the Cohesive Properties and Structure of Hexane and Polyethylene Using Molecular Dynamics Simulations

2.1 Summary

Molecular dynamics (MD) simulations using the OPLS-AA force field are conducted to compute pressure and molecular weight dependence of Hildebrand's solubility parameters of hexane and high-density polyethylene (HDPE) at high pressures. The pressure dependence investigation also captures density data computed at high temperature and for external pressures ranging from 100 to 3000 bar. The effect of electrostatic potential energy contribution to cohesive energy and density is investigated and it is shown that the solubility parameter increases monotonically with increasing external pressure for both molecular mechanical models with and without electrostatic terms. Analysis of the pair distribution function is carried out versus pressure together with the influence of electrostatic energy contribution reflecting structural change of the condensed phase.

2.2 Introduction

Understanding the phase behavior of polyethylene (PE) in hydrocarbon solutions is of great theoretical and practical interest especially in the industrial solution polymerization process of PE manufacturing. Solution polymerization involves chemical reaction of monomer ethylene in an inert hydrocarbon solvent (e.g. hexane) under high pressure to produce PE. The polymerization reaction is carried out at high pressure to maintain the fluid mixture in a single phase at the reaction temperature since at these conditions the reaction rate and product quality can be controlled effectively.[1] Further, to avoid flow

problems the reactor effluent needs to remain a homogeneous mixture prior to the separation phase as polymer-rich phase is viscous. Ultimately, phase separation of PE from the solvent and unreacted ethylene is accomplished through high-pressure separators by reducing the pressure to bring the one-phase polymer solution into the multi-phase region. Thus, the knowledge of thermodynamics and physical properties of PE in hydrocarbon solutions is essential in process design and control. Hence, this work seeks to contribute to the evolving understanding of the cohesive properties and solubility parameters of PE and hexane as functions of pressure and molecular weight which provide a rational basis for estimations of miscibility of PE in hexane solutions.

Solubility parameter theory[2-3] provides estimates of numerous thermodynamic solution properties including heat of mixing and miscibility. In particular, the theory has been shown to be useful in characterizing thermodynamic behavior of dilute solutions and especially when the constituting substances are non-polar.[4] Furthermore, this theory has been found extremely useful in correlating physical properties of materials such as glass transition temperature of polymers, dielectric constant, mechanical properties, permeability of molecules through membranes, permeation rates, surface tension, characterising surfaces, wettability, and the ratio of the thermal expansion coefficient to compressibility.[5-6] In recent years, solubility parameter concept has generated significant interest in a diverse number of practical applications such as in predicting the cohesive property (sorption) of flavor compounds for middle-density polyethylene (MDPE) films to evaluate the MDPE-flavor (solvent) affinity in plastic materials for food packaging.[7] Other examples include applications to dentin-bonding systems to aid development of polymeric adhesives and their strength correlations[8] and also in estimation of the aging resistance of asphalts which could be considered a kind of polymer solution in which maltene is the solvent and the asphaltene is the solute.[9] It was found that similar solubility parameters of asphaltene and maltene of the paving asphalt contributes to its good aging resistance. Further, the theory has received much interest in industrial applications including oil explorations, storage of oil/natural gas, selecting solvents in industry, polymer foaming, and blending. The above examples demonstrate that the knowledge of solubility parameter provides useful information on numerous material properties.

The solubility parameter (δ) is defined as the square root of the cohesive energy density (CED), representing the energy of vaporization per unit volume:

$$\delta(P, M_w) = \sqrt{\frac{\Delta U_{\text{vap}}}{V}} = \sqrt{\frac{\Delta H_{\text{vap}} - RT}{V}} \qquad (2.1)$$

where P is the pressure, T the temperature, M_w the molecular weight, ΔU_{vap} the increase in the internal energy (energy content) per mole as a result of eliminating intermolecular forces, and V is the molar volume of the substance at the pressure and temperature at which the vaporization occurs. By definition the energy of vaporization is the energy difference between vapor and liquid states. Equation (**1.1**) shows the connection between energy, ΔU_{vap} and the heat of vaporization ΔH_{vap}.

Nevertheless, unlike low-molecular-weight liquids, the cohesive energy of high-molecular-weight polymers cannot be conveniently measured since polymers have a hard-to-measure vapour pressure due to their low volatility. Hence, indirect methods such as determination of equilibrium swelling of polymers, intrinsic viscosity measurements, and additive group (molar-attraction constants) concept,[10] where solubility parameter (δ) is evaluated using knowledge of the structural formula of the substance, have been applied. However, the molar volume of the polymer still needs to be determined experimentally. Moreover, of greater interest is the ability to estimate pressure and temperature dependence of solubility of organic liquids and polymer blends/solutions, especially at elevated conditions which involves costly and time consuming experimental work. Accordingly, a great deal of effort has been expended to develop alternative methods for correlating and predicting solubility parameter.

To date, a number of theoretical and equation of state (EOS) studies have been reported to capture pressure and temperature dependence of solubility parameters of several pure compounds.[11-15] EOS models provide analytical expressions for cohesive energy and molar volume as functions of pressure, temperature, and concentration. However, in some cases EOS approaches are subject to practical limitations due to inaccuracy and the need for the determination of the molecular characteristic parameters in the model. Recently, Monte Carlo (MC) and molecular dynamics (MD) simulations have been introduced allowing for

precise determination of cohesive properties.[16-18] The advantage of molecular modeling methods is that they are able to provide molecular-level information besides macroscopic thermodynamic properties. Nonetheless, although a number of investigations have been performed to predict pressure and temperature dependence of cohesive properties, there is an incomplete molecular-level characterization at conditions of technological interest, as in the high-pressure production process of PE.[19-21]

This investigation seeks to develop a molecular-level understanding of thermodynamic properties that play a significant role in pressure-induced phase separation (PIPS).[22-25] To achieve this, isobaric-isothermal (NPT) MD simulations were carried out to characterize $\delta(P, M_w)$ of high-density polyethylene (HDPE) and hexane which lays a foundation to understand miscibility in these binary solutions. This investigation requires a detailed insight on the pressure effect upon the individual energy terms contributing to the total system energy, density, and accordingly the intrinsic structural properties. Since the accuracy of the MD results depends upon the molecular mechanics model parameters, this work is based on the widely-used optimized potentials for liquid simulations all-atom (OPLS-AA) force field, discussed below.

The organization of this paper is as follows. The method section presents the computational method followed by a detailed model description for NPT simulations employed to explore the pressure effects at 425 K, the temperature at which PE in hexane solutions are commonly processed. Results and discussion section presents the density and solubility parameter results together with pressure effects on potential energy contributions and structural properties. The final section presents the conclusions.

2.3 Model and Simulation Method

In the present work the molecular modeling software package GROMACS,[26-29] version 4.5.4 has been employed and the visual molecular dynamics (VMD) molecular graphics software[30] version 1.8.6 was used for visualization purposes. The force field OPLS-AA[31] was adopted which is appropriate for liquid hydrocarbon systems. This molecular mechanical model was developed by optimization of non-bonded parameters against experimental density, vaporization energy, and liquid heat capacity. The total system energy E_{total} is represented by the sum of bonded and non-bonded interactions:

$$E_{\text{total}} = E_b + E_\theta + E_\phi + E_{\text{vdW}} + E_{\text{electrostatics}} \qquad (2.2)$$

The molecular mechanics model incorporates the intramolecular interactions of covalent bond stretching (2-body), E_b, angle bending (3-body), E_θ, and dihedral angle (4-body), E_ϕ, which are based on a fixed list of atoms. The 2-body and 3-body interaction terms are expressed in harmonic form and dihedrals are treated by cosine series potentials. The intermolecular interactions which are computed on the basis of a list of non-bonded atoms within a certain radius between atoms separated by more than three bonds or those belong to different molecules, maybe modeled by pairwise additive 12-6 Lennard-Jones, E_{vdW}, and electrostatic, $E_{\text{electrostatics}}$, potential energies. Table 2.1 describes the functional form of energy terms along with the corresponding OPLS-AA parameters. To alleviate the ill effect of plain cut-offs, non-bonded potentials were treated by a shift function[32] (over the region 1-1.1 nm) which ensures that the truncated forces are continuous and have continuous derivatives at the group-based cut-off radius of 1.1 nm.

Table 2.1. Potential energy functions and the OPLS-AA force field parameters.

Interaction Type	Functional Form	Parameters
Bonded energy (kJ/mol):		Bonded interaction parameters
Bond stretching	$E_b = \sum_{bonds} \frac{1}{2} k_{ij}^b \left(r_{ij} - r_{ij}^0 \right)^2$	CC 0.1529 (nm) 224262.4 (kJ mol^{-1} nm^{-2}) CH 0.1090 (nm) 284512.0 (kJ mol^{-1} nm^{-2})
Angle bending	$E_\theta = \sum_{angles} \frac{1}{2} k_{ijk}^\theta \left(\theta_{ijk} - \theta_{ijk}^0 \right)^2$	CCC 112.7 (deg) 488.273 (kJ mol^{-1} rad^{-2}) CCH 110.7 (deg) 313.800 (kJ mol^{-1} rad^{-2}) HCH 107.8 (deg) 276.144 (kJ mol^{-1} rad^{-2})
Torsion	$E_\phi = \sum_{torsions} C_n \left(\cos\left(\phi - 180^\circ \right) \right)^n$	CCCC 2.9288 -1.4644 0.2092 -1.6736 0 0 (kJ mol^{-1}) CCCH 0.6276 1.8828 0 -2.5104 0 0 (kJ mol^{-1}) HCCH 0.6276 1.8828 0 -2.5104 0 0 (kJ mol^{-1})
Non-bonded energy (kJ/mol):		Non-bonded interaction parameters
Lennard-Jones	$E_{\text{vdW}} = \sum_{i>j} 4\varepsilon_{ij} \left(\left(\frac{\sigma_{ij}}{r_{ij}} \right)^{12} - \left(\frac{\sigma_{ij}}{r_{ij}} \right)^{6} \right)$	C 0.35 (nm) 0.276144 (kJ mol^{-1}) H 0.25 (nm) 0.125520 (kJ mol^{-1})
Electrostatics	$E_{\text{electrostatics}} = \sum_{i>j} \frac{q_i q_j}{\varepsilon r_{ij}}$	

The linear molecular architecture of PE chains were energy minimized and subsequently system models of 8 chains possessing 60 (8PE60) and 120 repeating units

(8PE120), corresponding to molecular weights of 1685 and 3368 g/mol, respectively, were packed into a cubic simulation box which has 3-D periodicity. This pressure-induced compression using a pressure coupling algorithm was employed to increase the gas density of the system close to the experimental density. In the next step, initial molecular structures were energy minimized using the steepest descent algorithm to bring the system close to minimum energy and to release atomic clashes. Further, to relax the initial unfavorable structures, the canonical ensemble simulations (NVT) were carried out at 425 K for PE and hexane. The run time for the canonical ensemble simulations is 500 ps with time steps of 1 fs which ensures that thermodynamic equilibrium is achieved. Following the NVT runs, the NPT (isobaric-isothermal) simulations were conducted for 20 ns at external pressures of P=100, 500, 1000, 2000, and 3000 bar to achieve equilibrium densities. Berendsen barostat[33] with time constant of 1 ps and temperature coupling using velocity rescaling[34] were used to control the system pressure and temperature at the target values. Coordinates and energy values were stored at every 100 steps for the confirmation of the equilibration and analysis. The equilibration of the simulations was mainly monitored by the time evolution of the total energy and density, and the last 1 ns of each simulation was analyzed and used to compute δ values. In molecular simulations the pressure dependence of the heat of vaporization may be computed from the internal energy of the periodic simulation cell at bulk state, U_{bulk} and the sum of the internal energies of the isolated molecules in vacuum, $U_{\text{i,isolated}}$ (absence of intermolecular interactions) averaged over a certain number of samples via the NPT runs:

$$\Delta H_{\text{vap}}(P,T) = \left\langle \sum_{i=1}^{n} U_{\text{i,isolated}}(T) - U_{\text{bulk}}(P,T) \right\rangle_{NPT} + RT \qquad (2.3)$$

Since PE is often treated as non-polar system, the effect of electrostatic potential energy has also been investigated on densities, solubility parameters, and structural properties (the notation 0c indicates molecular mechanics model where the atomic partial charges are set to zero).

2.4 Results and Discussion

2.4.1 Cohesive Energy Density versus Pressure

Isobaric-isothermal thermodynamic ensemble simulations were employed to investigate the pressure dependence of heat of vaporization, potential energy contributions, densities, and structural properties including radius of gyration of the polymer and radial distribution functions (RDFs). Figure 2.1 (left) demonstrates the pressure and temperature fluctuations for 8PE60 model where the target values are 3000 bar and 425 K. The simulations were long enough for the densities to reach equilibrium where densities fluctuate around an average value.

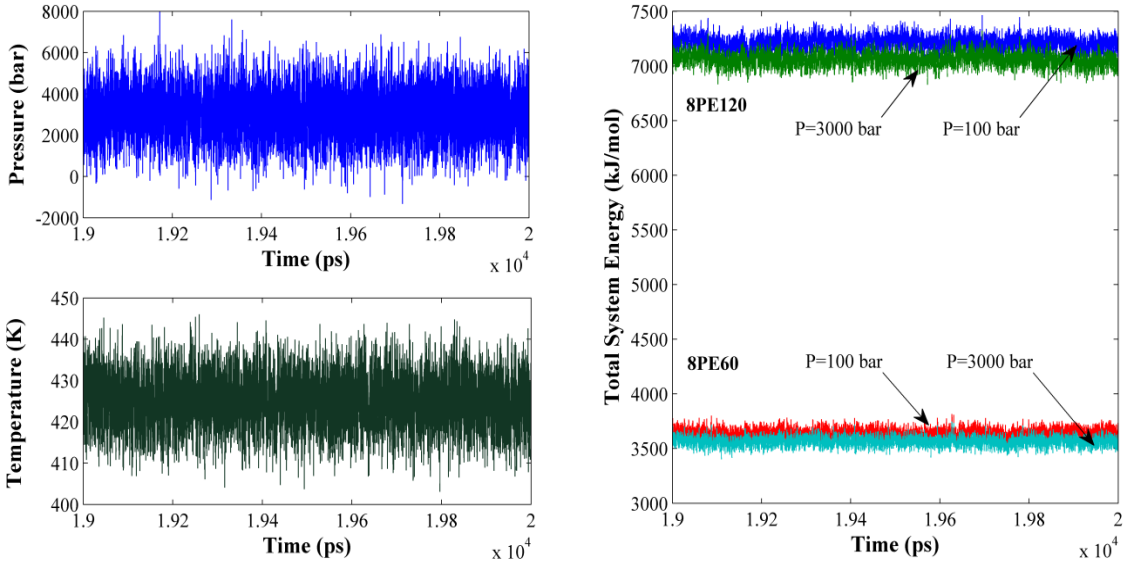

Figure 2.1. Pressure and temperature fluctuations (left) around target values of 3000 bar and 425 K for PE with 60 monomer units (8PE60). Time evolution of total system energy (right) for 8 polymer chains with 60 (8PE60) and 120 (8PE120) monomer units.

The total system energy leveled off during the first few nanoseconds, indicating the equilibrium state has been achieved. Figure 2.1 illustrates the total energy fluctuations obtained from the last 1 ns of the MD simulations for two molecular weights of the polymer at pressures of 100 and 3000 bar where the system energy decreases with increasing pressure. The bonded and non-bonded energy terms (listed in Table 2.2) were

calculated by averaging the corresponding values of the energies at varied pressures for different model systems.

Table 2.2. Computed values of energy components (kJ/mol) for PE and hexane models at 425 K.

Model System	P (bar)	Bonds	Angles	Torsions	Lennard-Jones	Electrostatics	Kinetic
	100	654.7	1022.6	334.2	-549.4	166.9	1917.5
	500	655.2	1021.1	331.2	-576.2	167.1	1917.5
8PE60	1000	653.5	1022.9	336.4	-591.4	164.2	1917.5
	2000	651.5	1024	342.6	-619.2	160.4	1917.5
	3000	650.3	1024	344.2	-640.3	160.4	1917.5
	100	1307.9	2039.4	649.8	-1143.6	342.2	3825.7
	500	1306.3	2044.6	671.2	-1159.2	331.7	3825.7
8PE120	1000	1301.1	2034	626.6	-1247.1	351.6	3825.7
	2000	1297.8	2029.9	615.9	-1310.8	357.1	3825.7
	3000	1296.9	2041.3	661	-1311.9	337.3	3825.7
	100	1301.2	2009.2	521.3	-1312.2	0	3825.8
	500	1299.5	2012.5	525.9	-1323.4	0	3825.8
8PE120-0c	1000	1297.9	2011.4	513.7	-1368.7	0	3825.8
	2000	1294.2	2016.3	538.8	-1386.7	0	3825.7
	3000	1293.5	2022.1	564.7	-1399.2	0	3825.7
	100	34.3	51.3	13.3	-19.1	8.7	105.9
	500	34.2	51.3	13.3	-23.6	8.6	105.9
hexane	1000	34.2	51.2	13.3	-26	8.6	105.9
	2000	34.1	51.3	13.4	-28.8	8.5	105.9
	3000	34	51.3	13.4	-30.4	8.4	105.9
	100	34.3	51.2	12.7	-18.7	0	105.9
	500	34.2	51.3	12.7	-23.6	0	105.9
hexane-0c	1000	34.1	51.3	12.7	-26.2	0	105.9
	2000	34	51.3	12.7	-29	0	105.9
	3000	34	51.3	12.7	-30.7	0	105.9

As may be inferred from the total energy break-down, the difference in total system energies is mainly due to the Lennard-Jones interactions and the remaining terms do not demonstrate significant pressure dependence. The results indicate that the differences in cohesive properties are essentially due to the Lennard-Jones interaction energies not bonded or electrostatic energy contributions.

The accuracy of the force field OPLS-AA was examined by comparing the equilibrated hexane densities at 50, 100, 500, and 1000 bar and at temperatures of 303 and 425 K. As depicted in Figure 2.2 simulated densities are in very good quantitative agreement with experimental values[35] (4% error at most in the range 50-1000 bar at 303 K). Figure 2.3 illustrates the density of PE models as a function of pressure and predictions based upon a corresponding-states theoretical method,[36] where densities show a slight increase with chains length. Predicted densities indicate a monotonic increase as a result of

pressure change from 100 to 3000 bar. For hexane electrostatics shows negligible impact on liquid densities. However, for the polymer, models that ignore electrostatic term predict higher density values for each molecular weight which is attributed to the lack of repulsive electrostatic interactions. Subsequently, the molar volume of the liquid was computed from densities predicted by NPT runs.

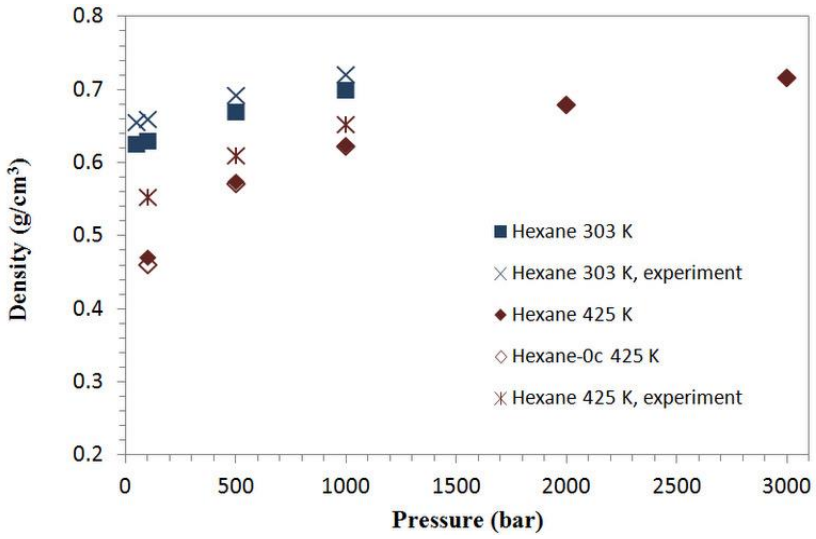

Figure 2.2. Pressure dependence of hexane density. The squares and diamonds represent simulation data at 303 and 425 K, respectively (0c notation indicates force field model with no electrostatic term).

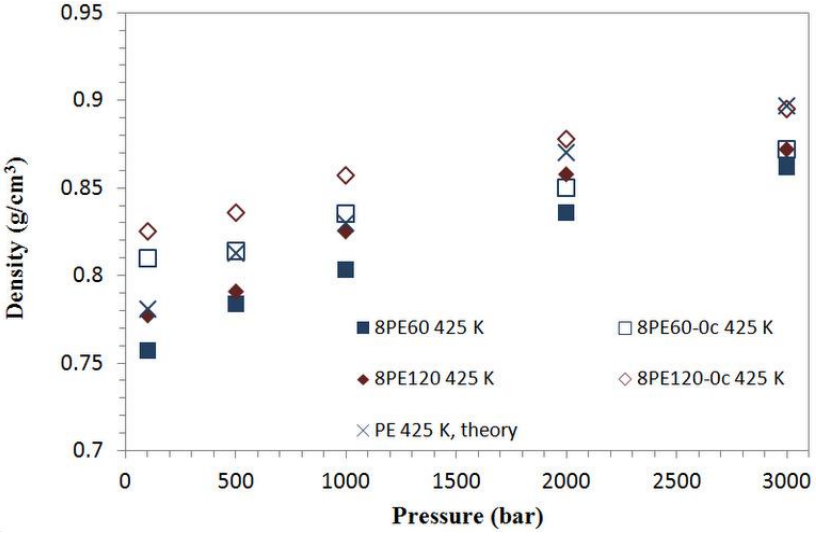

Figure 2.3. Pressure dependence of PE density at 425 K. The squares and diamonds represent simulation data for PE chains with 60 and 120 monomer units, respectively (0c notation indicates force field model with no electrostatic term).

The Hildebrand solubility parameters of PE and hexane obtained from the simulations were compared with experimental/theoretical/simulation data to confirm the validity of the model. Figure 2.4 shows the solubility parameters of hexane as a function of pressure obtained by reanalyzing the data in the final 1 ns of NPT runs. The computed solubility parameters of 14.3, 14.5, 15.4, and 16.2 $(MPa)^{1/2}$ (at P=50, 100, 500, and 1000 bar) correspond to a deviation of 2-5, 0.1-2, and 1-3% compared to the experimental,[14] MC and Peng–Robinson (PR)[15] data at 303 K, respectively. For hexane at 425 K and elevated external pressures we were not able to find experimental data to validate the NPT results. The computed values increase monotonically with pressure indicating that at higher pressures more energy is required to move the molecules to an infinite distance. This behavior is attributed to the absolute van der Waals (vdW) energies that increase with pressure (see Figure 2.5). At 425 K, solubility parameter varies in the range of 9.7-15.5 and 9.6-15.6 $(MPa)^{1/2}$ for two models with and without atomic partial charges which correspond to nearly 60% increase in the magnitude of δ for a pressure change from 100 to 3000 bar. Also since electrostatics energy term has slight influence on liquid densities and heat of vaporization, CED of the hydrocarbon liquid is insensitive to this potential energy term.

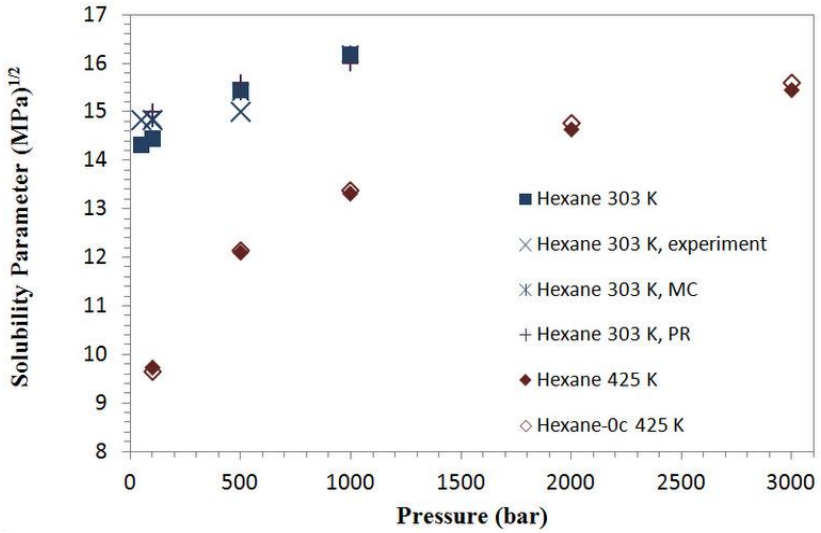

Figure 2.4. Pressure dependence of hexane solubility parameter. The squares and diamonds represent simulation data at 303 and 425 K, respectively (0c notation indicates force field model with no electrostatic term).

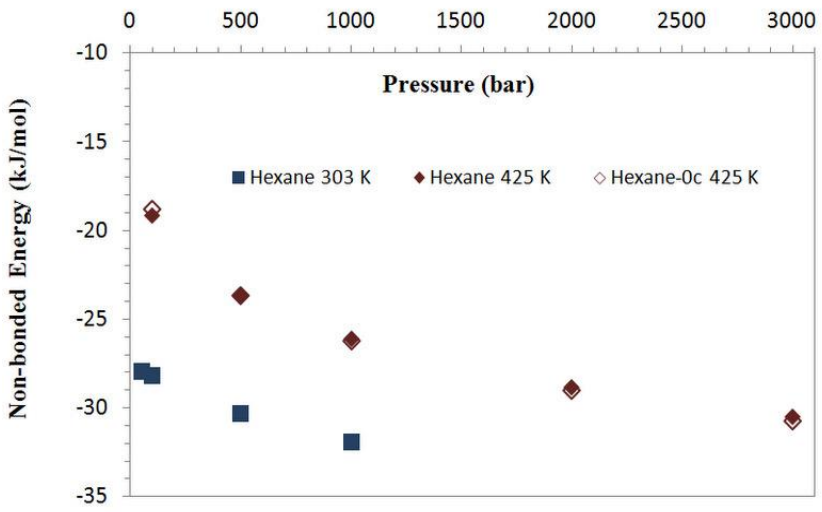

Figure 2.5. Pressure dependence of non-bonded energy contribution for hexane. The squares and diamonds represent simulation data at 303 and 425 K, respectively (0c notation indicates force field model with no electrostatic term).

Figure 2.6 represents the pressure dependence of the solubility parameter of PE where the computed δ value of 13 $(MPa)^{1/2}$ for PE60 at 425 K and 100 bar predicts accurately the measured 13 $(MPa)^{1/2}$ solubility parameter of HDPE by inverse gas chromatography[37] at 423.15 K (150 ^{o}C) and 1 bar. As may be seen, δ increases with increasing pressure and agree favorably with the corresponding-states theoretical results.[36] To investigate the effect of chain length, the solubility parameter of PE120 was estimated at P=100, 1000, and 2000 bar which demonstrates slight difference compared to the corresponding values for PE60 model. The non-bonded energies of the PE models with different chain lengths calculated at different pressures are presented in Figure 2.7 where the absolute energy values increase with pressure indicating that at higher pressure more energy is needed to vaporize the fluid resulting in larger CEDs at high pressure, in agreement with experimental and theoretical observations. Since electrostatic repulsion in the system leads to lower net non-bonded energies which play a key role in calculating cohesive properties, inclusion of this term is the main reason for the lower δ values of PE.[38] The other contribution to lower solubility parameters is due to lower densities of the system as depicted in Figure 2.3.

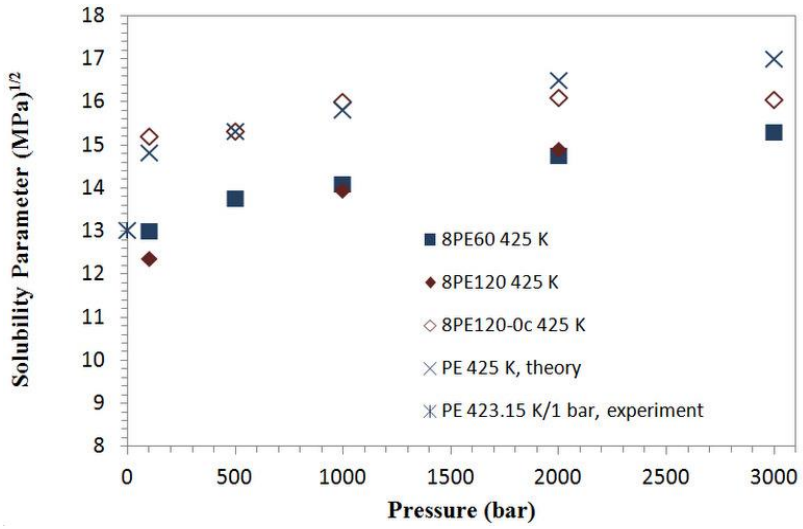

Figure 2.6. Pressure dependence of PE solubility parameter at 425 K. The squares and diamond represent simulation data for PE chains with 60 and 120 monomer units, respectively (0c notation indicates force field model with no electrostatic term).

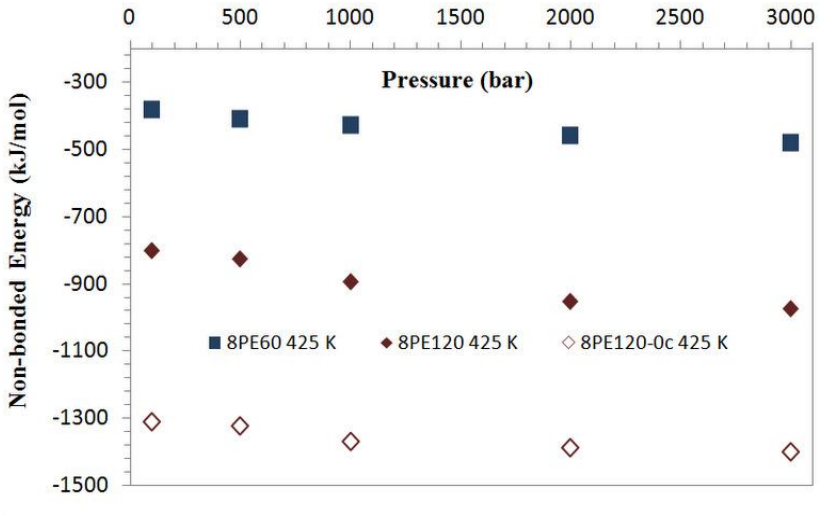

Figure 2.7. Pressure dependence of non-bonded energy contribution for PE at 425 K. The squares and diamond represent simulation data for PE chains with 60 and 120 monomer units, respectively (0c notation indicates force field model with no electrostatics term).

2.4.2 Radial Distribution Function and Radius of Gyration

Besides the influence of pressure on cohesive energy and liquid phase densities, the effect of external pressure (*P*=100, 500, 1000, 2000, and 3000 bar) on the structure of the liquid phase was analyzed via the polymer radius of gyration and the RDFs. The structural

stability was achieved in the first few nanoseconds; however, trajectories were analyzed in the last 1 ns of the runs to ensure that the structures are stabilized. It was noticed that as pressure increases, the height of the first peak increases and the distribution function is shifted to the left (see Figure 2.8 and Figure 2.9). This shift of the RDF is due to the increased local order upon increase in density which in turn is affected by external pressure. Table 2.3 lists the simulated densities for the model systems at 425 K. A magnified indication of the increased compactness of the structure at high pressure is noticed at a radius of 0.8-1 nm in the RDF of polymer and hexane. The increased local order with increasing pressure can also be deduced from the influence of pressure on radius of gyration indicating that the more packed structure is expected at higher pressure. Figure 2.10 reveals that high pressure causes the polymer to take a more compact conformation as radius of gyration decreases with increasing pressure.

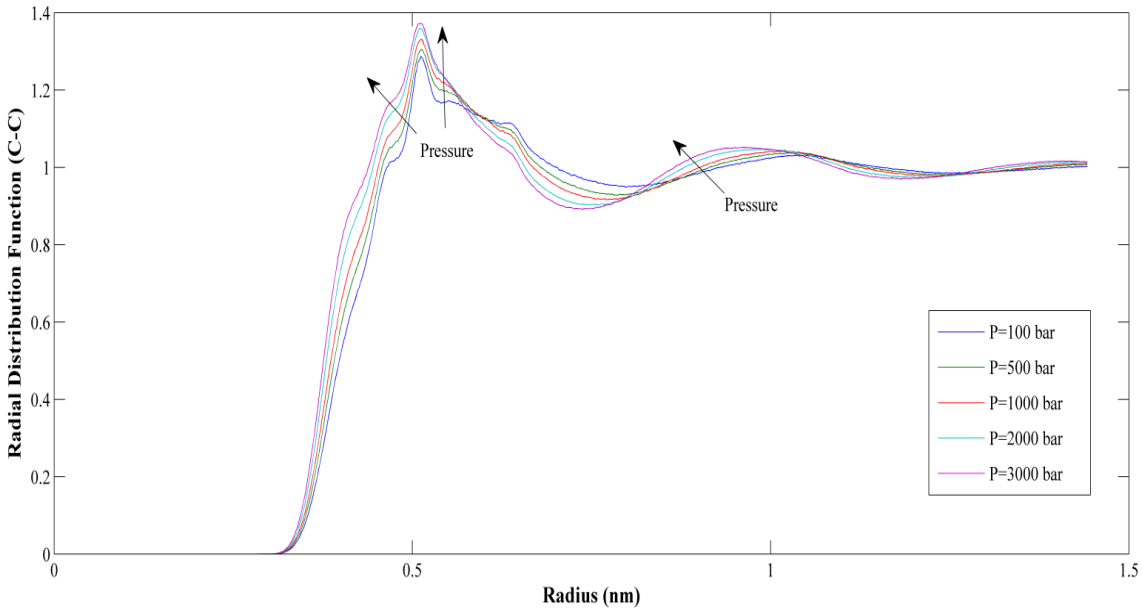

Figure 2.8. RDF for hexane at different external pressures of 100, 500, 1000, 2000, and 3000 bar.

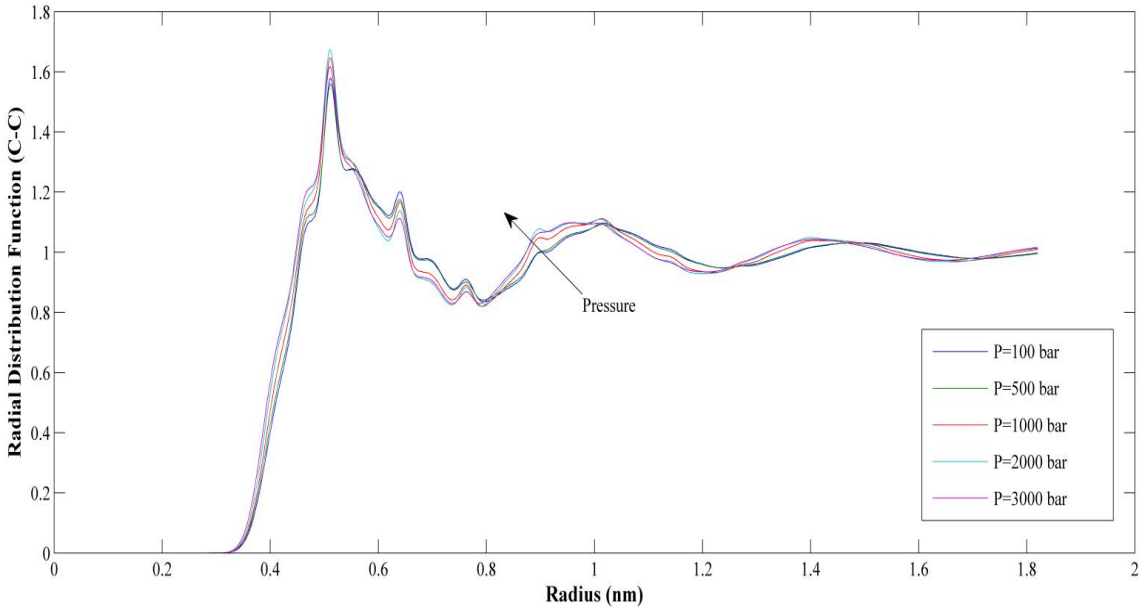

Figure 2.9. RDF for PE120 at different external pressures of 100, 500, 1000, 2000, and 3000 bar.

Table 2.3. Densities obtained by NPT-MD simulations at 425 K.

Model System	Density (g/cm^3)				
	100 (bar)	500 (bar)	1000 (bar)	2000 (bar)	3000 (bar)
8PE60	0.757	0.784	0.803	0.836	0.862
8PE60-0c	0.810	0.814	0.835	0.850	0.872
8PE120	0.777	0.791	0.825	0.858	0.872
8PE120-0c	0.825	0.836	0.857	0.878	0.895
hexane	0.470	0.574	0.624	0.680	0.716
hexane-0c	0.460	0.571	0.623	0.680	0.717

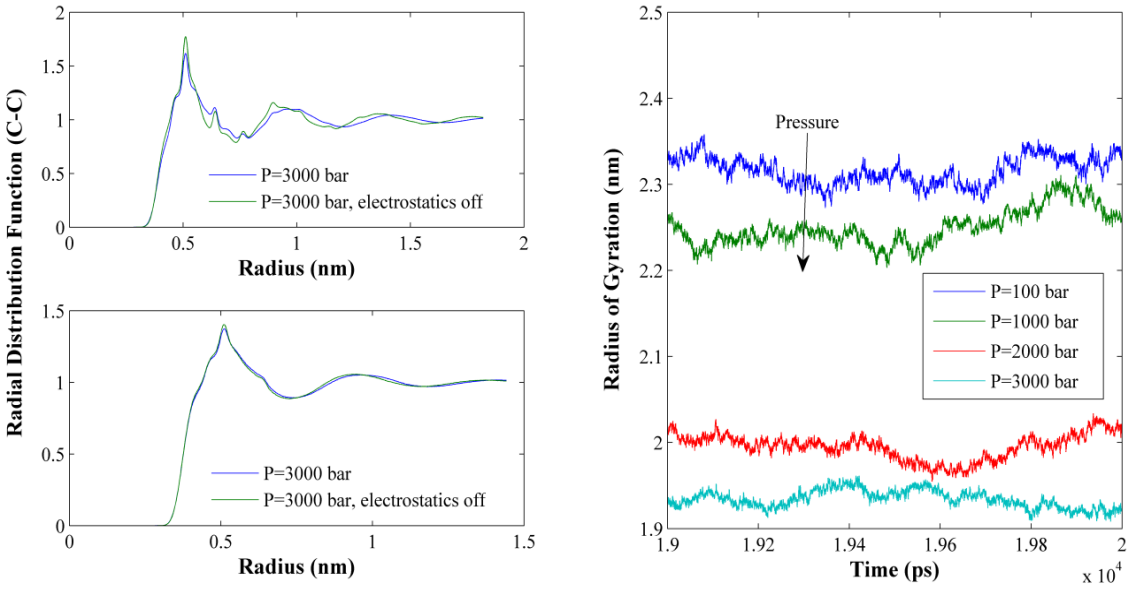

Figure 2.10. Effect of electrostatics on RDF of PE with 120 (PE120) monomer units (top) and hexane (bottom). Radius of gyration (right) of PE120 at different external pressures of 100, 1000, 2000, and 3000 bar.

Further, it is illustrated that for the PE the height of the first peak of the RDF increases and the curve shifts slightly to the left for the model where vdW is the only non-bonded energy term. The shift of the curve to the left is more pronounced in the range of 0.6-1 nm. This is due to the elimination of electrostatic repulsion potential from the system resulting in higher density and shorter separation. Unlike the RDF of PE, electrostatics does not shift RDF of hexane and only a very slight increase in the first peak (at radius of 0.5 nm) is observed for the model without electrostatic term owing to the lack of repulsion forces.

2.5 Conclusions

The Hildebrand solubility parameters and liquid phase densities for two molecular weights of HDPE and hexane were computed over a broad range of pressures using MD technique on the basis of the OPLS-AA force field. The solubility parameter and density increases monotonically with increasing pressure for all polymer model systems as well as for hexane due to increase in Lennard-Jones interactions. Liquid phase densities increase with degree of polymerization of the polymer, however, the solubility parameter remains

unchanged. The electrostatic potential has a significant impact on cohesive energy and density of PE. Exclusion of this term causes higher absolutes values of non-bonded energy and consequently higher heat of vaporization and also lower molar volumes due to lack of repulsion forces which is conducive to greater solubility parameters.

Structural analysis of PE chains and hexane reveals noticeable difference in the RDF (C-C atoms) where the height of the first peak increases and the pair distribution function shifts to shorter separations upon increasing pressure owing to increase in the positional compactness. This increase in the local order may be deduced from a decrease in the polymer radius of the gyration and increase of densities at high pressures. Further, elimination of electrostatic energy contribution causes the RDF of PE shift indicating shorter separation as a result of removing repulsive interactions.

The overall performance of the OPLS-AA force field employed to carry out NPT based on verifications with previously reported experimental/theoretical/simulation values of solubility parameters and densities, is very good. As MD simulations were performed on multiple-core processors simulation times were notably reduced enabling study of various model systems of thousands of atoms at varied pressures. Based on the results, we conclude that MD is a promising alternative to experimental and indirect methods for the determination of solubility parameters, densities, and structural properties of saturated hydrocarbon polymers and organic liquids at high pressures. Ultimately, using knowledge of solubility parameters of the polymer and solvent, the binary interaction parameters may be estimated enabling predictions of the miscibility of PE in the solvent at elevated pressures and temperatures which is a topic of significant industrial interest.

2.6 References

1. Trumpi, H.; de Loos, T. W.; Krenz, R. A.; Heidemann, R. A., High pressure phase equilibria in the system linear low density polyethylene + ethylene: Experimental results and modelling. *Journal of Supercritical Fluids* **2003,** *27* (2), 205-214.
2. Scatchard, G., Equilibria in non-electrolyte solutions in relation to the vapor pressures and densities of the components. *Chemical Reviews* **1931,** *8* (2), 321-333.
3. Hildebrand, J. H.; Scott, R. L., *The solubility of nonelectrolytes*. Dover Publications: New York, 1964.
4. Blanks, R. F.; Prausnitz, J. M., Thermodynamics of polymer solubility in polar and nonpolar systems. *Industrial and Engineering Chemistry Fundamentals* **1964,** *3* (1), 1-8.
5. Bicerano, J., *Prediction of polymer properties*. Marcel Dekker: New York, 2002.

6. Gardon, J. L., Relationship between cohesive energy densities of polymers and Zisman's critical surface tensions. *Journal of Physical Chemistry* **1963,** *67* (9), 1935-1936.
7. Matsui, T.; Nagashima, K.; Fukamachi, M.; Shimoda, M.; Osajima, Y., Application of the solubility parameter in estimating the sorption behavior of flavor into packaging film. *Journal of Agricultural and Food Chemistry* **1992,** *40* (10), 1902-1905.
8. Miller, R. G.; Bowles, C. Q.; Chappelow, C. C.; Eick, J. D., Application of solubility parameter theory to dentin-bonding systems and adhesive strength correlations. *Journal of Biomedical Materials Research* **1998,** *41* (2), 237-243.
9. Yang, P.; Cong, Q.; Liao, K. J., Application of solubility parameter theory in evaluating the aging resistance of paving asphalts. *Petroleum Science and Technology* **2003,** *21* (11-12), 1843-1850.
10. Fedors, R. F., A method for estimating both solubility parameters and molar volumes of liquids. *Polymer Engineering and Science* **1974,** *14* (2), 147-154.
11. Allada, S. R., Solubility parameters of supercritical fluids. *Industrial & Engineering Chemistry Process Design and Development* **1984,** *23* (2), 344-348.
12. Panayiotou, C., Solubility parameter revisited: An equation-of-state approach for its estimation. *Fluid Phase Equilibria* **1997,** *131* (1-2), 21-35.
13. Stefanis, E.; Tsivintzelis, L.; Panayiotou, C., The partial solubility parameters: An equation-of-state approach. *Fluid Phase Equilibria* **2006,** *240* (2), 144-154.
14. Verdier, S.; Andersen, S. I., Internal pressure and solubility parameter as a function of pressure. *Fluid Phase Equilibria* **2005,** *231* (2), 125-137.
15. Zeng, Z. Y.; Xu, Y. Y.; Li, Y. W., Calculation of solubility parameter using perturbed-chain SAFT and cubic-plus-association equations of state. *Industrial & Engineering Chemistry Research* **2008,** *47* (23), 9663-9669.
16. Rai, N.; Siepmann, J. I.; Schultz, N. E.; Ross, R. B., Pressure dependence of the Hildebrand solubility parameter and the internal pressure: Monte Carlo simulations for external pressures up to 300 MPa. *Journal of Physical Chemistry C* **2007,** *111* (43), 15634-15641.
17. Rai, N.; Wagner, A. J.; Ross, R. B.; Siepmann, J. I., Application of the TraPPE force field for predicting the Hildebrand solubility parameters of organic solvents and monomer units. *Journal of Chemical Theory and Computation* **2008,** *4* (1), 136-144.
18. Belmares, M.; Blanco, M.; Goddard, W. A.; Ross, R. B.; Caldwell, G.; Chou, S. H.; Pham, J.; Olofson, P. M.; Thomas, C., Hildebrand and Hansen solubility parameters from molecular dynamics with applications to electronic nose polymer sensors. *Journal of Computational Chemistry* **2004,** *25* (15), 1814-1826.
19. Folie, B.; Radosz, M., Phase equilibria in high-pressure polyethylene technology. *Industrial & Engineering Chemistry Research* **1995,** *34* (5), 1501-1516.
20. Gauter, K.; Heidemann, R. A., Modeling polyethylene-solvent mixtures with the Sanchez-Lacombe equation. *Fluid Phase Equilibria* **2001,** *183*, 87-97.
21. Haruki, M.; Takakura, Y.; Sugiura, H.; Kihara, S.; Takishima, S., Phase behavior for the supercritical ethylene + hexane + polyethylene systems. *Journal of Supercritical Fluids* **2008,** *44* (3), 284-293.
22. Ghiass, M.; Rey, A. D., Interfacial thermodynamics of compressible polymer solutions. *Journal of Chemical Physics* **2008,** *128* (7), 0711021-0711025.
23. Ghiass, M.; Rey, A. D., Interfacial properties of compressible polymer solutions. *Journal of Polymer Science Part B: Polymer Physics* **2009,** *47* (6), 640-654.

24. Ghiass, M.; Rey, A. D., Thermodynamic modeling of polymer solution interface. *Macromolecular Theory and Simulations* **2009,** *18* (2), 127-137.
25. Rasouli, G.; Rey, A. D., Acousto-spinodal decomposition of compressible polymer solutions: Early stage analysis. *Journal of Chemical Physics* **2011,** *134* (18), 1849011-18490119.
26. Berendsen, H. J. C.; van der Spoel, D.; van Drunen, R., Gromacs: A message-passing parallel molecular dynamics implementation. *Computer Physics Communications* **1995,** *91* (1-3), 43-56.
27. Lindahl, E.; Hess, B.; van der Spoel, D., GROMACS 3.0: A package for molecular simulation and trajectory analysis. *Journal of Molecular Modeling* **2001,** *7* (8), 306-317.
28. van der Spoel, D.; Lindahl, E.; Hess, B.; Groenhof, G.; Mark, A. E.; Berendsen, H. J. C., GROMACS: Fast, flexible, and free. *Journal of Computational Chemistry* **2005,** *26* (16), 1701-1718.
29. Hess, B.; Kutzner, C.; van der Spoel, D.; Lindahl, E., GROMACS 4: Algorithms for highly efficient, load-balanced, and scalable molecular simulation. *Journal of Chemical Theory and Computation* **2008,** *4* (3), 435-447.
30. Humphrey, W.; Dalke, A.; Schulten, K., VMD: Visual molecular dynamics. *Journal of Molecular Graphics & Modelling* **1996,** *14* (1), 33-38.
31. Jorgensen, W. L.; Madura, J. D.; Swenson, C. J., Optimized intermolecular potential functions for liquid hydrocarbons. *Journal of the American Chemical Society* **1984,** *106* (22), 6638-6646.
32. van der Spoel, D.; van Maaren, P. J., The origin of layer structure artifacts in simulations of liquid water. *Journal of Chemical Theory and Computation* **2006,** *2* (1), 1-11.
33. Berendsen, H. J. C.; Postma, J. P. M.; van Gunsteren, W. F.; Dinola, A.; Haak, J. R., Molecular dynamics with coupling to an external bath. *Journal of Chemical Physics* **1984,** *81* (8), 3684-3690.
34. Bussi, G.; Donadio, D.; Parrinello, M., Canonical sampling through velocity rescaling. *Journal of Chemical Physics* **2007,** *126* (1), 014101.
35. Daridon, J. L.; Lagourette, B.; Grolier, J. P. E., Experimental measurements of the speed of sound in n-hexane from 293 to 373 K and up to 150 MPa. *International Journal of Thermophysics* **1998,** *19* (1), 145-160.
36. Maloney, D. P.; Prausnitz, J. M., Thermodynamic properties of liquid polyethylene. *Journal of Applied Polymer Science* **1974,** *18* (9), 2703-2710.
37. Barton, A. F. M., *CRC handbook of polymer-liquid interaction parameters and solubility parameters*. CRC Press: Boca Raton, 1990.
38. Jo, W. H.; Choi, K., Determination of equation-of-state parameters by molecular simulations and application to the prediction of surface properties for polyethylene. *Macromolecules* **1997,** *30* (6), 1800-1805.

3 High Pressure Miscibility Predictions of Polyethylene in Hexane Solutions Based on Molecular Dynamics

3.1 Summary

Models that describe miscibility of polyethylene in hydrocarbon solvents at high pressures are of on-going interest in fundamental polymer physics and applied polymer processing. The present study aims to characterize the pressure dependence of the solubility of polyethylene (PE) in hexane using an atomistic-level simulation technique to avoid the need for expensive and difficult to obtain experimental data. To achieve this, isobaric-isothermal molecular dynamics (NPT-MD) simulations based upon a well-established force field (OPLS-AA) are utilized to predict the pressure dependence of Hildebrand's solubility parameter of high-density polyethylene (HDPE) and hexane at high pressure. The NPT simulations also capture molar volume data computed at high temperature (425 K) and high pressures ranging from 100 to 3000 bar. Further, internal pressures are estimated at high pressures and it is shown that for PE internal pressure is not identical to cohesive energy density (CED). However for PE the ratio of these two quantities tends to unity with increasing pressure. Subsequently, the Flory-Huggins binary interaction parameter is predicted from the knowledge of pressure dependence of solubility parameters and molar volumes. It is demonstrated that the computed binary interaction parameter decreases upon increasing the pressure indicating that the miscibility of the PE/hexane system improves by raising the pressure. This conclusion is in agreement with the solution polymerization process for producing PE where pressure-induced phase separation (PIPS) is applied to separate the polymer product from the polyolefin solution. Exclusion of electrostatic potentials in the molecular mechanics model results in larger interaction parameters while the monotonically decreasing trend remains intact in both molecular mechanics models

with and without electrostatic forces. In addition, it has been found that there is a pressure limit beyond which the binary interaction parameter demonstrates less sensitivity to pressure indicating that PE miscibility is not further affected by pressure changes. Based upon the pressure dependence of the interaction parameter the negative contribution of volume change on mixing is predicted where the change in volume upon mixing decays with increasing pressure. Moreover, it is shown that the increase in system pressure increases the chemical potential factor of the phase stability condition indicating that at higher pressures this term tends to stabilize the polymer-solvent system. It has also been revealed that the chemical potential factor estimated by the molecular mechanics model, incorporating the atomic partial charges, is qualitatively more consistent with the miscibility predictions from phase diagrams. The presented results contribute to the fundamental understanding of PIPS, an important demixing process poorly understood when compared to thermally-induced phase separation.

3.2 Introduction

Polyolefins are saturated hydrocarbon polymers representing the largest class of polymers in commercial applications in terms of production volume. A great portion of polyethylene (PE) is produced by solution polymerization process. Solution polymerization is a process in which a monomer is dissolved in a non-reactive solvent that contains a catalyst. This PE production process involves chemical reaction of ethylene in an inert hydrocarbon solvent (e.g. hexane) at high pressure. To maintain the fluid mixture in a single phase the polymerization reaction of ethylene in the hydrocarbon solvent is accomplished at sufficiently high pressure at the reaction temperature since at these conditions the reaction rate and product quality can be controlled effectively.[1] Moreover, as the polymer-rich phase is of high viscosity the polymer solution needs to remain as a homogeneous mixture prior to the separation stage to avoid flow problems. Ultimately, the separation of PE from the solvent and the unreacted monomer is carried out in a stagewise manner, i.e. the reactor effluent undergoes high and low pressure flash vaporizations as a result of which the solution is depressurized down to ambient pressure. The pressure quench transforms the one phase PE solution into two or more equilibrium phases. This thermodynamic instability is known as pressure-induced phase separation (PIPS) which

typically occurs by spinodal decomposition. Spinodal decomposition by PIPS, has distinguishing features from TIPS (temperature-induced phase separation), SIPS (solvent-induced phase separation), and RIPS (reaction-induced phase separation) and it is the subject of current interest.[2-6] The pressure decrease also affects the density of the mixture which consequently influences thermodynamic properties of the polymer solution. Thus, design and operation of the solution polymerization process requires accurate knowledge of thermodynamics and phase behavior of PE solutions including changes in pressure and mixture density. Moreover, understanding of the polymer solution thermodynamics helps to explore the micro structural and morphology evolution generated during the spinodal decomposition by PIPS.

In an effort to investigate the pressure effect on polymer miscibility in solutions, the traditional Flory-Huggins (FH) model which concentrates on the dissimilarity of contact energies or cohesive energies between polymer and solvent molecules, was extended through the introduction of a new factor accounting for dissimilarity between their respective free volumes. It was found that the free volume dissimilarity arising from difference in size or chain length has important thermodynamic consequences.[7-8] The pressure effect on the phase diagram of polymer solutions has been intensively investigated using experimental techniques.[9-17] There has also been much research on the theories (e.g. Sanchez-Lacombe model) of the pressure effects on the thermodynamics and phase behavior of polymer solutions.[18-19] Further, the Van Laar/Bragg-Williams (VLBW) model was extended based on an expression for the free enthalpy change on mixing to define the pressure dependence of the interaction parameter using definitions of thermal expansion coefficient and isothermal compressibility.[20] It has been shown that the first derivative of the interaction parameter with respect to pressure gives the deviation of the molar volume of the mixture from that of the constituents before mixing. As far as the polymer blend miscibility in concerned, experimental results indicate that the critical temperature is strongly affected by pressure. The pressure increase has been almost always found to increase the critical temperature in blends that display UCST (upper critical solution temperature) and LCST (lower critical solution temperature) behavior which indicates that the increasing pressure reduces the miscibility range in UCST blends and increases this range in LCST polymer blends.[21]

The present work aims to contribute to the evolving understanding of the pressure dependence of miscibility of PE in hexane solutions at conditions of industrial interest based upon the prediction of binary interaction parameters using the solubility parameters of PE and hexane validated in our previous work[22] that provides a rational basis for such an investigation.

To predict miscibility in binary mixtures, the solubility parameter (numerical estimate for intermolecular potential energies) concept has been widely employed. The solubility parameter may be estimated from the cohesive energy density (CED) that in turn is determined from the energy of vaporization and the molar volume of the liquid phase. For a solute-solvent system to form a homogenous mixture, the resulting solute-solvent interactions need to be strong enough to overcome the solvent-solvent and solute-solute intermolecular interactions. Hence, in a binary system the difference in the solubility parameters of the constituting substances maybe used to predict miscibility and change of enthalpy upon mixing. In particular, the theory has been widely applied in characterizing thermodynamic behavior of dilute solutions and especially when the constituting substances are non-polar.[23] According to the solubility parameter concept, non-polar molecules having nearly the same numerical values for solubility parameter are soluble.

The solubility parameter (δ) is defined as the square root of the CED representing the energy of vaporization per unit volume:

$$\delta(P) = \sqrt{\frac{\Delta U_{vap}}{V}} = \sqrt{\frac{\Delta H_{vap} - RT}{V}} \qquad (3.1)$$

where P is the pressure, T the temperature, ΔU_{vap} the increase in the internal energy (energy content) per mole as a result of eliminating intermolecular forces, and V is the molar volume of the condensed phase at the pressure and temperature at which the vaporization occurs. By definition the energy of vaporization is the energy difference between vapor and liquid states. Equation 3.1 shows the connection between energy, ΔU_{vap} and the heat of vaporization ΔH_{vap}.

In this paper from the solubility parameters we determine miscibility of a polymer in a solution by estimating the interaction parameter χ which is proportional to the enthalpy of mixing:

$$\chi = \frac{V\left(\delta_{solvent} - \delta_{polymer}\right)^2}{RT} \qquad (3.2)$$

V in this expression is the molar volume of the solvent and *RT* has the usual meaning. It is noteworthy that, the pressure and temperature dependence of the FH interaction parameter has been derived from Equation 3.2 using the knowledge of pressure and temperature dependence of solubility parameter differences and compared with measured interaction parameters for polymer blends.[24]

Besides quantifying the polymer-solvent interactions, the solubility parameter has been found useful in correlating a broad range of material properties.[25] Nevertheless, unlike low molecular weight liquids, the cohesive energy of synthetic polymers cannot be conveniently measured due to low volatility at room temperature and chemical degradation at the boiling point. Hence, indirect methods such as determination of equilibrium swelling of polymers, intrinsic viscosity measurements, and additive group (molar-attraction constants) concept where solubility parameter is evaluated using knowledge of the structural formula of the substance, have been applied. In the swelling measurement method the solubility parameter of the polymer is assigned to that of the solvent causing the maximum extent of equilibrium swelling in a series of polymer swelling measurements.[26] However, the molar volume of the polymer still needs to be determined experimentally. Further, estimation of pressure and temperature dependence of solubility of organic liquids and polymer blends/solutions, especially at elevated conditions is of great practical importance which involves costly and time consuming experimental effort.

Therefore, although estimation of the thermodynamic and physical properties of PE in hydrocarbons (solvent) is significant in a variety of industrial processes for PE production, due to the difficulty of carrying out experiments at high pressures and temperatures there has been a demand for alternative methods to capture pressure dependence of physical properties of PE solution systems.

In this regard, molecular-level physics supplies a powerful basis for the prediction of the thermodynamic properties of polymer-solvent systems. In the present study, molecular mechanics (MM) and molecular dynamics (MD) have been applied on the basis of an atomistic-level model to explore the binary interaction parameter χ as a function of pressure which provides the basis to characterize miscibility predictions of polymer solution. To the best of our knowledge, no such studies have been made earlier for a PE in hydrocarbon solution based on a molecular modeling approach. In addition, pressure dependence of internal pressure π for PE and hexane at high pressure has been evaluated as this topic has not been completely characterized and its nature remains partially understood. Internal pressure is a measure of the change in the internal energy upon an infinitesimal isothermal change in volume, defined as:

$$\pi = \left(\frac{\partial U}{\partial V}\right)_T = T\left(\frac{\partial P}{\partial T}\right)_V - P = T\frac{\alpha_P}{\kappa_T} - P \qquad (3.3)$$

where U, α_P, and κ_T are the internal energy, thermal expansivity, and isothermal compressibility, respectively. Although δ and π are defined differently, both describe the cohesive properties of a liquid. Here, we discuss the relationship between CED and internal pressure π with emphasis on the effect of pressure on the ratio π/CED.

Based upon the principles that govern the pressure dependence of χ, the PIPS phenomenon may be characterized over a broad range of pressures using the thermodynamic criterion for phase stability commonly expressed as:[27]

$$\frac{\partial^2 g}{\partial \phi^2} - v\beta P_\phi^{\,2} > 0 \qquad (3.4)$$

where g is free energy per unit volume, ϕ the polymer volume fraction, v the specific volume, β the isothermal compressibility, and $P_\phi = \left(\frac{\partial P}{\partial \phi}\right)_{T,v}$ the pressure change with composition. The derivative of the chemical potential with respect to concentration $\frac{\partial^2 g}{\partial \phi^2}$

represents the incompressible contribution (chemical potential factor), whereas the second term identifies the compressible contribution to phase stability. Hence, the stability criterion is composed of a chemical $\left(\frac{\partial^2 g}{\partial \phi^2}\right)$ and a mechanical part $\left(v\beta P_\phi^{\ 2}\right)$, as opposed to incompressible mixtures whose stability is determined only by chemical potential factor. It is important to recognize that since the second term in the above equation is always non-negative the above stability criterion indicates that the compressibility destabilizes the polymer solution promoting phase separation. In other words, phase stability of a compressible solution is more restricted than for the corresponding incompressible solution. Lastly, we note that if we neglect the mechanical factor $\left(v\beta P_\phi^{\ 2}\right)$, the partial stability criterium $\left(\frac{\partial^2 g}{\partial \phi^2}\right)$ is a very useful upper-bound to the total stability criterium, given the scarcity of high pressure measurements and predictions.

In the present paper, we seek to demonstrate the effect of pressure on the chemical potential factor (i.e. incompressible or constant volume contribution) $\frac{\partial^2 g}{\partial \phi^2}$ to phase stability using the well-known Flory-Huggins expression which reads:

$$\frac{\partial^2 g}{\partial \phi^2} = RT\left[\frac{1}{V_{hex}\phi_{hex}} + \frac{1}{V_{PE}\phi_{PE}} - 2\frac{\chi}{V_{hex}}\right] \tag{3.5}$$

Since for a PE solution V_{PE}, the molar volume of the polymer tends to infinity the second term may be ignored giving:

$$\frac{\partial^2 g}{\partial \phi^2} = \frac{RT}{V_{hex}}\left[\frac{1}{\phi_{hex}} - 2\chi\right] \tag{3.6}$$

where the volume fraction is defined in terms of mass fractions and mass density of pure components as:

$$\phi_{hex}(P) = \frac{\omega_{hex} / \rho_{hex}(P)}{\sum_{i=hex,PE} \omega_i / \rho_i(P)} \tag{3.7}$$

Based on the aforementioned aims we summarize the specific objectives of the present paper as follows which are essentially focused on pressure dependence of polymer solution properties: (I) The effect of pressure on internal pressure by MD (which is not well understood to our knowledge); (II) estimations of interaction parameter as a function of pressure, and lastly (III) phase stability predictions, by characterizing the significant aspect of the phase instability deriving force to shed light on the PIPS mechanism all based on the fully-atomistic model verified in our earlier computational work[22] that focuses on developing a MD computational platform to calculate solubility parameters of PE and hexane.

The organization of this paper is as follows. The methodology section presents the computational method and detailed model description for conducting NPT simulations employed to explore pressure effects. In the results and discussion section, part I evaluates the internal pressure (Equation 3.3) as a function of pressure together with the pressure effect on the ratio $\pi/$CED; part II utilizes the pressure dependence of solubility parameters of the constituents obtained in our previous work[22] to estimate pressure dependence of interaction parameter (Equation 3.2) using scaling law from which the miscibility of PE in hexane is evaluated, and part III characterizes the pressure dependence of the chemical potential contribution to the spinodal instability threshold to reveal the mechanism of PIPS, using interaction parameters predicted in part II. The final section presents the conclusions.

3.3 Model and Simulation Method

The molecular modeling software package GROMACS,[28-31] version 4.5.4 was employed to carry out MD simulations, and the force field OPLS-AA[32] (optimized potentials for liquid simulations all-atom) was adopted which has been shown to be appropriate in simulating liquid hydrocarbon systems. This force field is developed through optimization of non-bonded parameters with respect to experimental density, vaporization energy, and liquid heat capacity. The total system energy, E_{total} of the employed force field is described by the sum of bonded and non-bonded interactions:

$$E_{\text{total}} = E_b + E_\theta + E_\phi + E_{\text{vdW}} + E_{\text{electrostatics}} \quad (3.8)$$

The MM model incorporates the intramolecular interactions of covalent bond stretching (2-body), E_b, angle bending (3-body), E_θ, and dihedral angle (4-body), E_ϕ, which are based on a fixed list of atoms. The 2-body and 3-body interaction terms are expressed in harmonic form and dihedral angles are governed by cosine series potentials. The intermolecular interactions are described by the last two terms which consist of pairwise additive 12-6 Lennard-Jones, E_{vdW}, and electrostatic, $E_{\text{electrostatics}}$, potential energies. A neighbor list with cut-off distance of 1.35 nm and update frequency of every 10 steps was used for calculating the non-bonded interactions. To alleviate the ill effect of plain cut-offs, non-bonded potentials were treated by a shift function[33] which ensures that the truncated forces are continuous and have continuous derivatives at the group-based cut-off radius of 1.1 nm.

The molecular architecture of PE chains and hexane were built and the geometry was optimized by minimizing the energy of the system. Subsequently PE model systems composed of 60 (PE60) and 120 repeating units (PE120) were packed into a cubic simulation box with the 3-D periodic boundary conditions. This pressure-induced compression using a pressure coupling algorithm was employed to increase the gas density of the system close to the experimental density. In the next step, steepest descent algorithm was utilized to energy minimize the initial molecular structures to bring the system close to the minimum energy.

The initial unfavorable structure was relaxed by performing the canonical ensemble simulations (NVT) at 425 K for PE and hexane. The run time for the NVT-MD simulations is 500 ps where time step is set to 1 fs which ensures that thermodynamic equilibrium is achieved. On the basis of the relaxed models produced by NVT runs, the isobaric-isothermal (NPT) simulations were conducted for 20 ns at external pressures of P = 100, 500, 1000, 2000, and 3000 bar to achieve equilibrium densities. Berendsen barostat[34] with time constant of 1 ps and temperature coupling using velocity rescaling[35] with a relaxation constant of 0.1 was applied throughout the simulations to maintain the system pressure and temperature at the target values. The equations of motion were solved using a leap-frog

integration step and the coordinates and energy values were stored at every 100 steps for the confirmation of the equilibration and analysis. The total energy, pressure, and density were monitored to ensure equilibration of the system and ultimately, the last 1 ns of each simulation was analyzed and used to compute the quantities of interest. Since PE is often treated as non-polar system,[36-37] the effect of pressure on interaction parameter has been investigated for two force field models: PE60 model which incorporates E_{vdW} and $E_{\text{electrostatics}}$, and PE120-0c model where atomic partial charges are set to zero. The notation PE120-0c indicates a model system with PE chains having 120 units simulated using a molecular mechanics model which excludes the electrostatics energy term. The interaction parameter χ for the zero charge model (notation 0c) was evaluated using solubility parameters of PE and hexane based on the force field which excludes $E_{\text{electrostatics}}$.

3.4 Results and Discussion

3.4.1 Internal Pressure

MD simulations in isobaric-isothermal (NPT) thermodynamic ensemble were conducted to compute pressure dependence of internal pressure π. This requires computation of the pressure dependence of internal energy and molar volume obtained from the simulations as discussed below. Figure 3.1 demonstrates the pressure and temperature fluctuations versus simulation time (ps) for the PE60 model where the target values are 500 bar and 425 K. Figure 3.2 illustrates the time evolution of density profiles for PE and hexane where density reaches an equilibrium value and fluctuates about an average value. Subsequently, the molar volume of the condensed phase was computed from densities predicted by NPT runs.

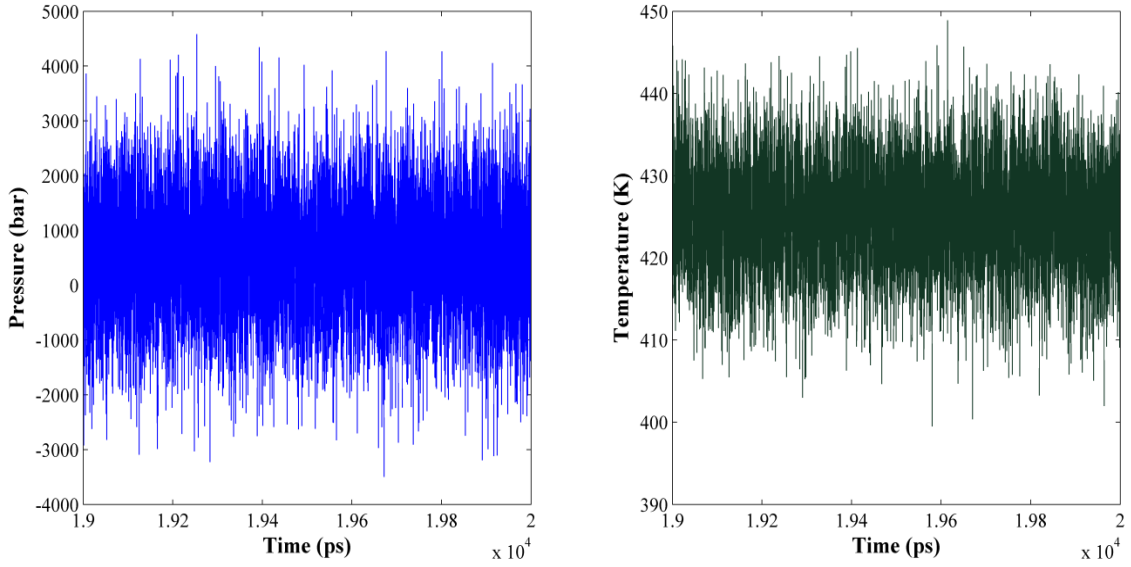

Figure 3.1. Pressure and temperature fluctuations around target values of 500 bar and 425 K for PE chains composed of 60 monomer units (PE60).

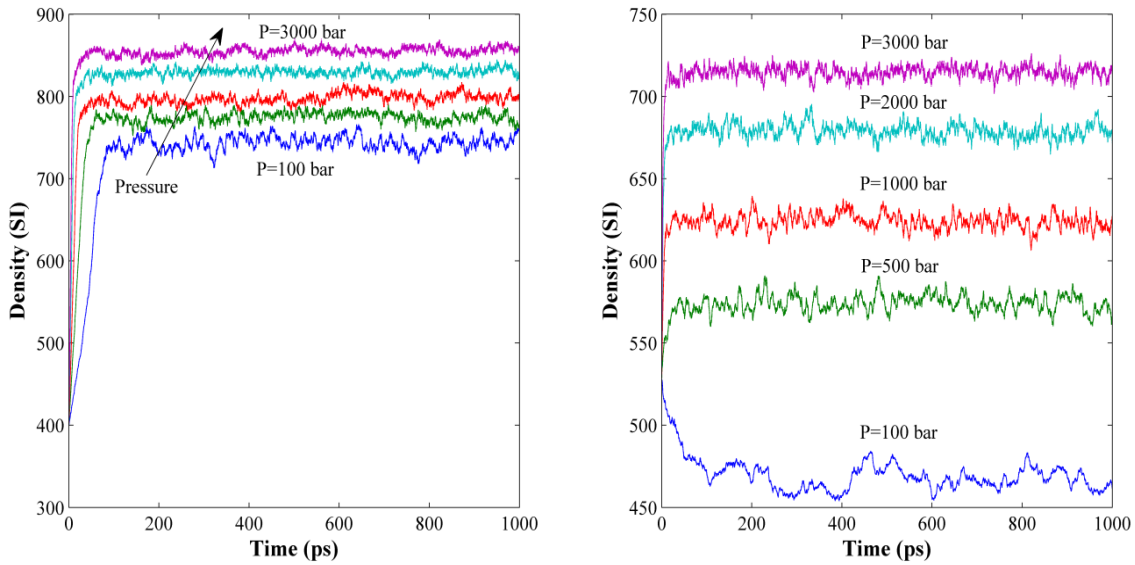

Figure 3.2. Time evolution of densities for PE composed of 60 repeating units (left) and hexane (right) obtained by NPT-MD simulations at different external pressures of 100, 500, 1000, 2000, and 3000 bar.

As has been depicted in Figure 3.3-Figure 3.6, the internal energy U and molar volume V decrease upon increasing external pressure P causing the CEDs to increase.

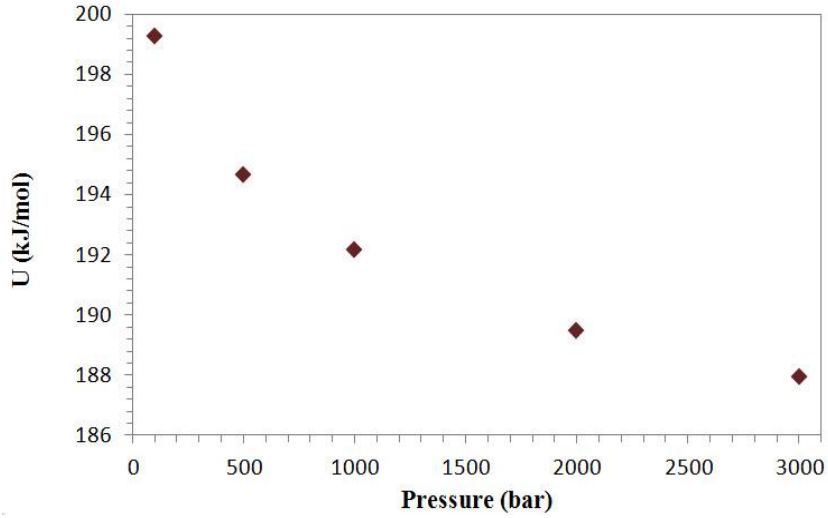

Figure 3.3. Pressure dependence of internal energy for hexane at 425 K.

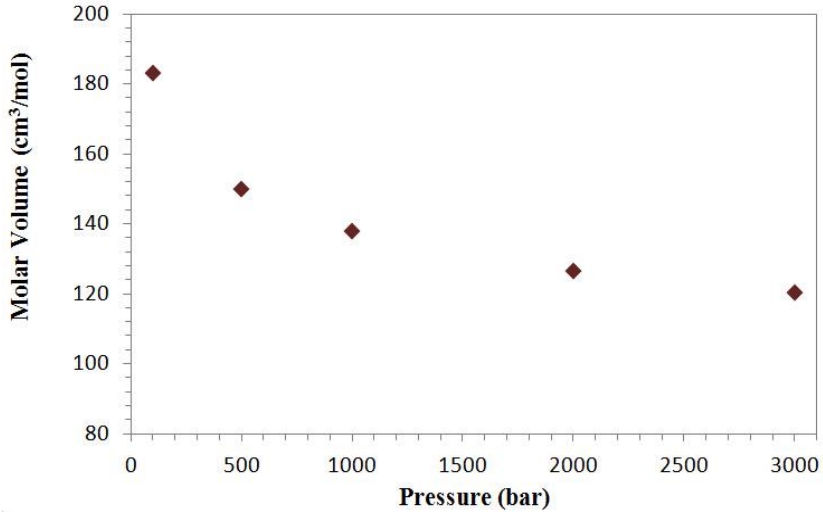

Figure 3.4. Pressure dependence of molar volume for hexane at 425 K.

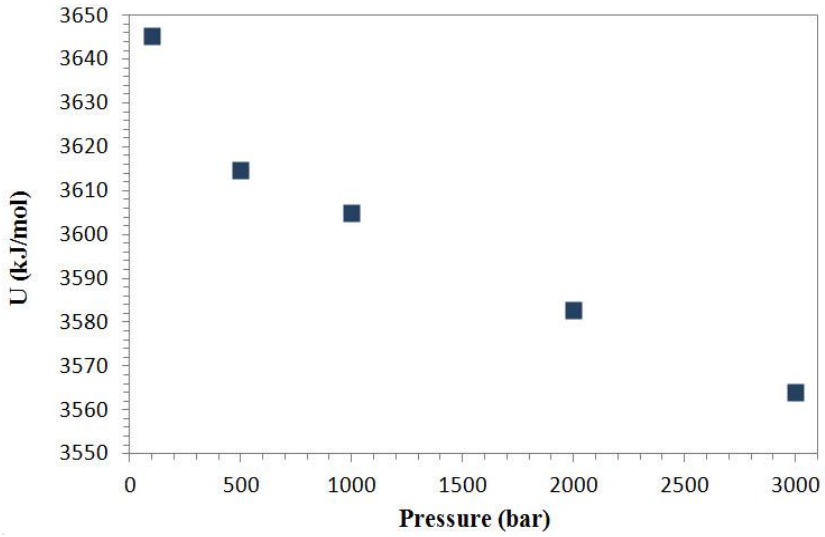

Figure 3.5. Pressure dependence of internal energy for PE60 at 425 K.

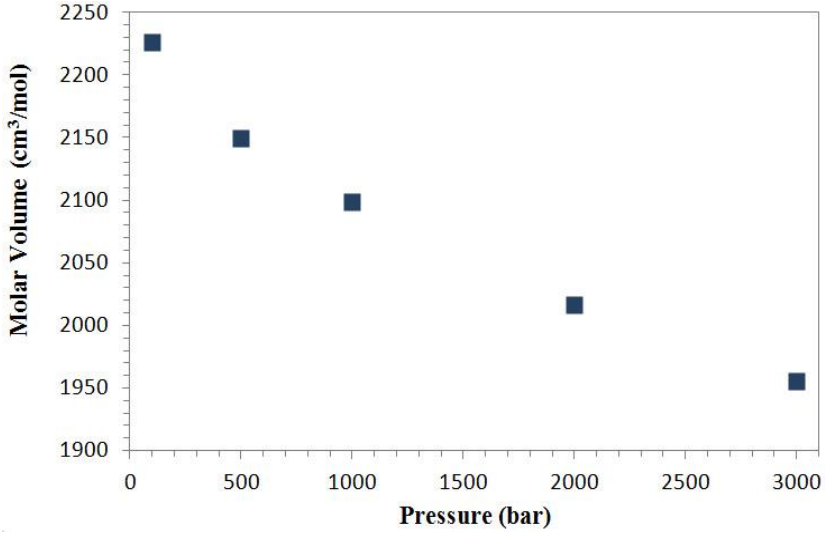

Figure 3.6. Pressure dependence of molar volume for PE60 at 425 K.

The computation of internal pressure based on Equation 3.3 requires the partial derivative of internal energy with respect to molar volume $\pi = \left(\frac{\partial U}{\partial V} \right)_T$ deriving the need to establish a connection between these two quantities. This relationship is established in Figure 3.7 and Figure 3.8 for hexane and PE where the internal energy has been fitted by a second order polynomial in molar volume. The plots show that, the fitted curves superpose

perfectly on the simulated data. Subsequently, on the basis of the polynomial fit, the first derivative of the internal energy with respect to molar volume $\pi = \left(\frac{\partial U}{\partial V}\right)_T$ at different external pressures was estimated (see Table 3.1) and compared with published data (see "Validation" rows). Since we were not able to find internal pressure values for PE60 (120 backbone carbons) at 425 K and high pressures (100-3000 bar) the simulation results were compared with data available in the literature. Internal pressure π of hexane was compared with Monte Carlo simulations[38] at 303.15 K and P = 1, 2000 bar while the PE results were compared with the reported simulation (NVT-MD) data[39] at 423.15 K and 1 bar for a PE chain with 30 carbons. The observed departure may be justified due to different PE chain length, high pressure effect, and the fact that our molecular mechanical model incorporates electrostatics and bond energy terms as well. Also experimental[40] internal pressure for PE at 440.15 K (167 ^{o}C) was used to compare results. For all pressures the simulated internal pressures are greater than CED values[22] (CED = 169, 189, 198, 217, and 234 MPa for P = 100, 500, 1000, 2000, and 3000 bar, respectively). A similar behavior was previously observed for various polymers at ambient pressure.[39]

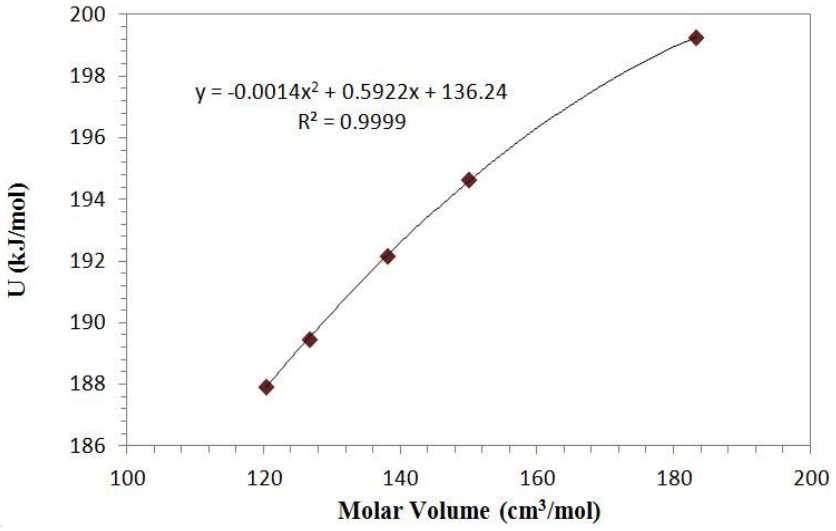

Figure 3.7. Internal energy as a function of molar volume for hexane at 425 K.

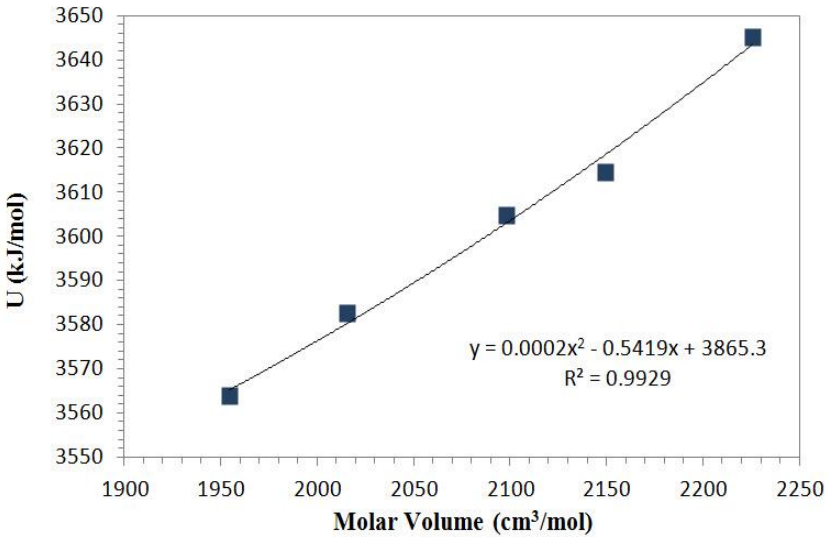

Figure 3.8. Internal energy as a function of molar volume for PE60 at 425 K.

Table 3.1. Internal pressures obtained by NPT-MD simulations at 425 K.

Model System	Internal Pressure (π) & CED (MPa)				
	100 (bar)	500 (bar)	1000 (bar)	2000 (bar)	3000 (bar)
PE60	343	312	292	259	235
Validation	Simulation:[39] 274 (423.15 K/1 bar); Experiment:[40] 312 (440.15 K)				
CED	169	189	198	217	234
π /CED	2	1.65	1.47	1.19	1
Hexane	79	172	205	237	255
Validation	Simulation:[38] 210, 260 (303.15 K/1, 2000 bar, respectively)				
CED	95	147	178	215	239
π /CED	0.83	1.17	1.16	1.11	1.07

Although both CED and π are used to characterize intermolecular interactions in liquids, CED is a measure of the total molecular cohesion per unit volume of the material, while π describes how internal energy changes upon infinitesimal isothermal changes in volume. Since for polymers the direct estimation of ΔH_{vap} is impossible, CED may be approximated by internal pressure which is experimentally obtainable through *PVT* measurements.[40-42] This approximation has been shown to be accurate for non-polar monomeric liquids interacting through dispersive forces, and in this study we find that over a wide range of pressures $CED = \pi$ for hexane. On the other hand, as may be seen in Table 3.1, for the polymer CED is not equal to internal pressure, however, at high pressures a significantly lower ratio for π/CED is predicted, to the extent that at 3000 bar $CED = \pi$.

3.4.2 Binary Interaction Parameter

Using the knowledge of solubility parameters of the polymer and solvent as a function of pressure, the pressure dependence of FH interaction parameter, χ has been computed for two molecular weight of PE based on Equation 3.2. The computed Hildebrand solubility parameters of PE and hexane predicted in our previous work[22] were utilized where PE simulation data are compared with the corresponding-states theoretical data[43] to confirm the validity of the model. The δ values increase with increasing pressure for both polymer and hexane indicating that at higher pressures more energy is required to move the molecules to an infinite distance. This behavior may be justified from the definition of cohesive energy.

The miscibility of PE in the solvent has been predicted by characterizing the pressure dependence of cohesive energy and densities which are in turn affected by the pressure dependence of non-bonded interaction energies. As shown in Figure 3.9 the computed binary interaction parameters decrease upon increasing pressure indicating that the miscibility of the PE/hexane system may be improved by raising the pressure. The best fitted curves in a form of power equation are plotted for PE60 and PE120-0c zero charge model (where E_{vdW} is the only non-bonded interaction) representing the pressure dependence of the interaction parameter. For PE120-0c polymer model interaction parameter is estimated to be $\chi\left(P,\text{PE120-0c}\right)=\frac{205}{P}$ while for PE60 we find $\chi\left(P,\text{PE60}\right)=\frac{33483}{P^{2.2}}$, where the higher power law exponent is the result of the electrostatic interaction which were excluded in the former P120-0c model but included in PE60. We have previously[22] demonstrated that the cohesive energies are not influenced for such a range of chain lengths (PE60/PE120), which implies that the observed change in the resulting interaction parameters is essentially due to $E_{\text{electrostatics}}$. As may be seen, exclusion of $E_{\text{electrostatics}}$ shifts up the interaction parameters with no impact on the monotonically decreasing trend upon increase in external pressure. This shift of the curve is attributed to two main contributions. Firstly, increase in cohesive energy of the PE120-0c compared to PE60 occurs, since exclusion of the electrostatic repulsion (in PE120-0c model) leads to higher net non-bonded energies which play a key role in calculating cohesive properties.

Secondly, for the polymer, models that ignore electrostatic terms predict higher density values which is attributed to the lack of repulsive electrostatic interactions. Owing to the aforementioned contributions, neglecting electrostatic forces is conducive to larger solubility parameters for the polymer while not significantly affecting the density nor the cohesive energy of hexane. This consequently gives rise to a greater difference in solubility parameters of polymer and solvent and subsequently, leads to higher interaction parameters.

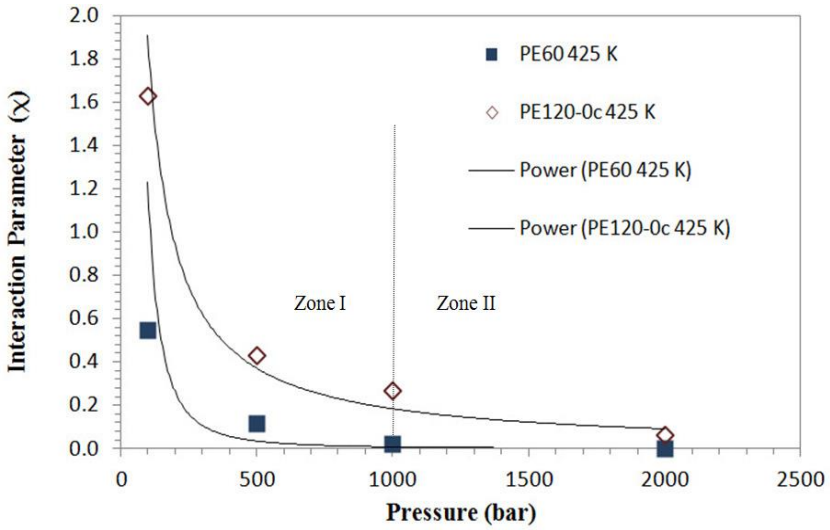

Figure 3.9. Binary interaction parameter as a function of pressure for PE/hexane system at 425 K.

The predicted pressure dependence of $\chi(P)$ for PE in hexane is consistent with the observed PIPS predictions where the pressure quench method is used to phase separate the homogeneous PE solutions into polymer-rich and polymer-lean phases.[1, 14-17] As may be seen in the adapted[14] Figure 3.10, computed using the Sanchez-Lacombe equation of state for the system PE and hexane, pressure quench denoted by the downward arrow brings the one-phase polymer solution into the unstable spinodal region, conducive to phase separation. The increase in PE solubility in hexane as a result of raising the pressure has also been reported for PE in alkane solvents i.e. pentane, butane, propane, and ethane based on the Prigogine-Flory expression[7] for the interaction parameter where the free volume difference of polymer and solvent decreases at high pressures. PE chains with 120

monomers (240 backbone carbons) show higher interaction parameters especially for *P* below 1000 bar which is due to larger CED compared to PE60 model due to eliminating the repulsive electrostatic interactions. It is noteworthy that two zones may be identified from the plot of the interaction parameter as a function of pressure: the zone corresponding to pressures below 1000 bar in which χ displays a large pressure dependence and the other for pressures above 1000 bar where the binary interaction parameter demonstrates weak sensitivity to pressure changes.

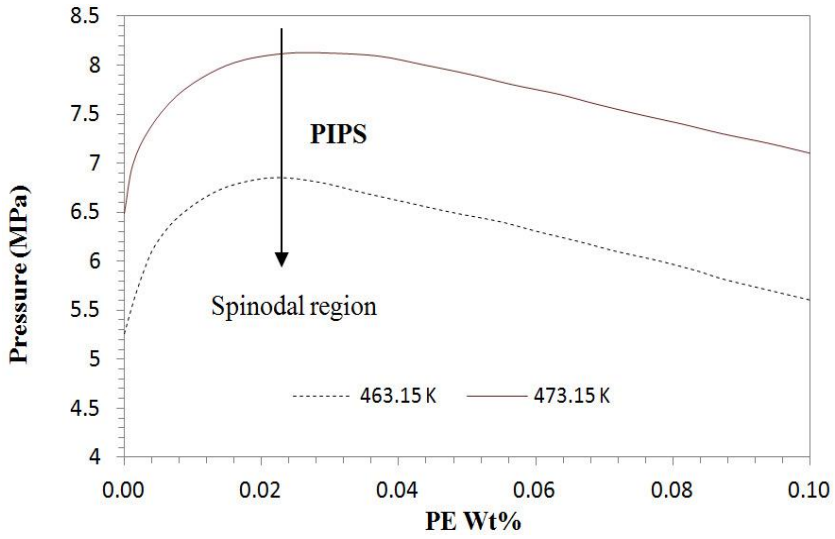

Figure 3.10. Pressure versus composition phase diagram for the system PE (*M*w = 108000) + hexane at 473.15 and 463.15 K. Spinodal curves predicted by the Sanchez-Lacombe EOS (adapted[14]).

It is widely recognized that PE solutions in hydrocarbons exhibit LCST fluid phase behavior. This type of phase behavior may be described by introducing an empirical temperature, concentration,[44-47] and pressure[48] dependence of interaction parameter. LCST is a consequence of dissimilarity in compressibility (density) between polymer and the solvent which induces a negative volume of mixing as a result of raising the temperature.[49] In the same fashion, reduction in pressure reduces drastically the density of solvent and hence free volume effects become more apparent.[47] Although, no free volume effect has been incorporated in the employed χ definition which is expressed in terms of cohesive

energies, the slope of the plot of χ versus pressure, $\frac{d\chi}{dP}$ in Figure 3.9 predicts the negative contribution in the volume of mixing over the entire range of pressure. It may be deduced from the high sensitivity of the interaction parameter in zone I that volume change on mixing is more pronounced at lower pressures than at higher pressures, which implies compressibility effects are more significant in zone I.

3.4.3 Phase Stability

To predict the derivative of the chemical potential with respect to concentration $\frac{\partial^2 g}{\partial \phi^2}$ as a function of pressure at 425 K, the pressure dependence of molar volume $V_{hex}(P)$, the volume fraction $\phi_{hex}(P)$ of hexane together with $\chi(P)$ were extracted from NPT-MD simulations at 425 K and pressures up to 2000 bar. Figure 3.11 illustrates the $\frac{\partial^2 g}{\partial \phi^2}(P)$ for PE60 and PE120 and polymer solutions of weight percent ω_{PE} = 5, 10, 20, and 30%. The figure shows that the chemical potential factor $\frac{\partial^2 g}{\partial \phi^2}$ increases with pressure for all concentrations and molecular weight models. This increase of the chemical potential factor as a result of raising the pressure indicates that this term tends to increase the stability of the polymer-solvent system at higher pressures, predicted by the phase diagram shown in Figure 3.10. Moreover, it can be seen that $\frac{\partial^2 g}{\partial \phi^2}$ is more sensitive to pressure and molecular weight of PE for pressures below 1000 bar and further increase in pressure has no significant impact on the incompressible contribution to phase stability criterion. As has been revealed the more realistic molecular mechanics model, which incorporates electrostatic forces, predicts more accurately the PE/hexane miscibility due to larger (and positive) chemical potential factor particularly at lower pressures (around 100 bar) where the mixture is expected to remain homogeneous at the investigated temperature, as predicted by the phase diagrams.[50]

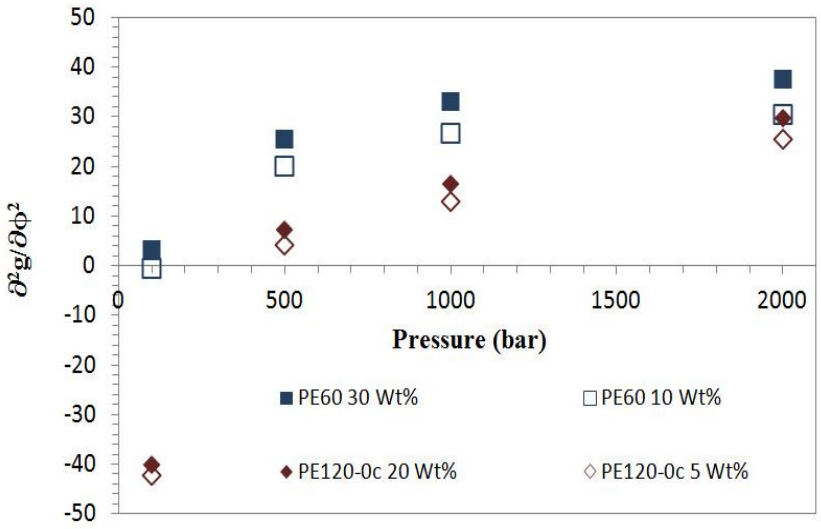

Figure 3.11. Second derivative of Gibbs free energy as a function of pressure for PE solutions of 5%, 10%, 20%, and 30% polymer weight fractions (PE chains consist of 60 and 120 monomer units).

3.5 Conclusions

MD simulations in isobaric-isothermal (NPT) thermodynamics ensemble using accurate OPLS-AA force field were conducted to compute the internal pressure of HDPE and hexane over a broad range of pressures up to 3000 bar. It has been shown that for non-polar monomeric liquids as hexane CED may be approximated by internal pressure. Also it can be concluded that for polymer CED is not identical to the internal pressure and for all pressures the internal pressure is larger than CED. However, the results imply that the ratio of π/CED for PE approaches unity with increasing pressure (Table 3.1). The computed binary interaction parameters were predicted to decrease upon increasing the pressure (Figure 3.9) indicating that the miscibility of the PE/hexane system may be improved by raising the pressure, in agreement with theoretical and experimental data (Figure 3.10). It has been postulated that the role of pressure is to increase the CED which in turn is influenced by changes in the non-bonded interaction energies and the system density. This finding assists to build a molecular level understanding of the pressure effect upon the interaction parameter. The increase in PE miscibility at high pressures is consistent with PIPS predictions where the pressure quench method is used to separate the PE from the homogeneous PE solution and also in qualitative agreement with PE solubility estimations

in alkane solvents made via free volume theory. Exclusion of electrostatics potentials in the molecular mechanics model shifts up the interaction parameters while the monotonically decreasing trend is observed for both molecular mechanics models with and without electrostatic forces (Figure 3.9). As far as the pressure dependence of the interaction parameter is concerned, it was shown that there is a pressure limit beyond which the binary interaction parameter displays less sensitivity to changes in pressure. This implies that PE miscibility is not influenced by changes in the system's pressure. In addition, it may be concluded that the solubility parameter theory is capable of semi-quantitatively predicting miscibility of PE in hydrocarbon solutions at high temperature and over a wide range of pressures.

The negative contribution of volume change on mixing is predicted from plot of χ versus pressure where the change in volume upon mixing decays with increasing pressure. Moreover, the upper bound for phase stability criteria (Equation 3.4) has been estimated and it was shown that the increase in the system's pressure increases the incompressible contribution to the phase stability condition (Equation 3.6) indicating that this term tends to increase the stability of the polymer-solvent system at higher pressures (Figure 3.10 and Figure 3.11). However, this increasing trend reaches a plateau for pressures beyond 1000 bar. Moreover, the force field model incorporating electrostatic energy contributions predicts more accurately the PE in hexane miscibility by predicting a larger chemical potential factor particularly at lower pressures. It is worth noting that even though the lattice-based thermodynamic formalism presented here can not accurately predict the experimental phase diagrams due to incorporating only the interactional energies, neglect of free volume dissimilarities, and limitations of the FH theory, the presented results reinforce that the PIPS mechanism can still be predicted in the framework of solubility parameter approach.

Our current direct numerical MD approach based on a well-established force field provides the basis to semi-quantitatively characterize the miscibility predictions of polymer solution which is consistent with PIPS and is a good complement for experimental and EOS methods. A similar approach can be undertaken to predict the LCST via MD simulations using the canonical ensemble (NVT) to explore the temperature dependence of cohesive energies and subsequently that of the interaction parameter. Ultimately, MD has

been found to be a promising alternative to predict miscibility-related thermodynamic properties of polyolefins and hydrocarbon solvents at conditions of technological interest for industrial polyolefin synthesis and processing which involves costly and time consuming experimental work.

3.6 Acknowledgements

This work is supported by a grant from the Natural Sciences and Engineering Research Council of Canada. Moeed Shahamat gratefully acknowledges scholarship support from McGill University.

3.7 References

1. Trumpi, H.; de Loos, T. W.; Krenz, R. A.; Heidemann, R. A., High pressure phase equilibria in the system linear low density polyethylene + ethylene: Experimental results and modelling. *Journal of Supercritical Fluids* **2003,** *27* (2), 205-214.
2. Lin, C. C.; Jeon, H. S.; Balsara, N. P.; Hammouda, B., Spinodal decomposition in multicomponent polymer blends. *Journal of Chemical Physics* **1995,** *103* (5), 1957-1971.
3. Chan, P. K.; Rey, A. D., Polymerization-induced phase separation. 1. Droplet size selection mechanism. *Macromolecules* **1996,** *29* (27), 8934-8941.
4. Graham, P. D.; Pervan, A. J.; McHugh, A. J., The dynamics of thermal-induced phase separation in PMMA solutions. *Macromolecules* **1997,** *30* (6), 1651-1655.
5. Barton, B. F.; Graham, P. D.; McHugh, A. J., Dynamics of spinodal decomposition in polymer solutions near a glass transition. *Macromolecules* **1998,** *31* (5), 1672-1679.
6. Rappl, T. J.; Balsara, N. P., Does coarsening begin during the initial stages of spinodal decomposition? *Journal of Chemical Physics* **2005,** *122* (21).
7. Patterson, D., Free volume and polymer solubility. A qualitative view. *Macromolecules* **1969,** *2* (6), 672-677.
8. Patterson, D.; Robard, A., Thermodynamics of polymer compatibility. *Macromolecules* **1978,** *11* (4), 690-695.
9. Wolf, B. A.; Blaum, G., Pressure influence on true cosolvency. Measured and calculated solubility limits of polystyrene in mixtures of acetone and diethyl ether. *Makromolekulare Chemie-Macromolecular Chemistry and Physics* **1976,** *177* (4), 1073-1088.
10. Blaum, G.; Wolf, B. A., The generation of true cosolvency by pressure. Solubility limits of high molecular weight polystyrene in mixtures of acetone and diethyl ether. *Macromolecules* **1976,** *9* (4), 579-582.
11. Wolf, B. A.; Geerissen, H., Pressure dependence of the demixing of polymer solutions determined by viscometry. *Colloid and Polymer Science* **1981,** *259* (12), 1214-1220.
12. Kennis, H. A. J.; de Loos, T. W.; de Swaan Arons, J.; Vanderhaegen, R.; Kleintjens, L. A., The influence of nitrogen on the liquid-liquid phase behaviour of the system n-

hexane-polyethylene: Experimental results and predictions with the mean-field lattice-gas model. *Chemical Engineering Science* **1990,** *45* (7), 1875-1884.
13. de Loos, T. W.; de Graaf, L. J.; de Swaan Arons, J., Liquid-liquid phase separation in linear low density polyethylene-solvent systems. *Fluid Phase Equilibria* **1996,** *117* (1-2), 40-47.
14. Chen, X. N.; Yasuda, K.; Sato, Y.; Takishima, S.; Masuoka, H., Measurement and correlation of phase equilibria of ethylene + n-hexane + metallocene polyethylene at temperatures between 373 and 473 K and at pressures up to 20 MPa. *Fluid Phase Equilibria* **2004,** *215* (1), 105-115.
15. Krenz, R. A. Correlating the fluid phase behaviour of polydisperse polyethylene solutions using the Modified Sanchez-Lacombe equation of state. Ph.D. Thesis, University of Calgary, Calgary, 2005.
16. Nagy, I.; de Loos, T. W.; Krenz, R. A.; Heidemann, R. A., High pressure phase equilibria in the systems linear low density polyethylene + n-hexane and linear low density polyethylene + n-hexane + ethylene: Experimental results and modelling with the Sanchez-Lacombe equation of state. *Journal of Supercritical Fluids* **2006,** *37* (1), 115-124.
17. Haruki, M.; Takakura, Y.; Sugiura, H.; Kihara, S.; Takishima, S., Phase behavior for the supercritical ethylene + hexane + polyethylene systems. *Journal of Supercritical Fluids* **2008,** *44* (3), 284-293.
18. An, L. J.; Horst, R.; Wolf, B. A., Pressure dependence of the miscibility of poly(vinyl methyl ether) and polystyrene: Theoretical representation. *Journal of Chemical Physics* **1997,** *107* (7), 2597-2602.
19. An, L. J.; Wolf, B. A., Combined effects of pressure and shear on the phase separation of polymer solutions. *Macromolecules* **1998,** *31* (14), 4621-4625.
20. Koningsveld, R.; Stockmayer, W. H.; Nies, E., *Polymer phase diagrams: A textbook*. Oxford University Press: Oxford; New York, 2001.
21. Rabeony, M.; Lohse, D. J.; Garner, R. T.; Han, S. J.; Graessley, W. W.; Migler, K. B., Effect of pressure on polymer blend miscibility: A temperature-pressure superposition. *Macromolecules* **1998,** *31* (19), 6511-6514.
22. Shahamat, M.; Rey, A. D., Characterization of pressure effects on the cohesive properties and structure of hexane and polyethylene using molecular dynamics simulations. *Macromolecular Theory and Simulations* **2012,** *21* (8), 535-543.
23. Blanks, R. F.; Prausnitz, J. M., Thermodynamics of polymer solubility in polar and nonpolar systems. *Industrial and Engineering Chemistry Fundamentals* **1964,** *3* (1), 1-8.
24. Graessley, W. W., *Polymeric liquids and networks: Structure and properties*. Garland Science: New York, 2004.
25. Bicerano, J., *Prediction of polymer properties*. Marcel Dekker: New York, 2002.
26. Bristow, G. M.; Watson, W. F., Cohesive energy densities of polymers. 1. Cohesive energy densities of rubbers by swelling measurements. *Transactions of the Faraday Society* **1958,** *54* (11), 1731-1741.
27. Sanchez, I. C., Volume fluctuation thermodynamics of polymer solutions. *Macromolecules* **1991,** *24* (4), 908-916.
28. Berendsen, H. J. C.; van der Spoel, D.; van Drunen, R., Gromacs: A message-passing parallel molecular dynamics implementation. *Computer Physics Communications* **1995,** *91* (1-3), 43-56.

29. Lindahl, E.; Hess, B.; van der Spoel, D., GROMACS 3.0: A package for molecular simulation and trajectory analysis. *Journal of Molecular Modeling* **2001,** *7* (8), 306-317.
30. van der Spoel, D.; Lindahl, E.; Hess, B.; Groenhof, G.; Mark, A. E.; Berendsen, H. J. C., GROMACS: Fast, flexible, and free. *Journal of Computational Chemistry* **2005,** *26* (16), 1701-1718.
31. Hess, B.; Kutzner, C.; van der Spoel, D.; Lindahl, E., GROMACS 4: Algorithms for highly efficient, load-balanced, and scalable molecular simulation. *Journal of Chemical Theory and Computation* **2008,** *4* (3), 435-447.
32. Jorgensen, W. L.; Madura, J. D.; Swenson, C. J., Optimized intermolecular potential functions for liquid hydrocarbons. *Journal of the American Chemical Society* **1984,** *106* (22), 6638-6646.
33. van der Spoel, D.; van Maaren, P. J., The origin of layer structure artifacts in simulations of liquid water. *Journal of Chemical Theory and Computation* **2006,** *2* (1), 1-11.
34. Berendsen, H. J. C.; Postma, J. P. M.; van Gunsteren, W. F.; Dinola, A.; Haak, J. R., Molecular dynamics with coupling to an external bath. *Journal of Chemical Physics* **1984,** *81* (8), 3684-3690.
35. Bussi, G.; Donadio, D.; Parrinello, M., Canonical sampling through velocity rescaling. *Journal of Chemical Physics* **2007,** *126* (1), 014101.
36. Jo, W. H.; Choi, K., Determination of equation-of-state parameters by molecular simulations and application to the prediction of surface properties for polyethylene. *Macromolecules* **1997,** *30* (6), 1800-1805.
37. Choi, P., Molecular dynamics studies of the thermodynamics of HDPE/butene-based LLDPE blends. *Polymer* **2000,** *41* (24), 8741-8747.
38. Rai, N.; Siepmann, J. I.; Schultz, N. E.; Ross, R. B., Pressure dependence of the Hildebrand solubility parameter and the internal pressure: Monte Carlo simulations for external pressures up to 300 MPa. *Journal of Physical Chemistry C* **2007,** *111* (43), 15634-15641.
39. Maranas, J. K.; Mondello, M.; Grest, G. S.; Kumar, S. K.; Debenedetti, P. G.; Graessley, W. W., Liquid structure, thermodynamics, and mixing behavior of saturated hydrocarbon polymers. 1. Cohesive energy density and internal pressure. *Macromolecules* **1998,** *31* (20), 6991-6997.
40. Krishnamoorti, R.; Graessley, W. W.; Dee, G. T.; Walsh, D. J.; Fetters, L. J.; Lohse, D. J., Pure component properties and mixing behavior in polyolefin blends. *Macromolecules* **1996,** *29* (1), 367-376.
41. Allen, G.; Gee, G.; Mangaraj, D.; Sims, D.; Wilson, G. J., Intermolecular forces and chain flexibilities in polymers. 2. Internal pressures of polymers. *Polymer* **1960,** *1* (4), 467-476.
42. Barton, A. F. M., Internal pressure. A fundamental liquid property. *Journal of Chemical Education* **1971,** *48* (3), 156-162.
43. Maloney, D. P.; Prausnitz, J. M., Thermodynamic properties of liquid polyethylene. *Journal of Applied Polymer Science* **1974,** *18* (9), 2703-2710.
44. Qian, C. B.; Mumby, S. J.; Eichinger, B. E., Phase diagrams of binary polymer solutions and blends. *Macromolecules* **1991,** *24* (7), 1655-1661.

45. Solc, K.; Koningsveld, R., Coalescence of upper and lower miscibility gaps in systems with concentration-dependent interactions. *Journal of Physical Chemistry* **1992,** *96* (10), 4056-4068.
46. Bae, Y. C.; Shim, J. J.; Soane, D. S.; Prausnitz, J. M., Representation of vapor-liquid and liquid-liquid equilibria for binary systems containing polymers: Applicability of an extended Flory-Huggins equation. *Journal of Applied Polymer Science* **1993,** *47* (7), 1193-1206.
47. Schnell, M.; Stryuk, S.; Wolf, B. A., Liquid/liquid demixing in the system n-hexane/narrowly distributed linear polyethylene. *Industrial & Engineering Chemistry Research* **2004,** *43* (11), 2852-2859.
48. Vanopstal, L.; Koningsveld, R., Mean-field lattice equations of state. 4. Influence of pressure on the phase behavior of the system polystyrene/cyclohexane. *Polymer* **1992,** *33* (16), 3433-3444.
49. Paricaud, P.; Galindo, A.; Jackson, G., Understanding liquid-liquid immiscibility and LCST behaviour in polymer solutions with a Wertheim TPT1 description. *Molecular Physics* **2003,** *101* (16), 2575-2600.
50. Nies, E.; Stroeks, A.; Simha, R.; Jain, R. K., LCST phase behavior according to the Simha-Somcynsky Theory: Application to the n-hexane polyethylene system. *Colloid and Polymer Science* **1990,** *268* (8), 731-743.

4 Molecular Thermodynamic Characterization of LCST Fluid Phase Behavior and Exploring Electrostatic Algorithms to Compute Polymer/Solvent Solubility Parameters in the Canonical Ensemble

4.1 Summary

The present study aims to characterize the temperature dependence of polyethylene (PE) solubility in hexane at high pressure using an atomistic-level simulation technique, without the need for expensive and time-consuming experimental methods, to gain significant miscibility insights in polymer processes that are present in a wide range of industrial applications. To this end, various molecular dynamics (MD) simulations based upon the OPLS-AA force field are carried out over a range of 425-500 K at 50 and 200 bar to predict the temperature dependence of Hildebrand's solubility parameter of high-density polyethylene (HDPE) and hexane at these high pressures. The NVT simulation results compare quite favorably with the available experimental and theoretical data. The effect of electrostatic potential energy contribution to cohesive energy is also investigated, and it is shown that the solubility parameter decreases with increasing temperature for both molecular mechanical models with and without electrostatic terms. Subsequently, the Flory-Huggins (FH) binary interaction parameter is predicted from the knowledge of temperature dependence of solubility parameters. It is demonstrated that the computed binary interaction parameter increases upon increasing the temperature, indicating that the miscibility of the PE/hexane system decreases by raising the temperature. This conclusion is in agreement with the widely recognized lower critical solution temperature (LCST) fluid phase behavior. Moreover, it is shown that the increase in system temperature decreases the

chemical potential factor of the phase stability condition, indicating that at higher temperatures this effect tends to destabilize the polymer-solvent system. Comparisons of electrostatic forces evaluated based on shift functions and the particle mesh Ewald (PME) methods show slight difference, and it is also found that the grid spacing has no noticeable influence on non-bonded energy terms and total potential, employed in the calculation of cohesive energy, a result that is useful to increase the efficiency of future MD simulations.

4.2 Introduction

A full characterization of the effects of temperature on phase behavior of polymer solution at high pressure is required in order to achieve a fundamental understanding of polymer-solvent miscibility utilized, of relevance to polymer physics and applied polymer processing. However, the thermodynamic and phase behavior predictions in polymer solutions require accurate knowledge of polymer-solvent interactions, which is essential in controlling the phase behavior trends in such systems. In previous work[1] we focused on developing a molecular dynamics (MD) calculation platform under the isobaric-isothermal (NPT) ensemble to compute the effect of pressure on densities, structure (i.e. polymer radius of gyration and pair distribution functions), and cohesive energies of polyethylene (PE) and hexane over a wide range of pressures from 100 up to 3000 bar by quantifying specific contributions of bonded/non-bonded interactions to gain a fundamental understanding of phase behavior in polymer solutions at high pressures. Furthermore, on the basis of the NPT-MD ensemble predictions of internal pressures were performed at elevated pressures and the knowledge of pressure dependence of solubility parameters and molar volumes was further utilized to build a molecular thermodynamic characterization of compressible PE solutions. In this regard, the Flory-Huggins (FH) binary interaction parameter, volume change upon mixing, and the chemical potential factor as functions of pressure were computed to predict miscibility and phase stability and to shed light on the pressure-induced phase separation mechanism in binary solutions of PE in hexane.[2] The present work aims to elucidate the fundamental understanding of the cohesive properties and solubility parameters of PE and hexane as a function of temperature, which provides a rational basis for estimations of miscibility, stability, and lower critical solution

temperature (LCST) fluid phase behavior of PE in hexane solutions, using canonical ensemble that is consistent with the present objectives.

The solubility parameter (δ) is defined as the square root of the cohesive energy density (CED) which corresponds to the increase in the molar energy per unit volume if all intermolecular forces are eliminated, as formulated below:

$$\delta(T) = \sqrt{\text{CED}} = \sqrt{\frac{\Delta U_{\text{vap}}}{V}} \tag{4.1}$$

where T is the temperature, ΔU_{vap} the increase in the internal energy (energy content) per mole as a result of eliminating intermolecular forces and V is the molar volume of the substance at the pressure and temperature at which the vaporization occurs. By definition the energy of vaporization is the energy difference between vapor and liquid states. Subsequently, from the solubility parameters one can determine the miscibility of a polymer in a solvent by estimating the FH interaction parameter χ which is proportional to the enthalpy of mixing:

$$\chi = \frac{V\left(\delta_{\text{solvent}} - \delta_{\text{polymer}}\right)^2}{RT} \tag{4.2}$$

where V is the molar volume of the solvent and RT has the usual meaning. Nevertheless, unlike low molecular weight liquids, the cohesive energy of high molecular weight polymers cannot be conveniently determined experimentally since polymers have a difficult-to-measure vapor pressure due to their low volatility and in some cases they are poorly characterized. Hence, a detailed molecular-level strategy needs to be undertaken to understand the physical interactions and miscibility characteristics of such systems at elevated pressure and temperature, which are inherently difficult to estimate experimentally or for which experimental data are not available.

In this contribution, a molecular modeling investigation is performed to calculate the CED of PE and hexane to address this incomplete molecular-level characterization issues which have relevance to the LCST mechanism, as in the industrial production process of

PE.[3] The simulation methodology includes molecular mechanics (MM) and MD calculations based on the optimized potentials for liquid simulations all-atom (OPLS-AA) force field where the canonical ensemble simulations (NVT) were carried out to characterize $\delta(T)$ of high-density polyethylene (HDPE) and hexane which lays a foundation to understand miscibility in these binary solutions, as discussed below. This investigation requires a detailed insight on the temperature effect upon the individual energy terms contributing to the total system energy. In order to validate the simulation protocols using the OPLS-AA force field, solubility parameters have been compared with the available literature data.

To evaluate the phase stability of polymer solution, the thermodynamic criterion for phase stability has been employed, commonly expressed as:[4]

$$\frac{\partial^2 g}{\partial \phi^2} - v\beta P_\phi^{\,2} > 0 \qquad (4.3)$$

where g is free energy per unit volume, ϕ the volume fraction, v the specific volume, β the isothermal compressibility, and $P_\phi = \left(\frac{\partial P}{\partial \phi}\right)_{T,v}$ the pressure change with composition. The derivative of the chemical potential with respect to concentration $\frac{\partial^2 g}{\partial \phi^2}$ represents the incompressible contribution (chemical potential factor), whereas the second term corresponds to the compressible and unfavorable contribution to phase stability. Hence, as noted in the earlier work,[2] the stability criterion is composed of a chemical $\left(\frac{\partial^2 g}{\partial \phi^2}\right)$ and a mechanical contribution $\left(v\beta P_\phi^{\,2}\right)$, as opposed to incompressible mixtures whose stability is determined only by chemical potential factor. It is important to recognize that since the second term in the above equation is always non-negative the above stability criterion indicates that the compressibility destabilizes the polymer solution promoting phase separation. Lastly, we note that if we neglect the mechanical factor $\left(v\beta P_\phi^{\,2}\right)$, the partial

stability criterium $\left(\frac{\partial^2 g}{\partial \phi^2}\right)$ is a very useful upper-bound to the total stability criterium, given the scarcity of high-pressure measurements and predictions.

In the present paper, we seek to demonstrate the effect of temperature on the chemical potential factor (i.e. incompressible or constant volume contribution) $\frac{\partial^2 g}{\partial \phi^2}$ to phase stability at high pressure using the well-known FH expression which reads:

$$\frac{\partial^2 g}{\partial \phi^2} = RT\left[\frac{1}{V_{hex}\phi_{hex}} + \frac{1}{V_{PE}\phi_{PE}} - 2\frac{\chi}{V_{hex}}\right] \tag{4.4}$$

Since for a PE solution V_{PE}, the molar volume of the polymer tends to infinity the second term may be ignored giving:

$$\frac{\partial^2 g}{\partial \phi^2} = \frac{RT}{V_{hex}}\left[\frac{1}{\phi_{hex}} - 2\chi\right] \tag{4.5}$$

where the volume fraction is defined in terms of mass fractions ω and mass density ρ of pure components as:

$$\phi_{hex} = \frac{\omega_{hex}/\rho_{hex}}{\sum_{i=hex,PE}\omega_i/\rho_i} \tag{4.6}$$

The present paper also reports on a series of MD simulations with the aim to explore the effect of electrostatic schemes of shift functions as well as particle mesh Ewald (PME) on this particular partially charged system. This is necessary to identify the simplest and most accurate computational schemes for these systems due to the fact that with the increasing size of the systems involved, especially for binary mixtures, the calculation of all possible pairwise electrostatic interactions using the Coulomb law would take a substantial amount of the computational time and would make simulations unfeasible. As

computational efficiency is the ratio of accuracy to computational cost, the present investigation provides a guide to more efficient MD calculations for these polymer systems.

The organization of this article is as follows. The methodology section introduces the computational method with a brief description of the force field followed by a detailed model description for NVT simulations employed to explore the temperature effects at 50 and 200 bar. The results and discussion section presents the solubility parameter results where the values are compared with literature data, together with temperature effects on potential energy contributions (part I). Here, we also discuss the temperature dependence of interaction parameter (part II) essential for characterizing the stability condition for PE in solvent system (part III). This section finishes with comparisons of electrostatic schemes of shift functions and PME including studies of mesh sizing (part IV). The final section summarizes the presented findings and provides a number of concluding remarks.

4.3 Model and Simulation Method

The molecular modeling software package GROMACS,[5-8] version 4.5.4 was employed with the force field OPLS-AA,[9] which is appropriate for liquid hydrocarbon systems. The total system energy is represented by the sum of bonded and non-bonded interactions. The covalent bond stretching and valence angle bending are described by harmonic potentials and the twisting of the dihedral angles by periodic functions. The non-bonded van der Waals (vdW) type of interaction is modeled using pairwise additive 12-6 Lennard-Jones and the electrostatic contribution is evaluated based on charge groups to reduce cut-off artifacts of Coulomb interactions. The explicit functional form of the various interaction terms along with the corresponding OPLS-AA parameters is given in our previous work.[1] A neighbor list, used for calculating the non-bonded interactions, was kept to 1.35 nm and updated every 10 steps. Unless stated otherwise, to alleviate the ill effect of plain cut-offs, non-bonded potentials were treated by a shift function[10] (over the region 1-1.1 nm), which ensures that the truncated forces are continuous and have continuous derivatives at the group-based cut-off radius of 1.1 nm.

The PE chains composed of 60 monomer units (PE60; i.e. 120 CH_2/CH_3 units) using all-atom representation were first constructed and then the geometry was optimized by minimizing the energy of the system. Subsequently, 8 polymer chains, instead of a single

chain, were placed in a periodic cubic simulation box to minimize the influence of finite size effect. MD simulations under constant temperature and density (NVT ensemble) were performed for PE60 (1685 g/mol) and hexane model systems containing 2896 and 2500 atoms respectively, based on a leap-frog algorithm for integrating Newton's equations of motion. The dimension of the cubic periodic simulation cells for each molecular model was specified using the experimental/empirical density and the molecular weight of the substance being simulated. Thus, the canonical ensemble ensures that the resulting δ values correspond to the experimental/empirical densities. The validity of the force field was examined by comparing the calculated solubility parameters of PE to experimental data at 1 bar and temperature range of 425-525 K using the PE melt densities, which were taken from an empirical expression[11] describing the PE specific volume as a function of temperature. The densities of PE[12] applied in the simulations at different temperatures and 50 bar were estimated to be 0.787, 0.766, 0.759, and 0.746 (g/cm^3) corresponding to 425, 463, 475, and 500 K, respectively. At 200 bar PE densities of respectively 0.794, 0.772, 0.767, and 0.758 (g/cm^3) were utilized at the above mentioned temperatures. Densities of hexane at 425, 463, 475, and 500 K were 0.542, 0.506, 0.495, and 0.472 (g/cm^3), respectively obtained by extrapolating available data at lower temperatures deduced from ultrasonic measurements[13] at 50 bar. For hexane at 200 bar densities of 0.572, 0.541, 0.531, and 0.511 (g/cm^3) were employed at the aforementioned temperatures, respectively. From the molecular weight of the polymer and the number of chains, the total mass of the system may be calculated and subsequently, with the given densities, the size of the unit cells was determined. Each model system was subjected to energy minimization prior to the equilibration in the canonical ensemble. Equilibration and production runs were carried out in the NVT ensemble at 425-500 K for 10 ns where the time step is set to 1 fs. Temperature coupling using velocity-rescaling[14] was used to control the system temperature at the target values. Coordinates and energy values were stored at every 100 steps for the confirmation of the equilibration and analysis. The equilibration of the simulations was mainly monitored by the time evolution of the total energy and the last 1 ns of the trajectory files was analyzed and used to compute δ values.

4.4 Results and Discussion

4.4.1 Solubility Parameter

The canonical ensemble simulations were employed to investigate the temperature dependence of the heat of vaporization and potential energy contributions at 1, 50, and 200 bar. The total system energy leveled off during the first few nanoseconds, indicating the equilibrium state has been achieved. Figure 4.1 illustrates the total energy fluctuations obtained from the last 1 ns of the MD simulations for PE and hexane at 50 bar and at temperatures of 425, 463, 475, and 500 K, where the system energy increases with increasing temperature.

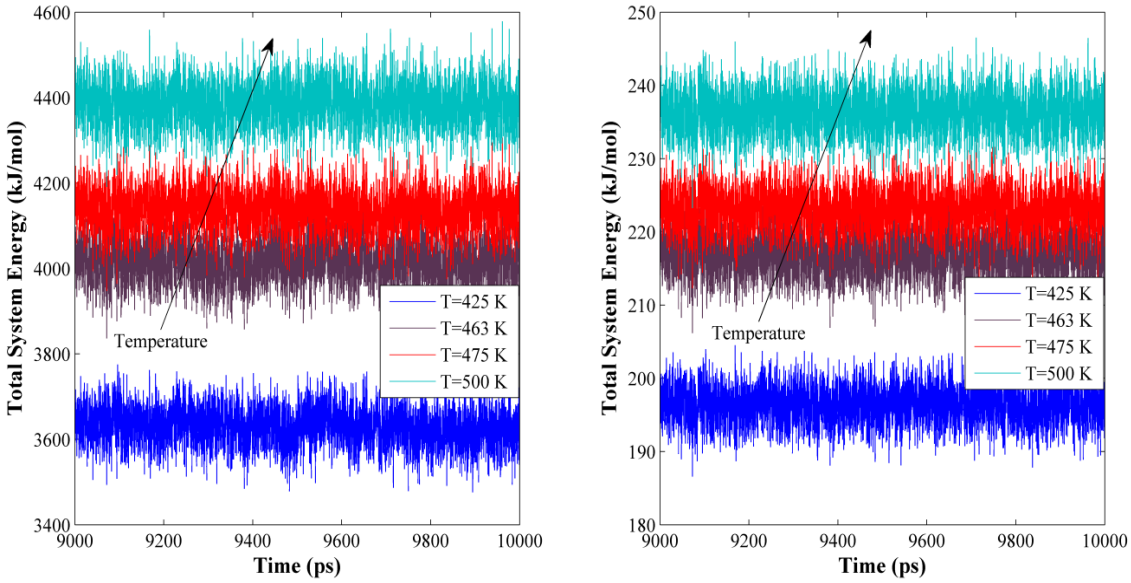

Figure 4.1. Time evolution of total system energy for PE (left) and hexane (right) at different temperatures and at 50 bar.

It is noteworthy that previous work shows that solubility parameters become independent of the degree of polymerization and molecular weight of the polymer above certain number of monomer units on the polymer chain. For instance, it was observed that for poly(carbonate) 21 repeating units were sufficient to perform the simulation.[15] Similar findings were observed for poly(ether imide) and poly(carbonate) with 10 and 23 repeating units, respectively.[16] It may be also noted that the solubility parameters of poly(L-lactide), PLL, and poly(vinyl alcohol), PVA, at certain molecular weights were computed wherein it

was found that the solubility parameters level off when the number of repeating units of PLL and PVA exceeds 10 and 20, respectively.[17] In a similar fashion, our simulations suggest that the solubility parameters of PE composed of 60 and 120 monomers do not vary much and compare quite favorably with experimental data.[1] Based on this validation we believe that the number of monomer units taken into account is sufficient representing a real polymer coil and does not introduce significant inaccuracies in the results.

As may be inferred from the total energy break-down, illustrated in Figure 4.2-Figure 4.9, the difference in total system energies arises from the temperature dependence of the energy components, which increase linearly with increasing temperature. Simulation data are shown at 1, 50, and 200 bar for various potential energy contributions. The total negative non-bonded energies versus temperature predicted by NVT (Figure 4.8 and Figure 4.9) for MM models that include electrostatics suggest that the magnitude of attractive vdW interactions is greater than that of repulsive electrostatics. Further, inclusion of the repulsive electrostatics forces decreases the net non-bonded interactions due to the fact that the vdW energy is negative. The analysis of non-bonded interactions indicates that the repulsive electrostatic energy contributes to between 23 and 30% of total non-bonded energy for PE and hexane, respectively suggesting that in such apolar systems partial electric charges of atoms can still affect the cohesive energy (see Figure 4.10 and Figure 4.11). Therefore, it is believed that although electrostatic forces are computationally expensive, one can achieve a more realistic model by including this interaction term in the MM model.

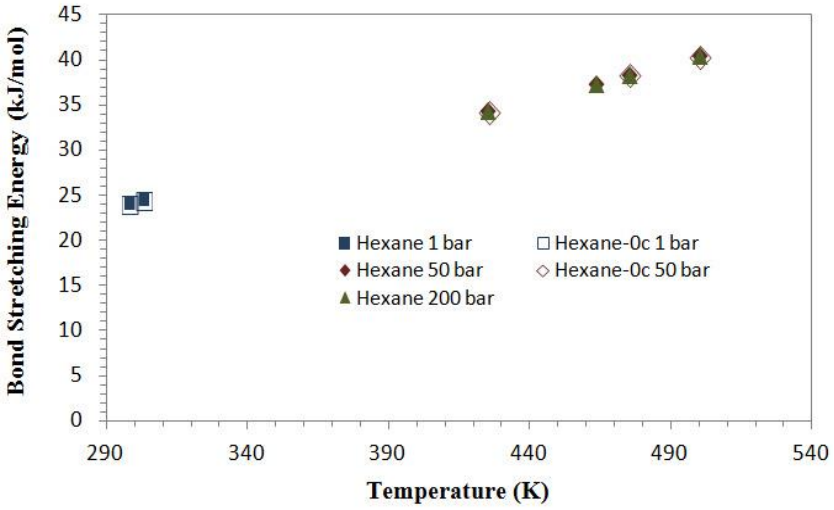

Figure 4.2. Temperature dependence of hexane bond energy. The squares, diamonds, and triangles represent simulation data at 1, 50, and 200 bar, respectively (0c notation indicates MM model with electrostatics switched off).

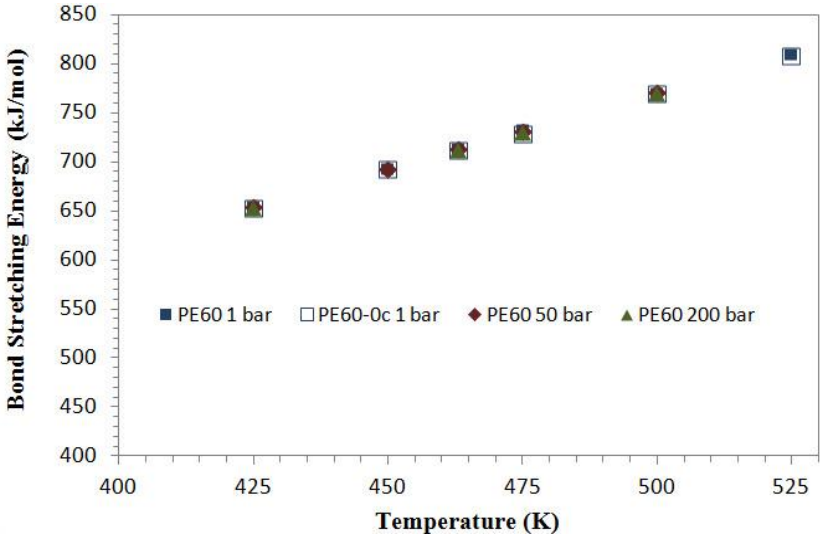

Figure 4.3. Temperature dependence of PE bond energy. The squares, diamonds, and triangles represent simulation data at 1, 50, and 200 bar, respectively (0c notation indicates MM model with electrostatics switched off).

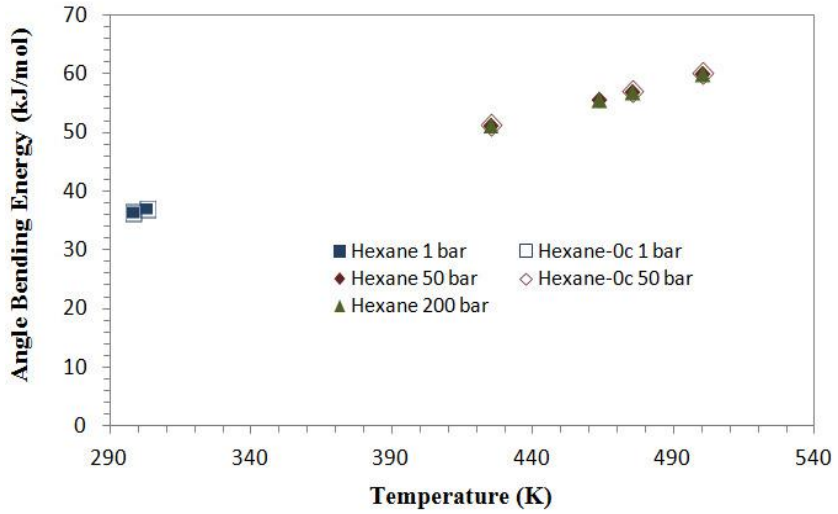

Figure 4.4. Temperature dependence of hexane angle energy. The squares, diamonds, and triangles represent simulation data at 1, 50, and 200 bar, respectively (0c notation indicates MM model with electrostatics switched off).

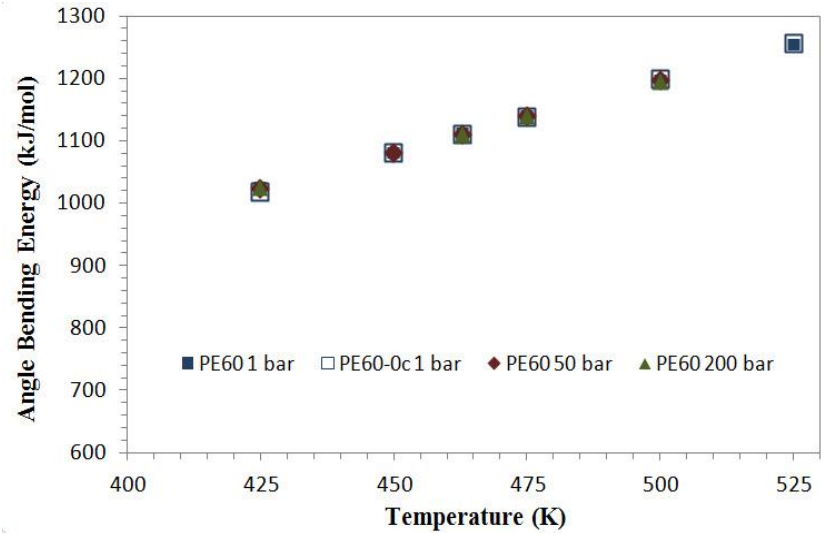

Figure 4.5. Temperature dependence of PE angle energy. The squares, diamonds, and triangles represent simulation data at 1, 50, and 200 bar, respectively (0c notation indicates MM model with electrostatics switched off).

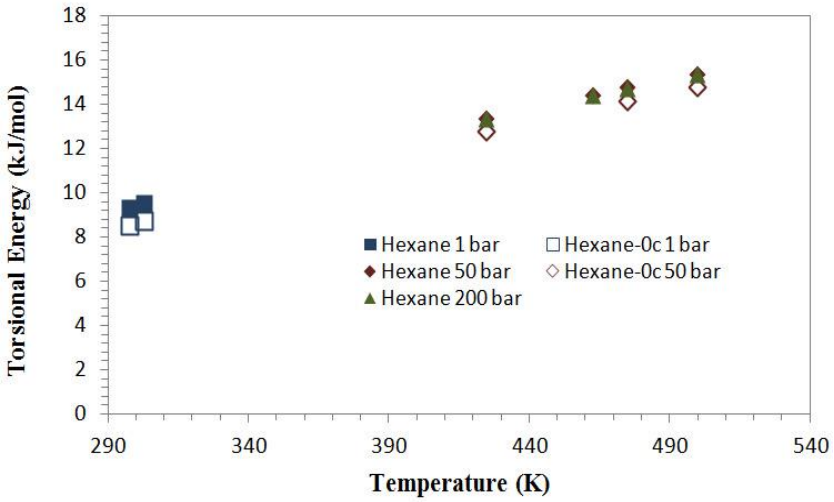

Figure 4.6. Temperature dependence of hexane torsional energy. The squares, diamonds, and triangles represent simulation data at 1, 50, and 200 bar, respectively (0c notation indicates MM model with electrostatics switched off).

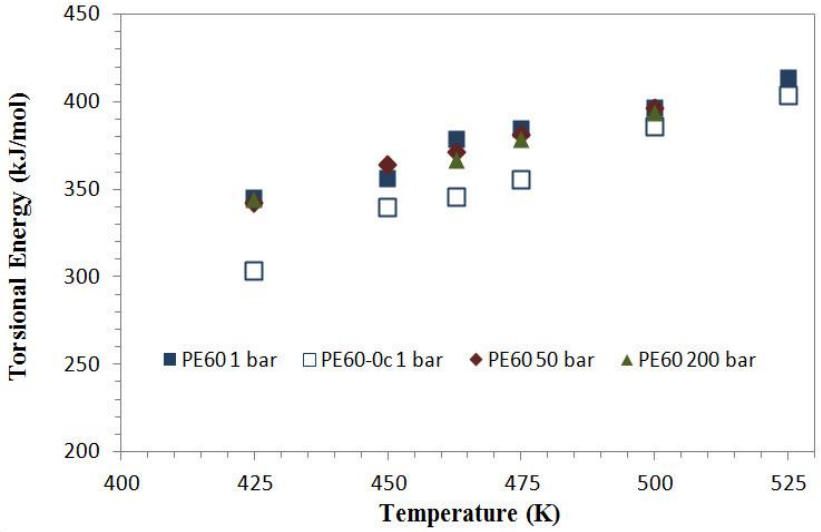

Figure 4.7. Temperature dependence of PE torsional energy. The squares, diamonds, and triangles represent simulation data at 1, 50, and 200 bar, respectively (0c notation indicates MM model with electrostatics switched off).

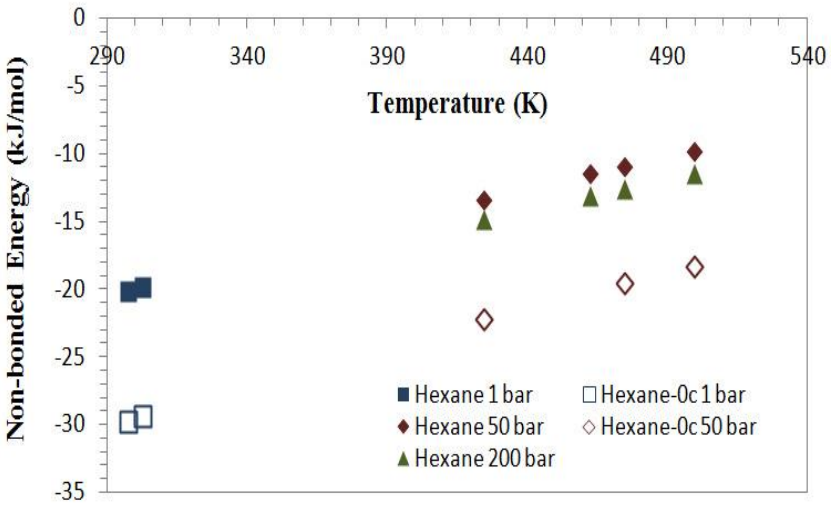

Figure 4.8. Temperature dependence of hexane non-bonded energy. The squares, diamonds, and triangles represent simulation data at 1, 50, and 200 bar, respectively (0c notation indicates MM model with electrostatics switched off).

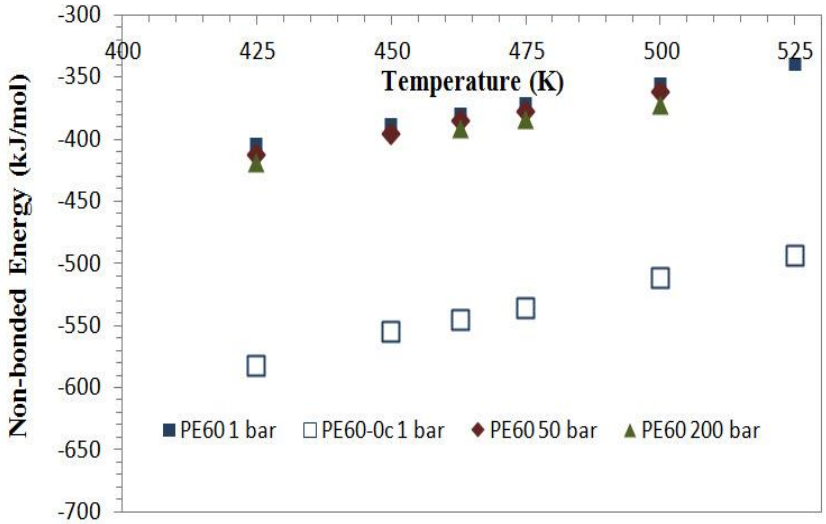

Figure 4.9. Temperature dependence of PE non-bonded energy. The squares, diamonds, and triangles represent simulation data at 1, 50, and 200 bar, respectively (0c notation indicates MM model with electrostatics switched off).

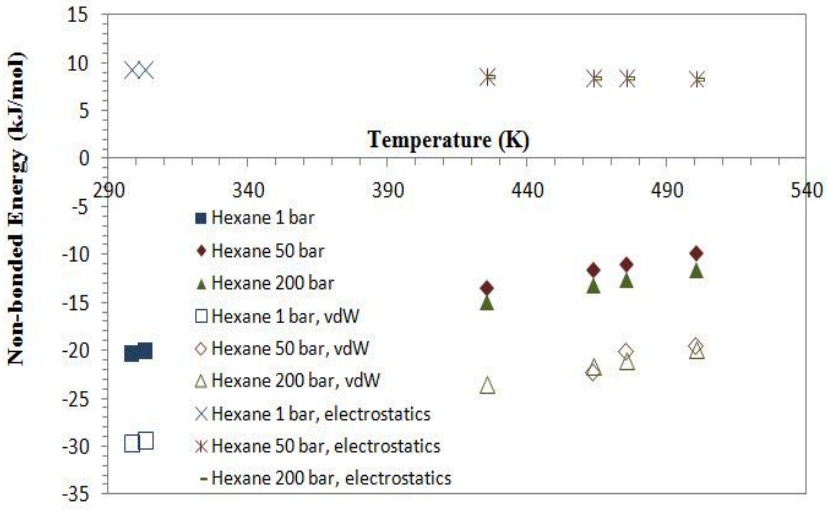

Figure 4.10. Temperature dependence of hexane total non-bonded energy (filled symbols), vdW, and electrostatics components.

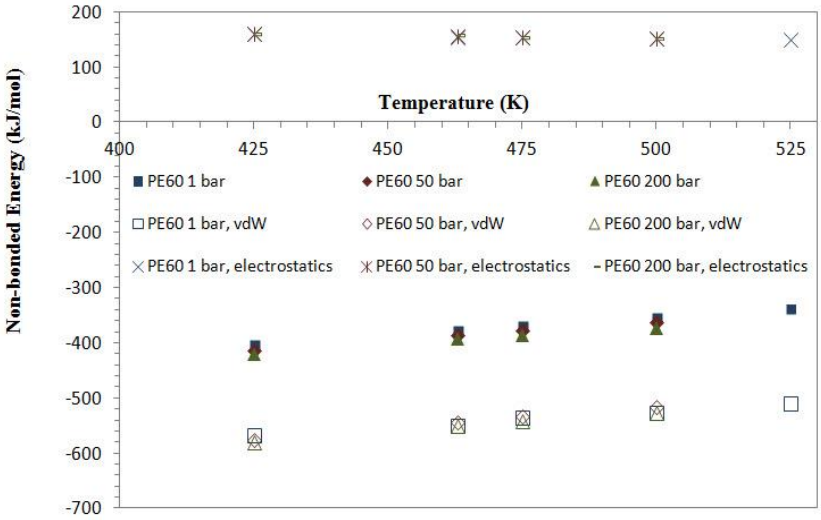

Figure 4.11. Temperature dependence of PE total non-bonded energy (filled symbols), vdW, and electrostatics components.

Table 4.1 provides statistical information on the total system energy of various model systems in the liquid state as well as gas phase. The error estimation of below 1% (2-3% for PE runs in vacuum) obtained from NVT runs suggests that the data were collected when the equilibrium state was achieved. The reported total drift is the difference of the least-squares fit of the data to a straight line evaluated at the first and last points. In addition, a few simulations were conducted to compare the velocity-rescaling against Nose-Hoover[18-19]

thermostats where the break-down of total energy indicates that Nose-Hoover produces similar results to the velocity-rescaling scheme (see Table 4.2). The calculated average pressures in the NVT simulations were found to be within a range of nearly +/- 200 and 300 bar for hexane and PE, respectively from the expected values under which the experimental density was measured, as reported in previous work.[20]

In molecular simulations the heat of vaporization may be computed from the internal energy of the periodic simulation cell at bulk state, U_{bulk} and the sum of the internal energies of the isolated molecules in vacuum, $U_{\text{i,isolated}}$ (in the absence of intermolecular interactions) averaged over a certain number of samples:

$$\Delta H_{\text{vap}}(T) = \left\langle \sum_{i=1}^{n} U_{\text{i,isolated}}(T) - U_{\text{bulk}}(T) \right\rangle_{NVT} + RT \qquad (4.7)$$

Figure 4.12 and Figure 4.13 present the computed δ of the model systems of PE and hexane as a function of temperature. The solubility parameter of hexane was validated at 298 and 303 K at 1 bar.[21-22] The PE system was validated[12] at 1 bar in the temperature range of 425-525 K and subsequently the temperature was increased to study δ(T) of hexane and PE in the range of 425-500 K at 50 and 200 bar. Verification of δ of hexane and PE at 50 bar was carried out utilizing perturbed-chain statistical associating fluid theory (PC-SAFT)[23] and corresponding-states theoretical[12] methods, respectively. In the literature the calculated values of PE solubility parameter lie in a broad range of 14.8-18 $(\text{MPa})^{1/2}$. The δ values by inverse gas chromatography for HDPE and LDPE (low-density polyethylene) were equal and were estimated to be 13 and 12 $(\text{MPa})^{1/2}$ (at 423 and 453 K, respectively). Also a value of 11 $(\text{MPa})^{1/2}$ at 413 K was reported by GLC technique.[24] As may be inferred from the NVT simulation results, the δ values decrease with increasing temperature. This slight decrease is justified due to the fact that ΔE_{vap} decreases and the molar volume increases with increasing temperature. The predicted δ of PE and hexane increases as a result of raising the pressure from 50 to 200 bar in the constant-temperature constant-volume ensemble indicating that at higher pressures more energy is required to move the molecules to an infinite distance as predicted under the isobaric-isothermal conditions.[1]

Table 4.1. Pressure and temperature dependence of internal energy of liquid and gas phases for PE and hexane models obtained via canonical ensemble simulations to compute CED.

Model System	Temperature (K)	Internal Energy (kJ/mol)	Error Estimation (kJ/mol)	RMSD (kJ/mol)	Total Drift (kJ/mol)
Hexane (1 bar)	298	127.1	0.03	1.7	0.09
	303	129.9	0.04	1.7	-0.2
Hexane (50 bar)	425	196.2	0.06	2.4	-0.09
	463	216.5	0.05	2.6	-0.2
	475	222.9	0.05	2.6	-0.1
	500	236.1	0.03	2.8	0.08
Hexane (200 bar)	425	194.8	0.02	2.4	-0.05
	463	214.9	0.02	2.6	-0.06
	475	221.2	0.04	2.6	-0.07
	500	234.4	0.05	2.8	0.08
Hexane (vacuum)	298	154.1	0.36	18.9	3.6
	303	159.5	0.36	19.2	2.2
	425	216.6	0.52	27.1	10.1
	463	237.4	0.51	29.3	2.6
	475	242.7	0.54	30.1	1.3
	500	253	0.57	31.6	2.1
PE60 (1 bar)	425	3640.7	0.83	42.1	-1
	463	4029.3	0.88	45.6	7.3
	475	4146.7	0.91	46.5	4.8
	500	4387.3	0.97	49.3	5.5
	525	4636.7	0.96	51	5.8
PE60 (50 bar)	425	3627.9	0.91	42.6	-21.8
	463	4012.8	0.88	45.3	-1.5
	475	4135.8	0.89	46.7	-9.4
	500	4381.7	0.89	48.9	-0.1
PE60 (200 bar)	425	3625.8	0.84	42.1	-16.5
	463	4001	0.91	45.7	6.8
	475	4124.2	0.96	47	-14
	500	4367.5	0.93	48.8	-12.1
PE60 (vacuum)	425	4020.9	2.4	122	2.5
	463	4404.3	2.8	134.4	-4.6
	475	4512.5	2.8	137	-4.2
	500	4759.2	3	144.5	-16.6
	525	4995.2	3.1	151.1	-5.7

Table 4.2. Computed values of energy components (kJ/mol) using velocity-rescaling and Nose-Hoover thermostats.

Thermostat	*P* (bar)/*T* (K)	Bonds	Angles	Torsions	Lennard-Jones	Electrostatics	Kinetic
PE: Velocity-rescaling	50/425	653.9	1023.3	342.2	-574.3	161.9	1918.1
PE: Nose-Hoover	50/425	653.1	1023.5	340.4	-575	163.4	1918.1
PE: Velocity-rescaling	50/475	731.7	1139.8	380.8	-532.2	155.1	2143.7
PE: Nose-Hoover	50/475	731.3	1139.6	379.3	-532.4	155.9	2143.7
Hexane: Velocity-rescaling	50/425	34.3	51.3	13.3	-22.1	8.6	105.9
Hexane: Nose-Hoover	50/425	34.3	51.3	13.2	-22.1	8.6	105.9

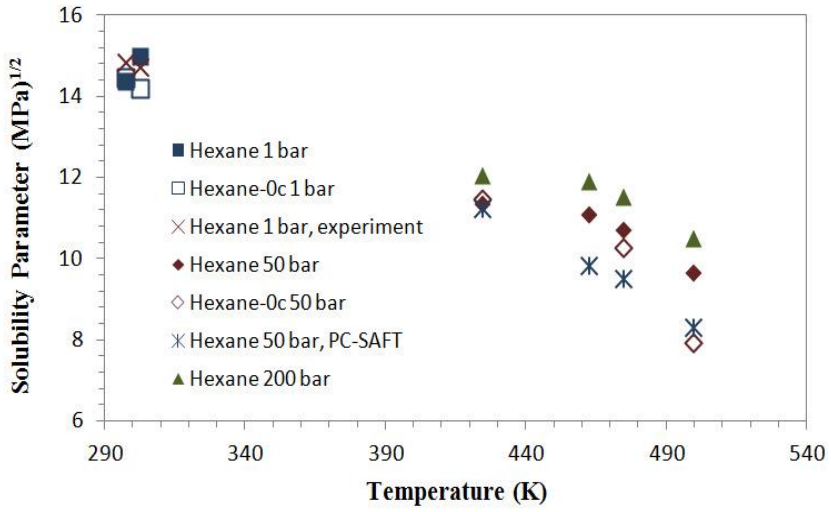

Figure 4.12. Temperature dependence of hexane solubility parameter. The squares, diamonds, and triangles represent simulation data at 1, 50, and 200 bar, respectively (0c notation indicates MM model with electrostatics switched off).

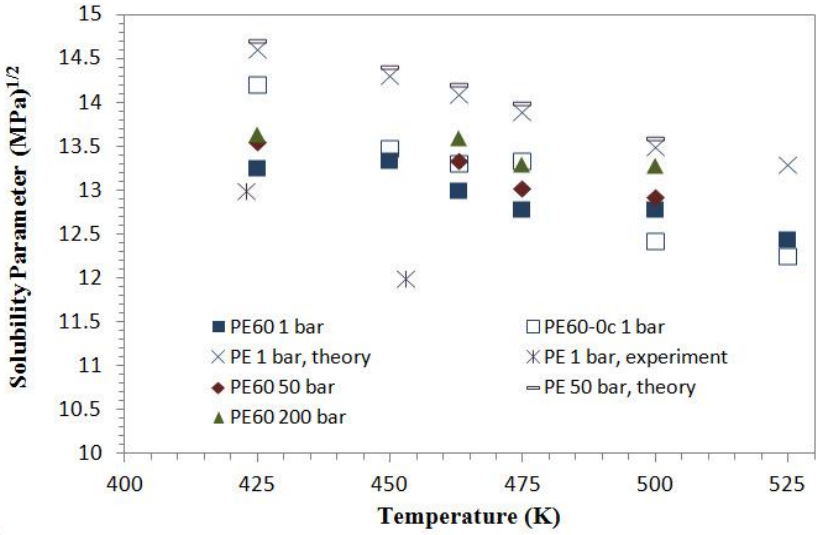

Figure 4.13. Temperature dependence of PE solubility parameter. The squares, diamonds, and triangles represent simulation data at 1, 50, and 200 bar, respectively (0c notation indicates MM model with electrostatics switched off).

4.4.2 Binary Interaction Parameter

Using the knowledge of solubility parameters of the polymer and solvent as a function of temperature, the temperature dependence of the FH interaction parameter, χ has been computed based on Equation 4.2 at 425, 463, 475, and 500 K. As shown in Figure

4.14, the computed binary interaction parameters increase upon increasing the temperature indicating that the miscibility of the PE/hexane system may be improved by decreasing the temperature. Since the cohesive energy of hexane is more sensitive to molar volume than PE, and both are decreasing functions of temperature (due to the fact that cohesive energies depend mainly on densities and higher temperature corresponds to lower pressure) with increasing temperature, solubility parameters of hexane decrease faster than that of PE. It is clear that the greater the difference in solubility parameters, the larger the interaction parameter at higher temperatures will be. The sharp rise in χ beyond 475 K is attributed to the drastic change in the density of the solvent as it undergoes phase change where the solvent expands rapidly from liquid to the gas density while the polymer tends to remain in the liquid state. The predicted $\chi(T)$ for PE in hexane is consistent with the widely recognized LCST fluid phase behavior. This type of phase behavior is a consequence of difference in compressibility between polymer and the solvent upon increasing temperature. It is believed that this increasing dissimilarity in density induces a negative volume of mixing as a result of raising the temperature.[25] Furthermore, the NVT computed binary interaction parameters decrease upon increasing pressure from 50 to 200 bar indicating that the miscibility of the PE/hexane system may be improved by raising the pressure as predicted by NPT runs.[2]

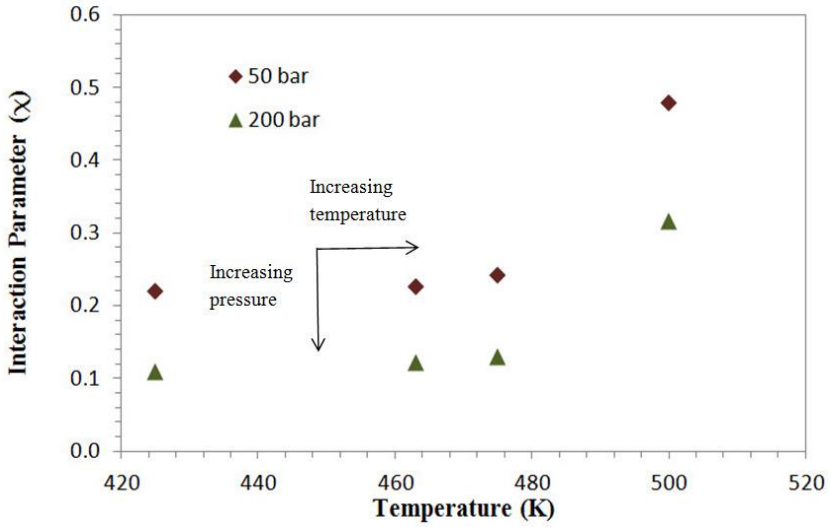

Figure 4.14. Binary interaction parameter as a function of temperature for PE/hexane system at 50 and 200 bar.

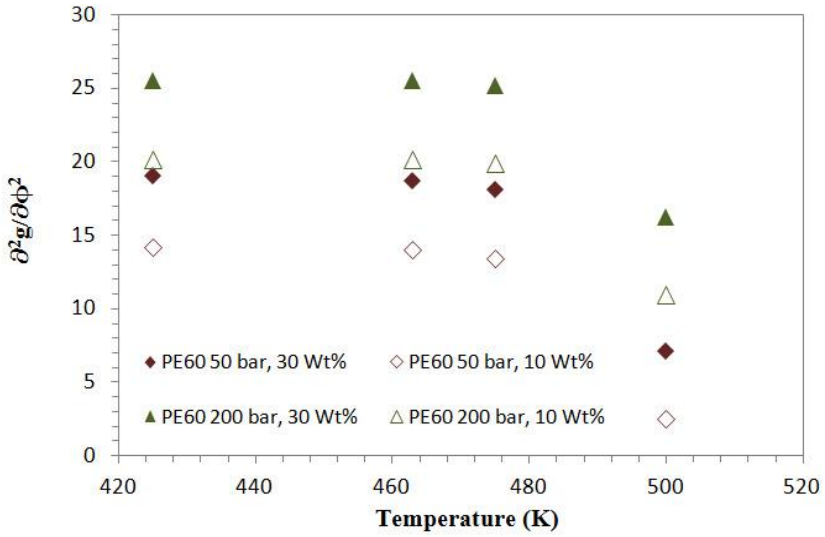

Figure 4.15. Second derivative of Gibbs free energy as a function of temperature for PE solutions of 10 and 30% polymer weight fractions.

4.4.3 Phase Stability

Figure 4.15 illustrates the chemical potential factor $\frac{\partial^2 g}{\partial \phi^2}(T)$ for PE60 and polymer solutions of weight percent ω_{PE} = 10 and 30% at 50 and 200 bar, respectively. The figure shows that the chemical potential factor $\frac{\partial^2 g}{\partial \phi^2}$ decreases with temperature and increases with pressure. This decrease of the chemical potential factor as a result of raising the temperature indicates that this term tends to decrease the stability of the polymer-solvent system at higher temperatures, as expected in the LCST type of phase diagram.[25-26] The sudden decrease in chemical potential factor beyond 475 K is attributed to the increasing dissimilarity in densities of polymer and solvent as discussed above. Moreover, the increase of the chemical potential factor as a result of raising the pressure from 50 to 200 bar predicted by NVT ensemble simulations indicates that this term tends to increase the stability of the polymer-solvent system at higher pressures, consistent with the pressure-induced phase separation predictions under NPT ensemble.[2]

4.4.4 Electrostatic Algorithm

In this section we present a series of simulations, based on the shift function and the PME[27-28] methods to establish efficient routes to polymer solution MD calculations. PME is an efficient and fast method, where the electrostatic energy is split into the short range (SR), computed in direct space, and the long range (LR) in reciprocal space using fast Fourier transforms. This method provides an improved performance of the reciprocal sum, which enables calculating accurately the LR interactions where the grid dimensions may be controlled. In this study, we report on the effect of the grid spacing of 0.12, 0.2, and 0.25 nm on the non-bonded terms together with total potential energy utilized in the calculation of cohesive energy at 425 K and 50 bar for both PE and hexane. A fourth-order interpolation was applied for PME, and the neighbor lists were computed with a 1.35 nm cut-off for both methods to evaluate the non-bonded interactions. A group-based cut-off radius of 1.35 nm was utilized for PME, while for the shift function the electrostatic interactions were switched smoothly to zero over the region 1-1.1 nm. An overview of the simulations performed with details of the implemented electrostatic scheme is given in Table 4.3. The non-bonded energy terms, Lennard-Jones and electrostatics (PME: SR + LR) do not demonstrate significant dependence on grid spacing, indicating that for partially charged molecules as PE and hexane the PME grid spacing may be increased up to 0.25 nm in order to accelerate the simulation runs. The total potential is shown to be insensitive with respect to electrostatic schemes predicted using shift functions and PME with various grid spacing values.

Table 4.3. Effect of electrostatic techniques on total potential energy (kJ/mol) for PE and hexane at 425 K and 50 bar.

Model System	Electrostatic Scheme	Lennard-Jones	Electrostatics (SR)	Electrostatics (LR)	Total Potential
PE60	PME-Grid spacing 0.12 nm	-575.9	142.9	34.1	1714.7
	PME-Grid spacing 0.2 nm	-574.4	141.1	33.5	1722.3
	PME-Grid spacing 0.25 nm	-575.5	142.7	34	1714.9
	Shift function (1-1.1 nm)	-574.3	161.9	-	1709.9
Hexane	PME-Grid spacing 0.12 nm	-22.1	5.7	5	92.3
	PME-Grid spacing 0.2 nm	-22.1	5.7	5	92.3
	PME-Grid spacing 0.25 nm	-22.1	5.7	5	92.3
	Shift function (1-1.1 nm)	-22.1	8.6	-	90.2

4.5 Conclusions

The Hildebrand solubility parameters for HDPE and hexane were computed over the range of 425-525 K, using the MD technique on the basis of the OPLS-AA force field. The simulations in the NVT ensemble at various temperatures were performed at which equilibration was achieved within the first few nanoseconds. The δ values decrease monotonically with increasing temperature for both MM models with and without electrostatic forces, indicating that at higher temperatures less energy is required to move the molecules to an infinite distance. The comparison of solubility parameter of PE between 1 and 50-200 bar indicates that the values are slightly sensitive to pressure in the investigated temperature range. The analysis of non-bonded interactive energy indicated that vdW interaction is of more importance than electrostatics in a PE-hexane solution. Nevertheless, the electrostatic energy was found to contribute considerably to the total non-bonded interactions suggesting that inclusion of this term is representative of a more realistic model. Comparisons with previously reported experimental/theoretical values of solubility parameters confirm the accuracy of the OPLS-AA force field.

The computed binary interaction parameters were predicted to increase upon increasing the temperature which underlines the fact that the miscibility of the PE/hexane system may be lowered by raising the temperature, in agreement with experimental and theoretical data. The decrease in PE miscibility at high temperatures is consistent with LCST fluid phase behavior. Moreover, it was shown that the increase in the system's temperature decreases the incompressible contribution to phase stability condition (Equation 4.3), indicating that this term tends to decrease the stability of the polymer-solvent system at higher temperatures. It should also be remarked that, although the implemented thermodynamic methodology presented here fails to represent quantitatively the experimental data, due to the limitations of the FH theory (e.g. neglect of the concentration dependence of interaction parameter), the presented results prove that the LCST mechanism can still be predicted in the framework of solubility parameter approach in which the binary interaction parameter is only a function of intermolecular forces. The present methodology complements the parametric EOS approaches, whose parameters require costly and difficult experimental measurements, and further provides atomistic-level insights that are difficult to capture experimentally.

Additionally, electrostatic interactions were calculated by the well-known PME method and compared with the shift function, where it was found that the grid spacing has no noticeable influence on non-bonded energy terms and total potential, employed in the calculation of cohesive energy. This suggests that the computations can be significantly accelerated by increasing grid spacing up to 0.25 nm without losing accuracy. Ultimately, the modeling approach employed in this research provides a significant insight into the molecular-level effects that control the miscibility-related thermodynamic properties of polyolefins and hydrocarbon solvents, as in the high-pressure production process of PE.

4.6 References

1. Shahamat, M.; Rey, A. D., Characterization of pressure effects on the cohesive properties and structure of hexane and polyethylene using molecular dynamics simulations. *Macromolecular Theory and Simulations* **2012,** *21* (8), 535-543.
2. Shahamat, M.; Rey, A. D., High pressure miscibility predictions of polyethylene in hexane solutions based on molecular dynamics. *European Polymer Journal* **2013,** *49* (2), 471-481.
3. Folie, B.; Radosz, M., Phase equilibria in high-pressure polyethylene technology. *Industrial & Engineering Chemistry Research* **1995,** *34* (5), 1501-1516.
4. Sanchez, I. C., Volume fluctuation thermodynamics of polymer solutions. *Macromolecules* **1991,** *24* (4), 908-916.
5. Berendsen, H. J. C.; van der Spoel, D.; van Drunen, R., Gromacs: A message-passing parallel molecular dynamics implementation. *Computer Physics Communications* **1995,** *91* (1-3), 43-56.
6. Lindahl, E.; Hess, B.; van der Spoel, D., GROMACS 3.0: A package for molecular simulation and trajectory analysis. *Journal of Molecular Modeling* **2001,** *7* (8), 306-317.
7. van der Spoel, D.; Lindahl, E.; Hess, B.; Groenhof, G.; Mark, A. E.; Berendsen, H. J. C., GROMACS: Fast, flexible, and free. *Journal of Computational Chemistry* **2005,** *26* (16), 1701-1718.
8. Hess, B.; Kutzner, C.; van der Spoel, D.; Lindahl, E., GROMACS 4: Algorithms for highly efficient, load-balanced, and scalable molecular simulation. *Journal of Chemical Theory and Computation* **2008,** *4* (3), 435-447.
9. Jorgensen, W. L.; Madura, J. D.; Swenson, C. J., Optimized intermolecular potential functions for liquid hydrocarbons. *Journal of the American Chemical Society* **1984,** *106* (22), 6638-6646.
10. van der Spoel, D.; van Maaren, P. J., The origin of layer structure artifacts in simulations of liquid water. *Journal of Chemical Theory and Computation* **2006,** *2* (1), 1-11.
11. Rudin, A.; Chee, K. K.; Shaw, J. H., Specific volume and viscosity of polyolefin melts. *Journal of Polymer Science, Part C: Polymer Symposium* **1970,** (30), 415-427.
12. Maloney, D. P.; Prausnitz, J. M., Thermodynamic properties of liquid polyethylene. *Journal of Applied Polymer Science* **1974,** *18* (9), 2703-2710.

13. Daridon, J. L.; Lagourette, B.; Grolier, J. P. E., Experimental measurements of the speed of sound in n-hexane from 293 to 373 K and up to 150 MPa. *International Journal of Thermophysics* **1998,** *19* (1), 145-160.
14. Bussi, G.; Donadio, D.; Parrinello, M., Canonical sampling through velocity rescaling. *Journal of Chemical Physics* **2007,** *126* (1), 014101.
15. Fan, C. F.; Cagin, T.; Chen, Z. M.; Smith, K. A., Molecular modeling of polycarbonate.1. Force-Field, static structure, and mechanical properties. *Macromolecules* **1994,** *27* (9), 2383-2391.
16. Zhang, M. Z.; Choi, P.; Sundararaj, U., Molecular dynamics and thermal analysis study of anomalous thermodynamic behavior of poly (ether imide)/polycarbonate blends. *Polymer* **2003,** *44* (6), 1979-1986.
17. Jawalkar, S. S.; Aminabhavi, T. M., Molecular modeling simulations and thermodynamic approaches to investigate compatibility/incompatibility of poly(L-lactide) and poly(vinyl alcohol) blends. *Polymer* **2006,** *47* (23), 8061-8071.
18. Nose, S., A unified formulation of the constant temperature molecular dynamics methods. *Journal of Chemical Physics* **1984,** *81* (1), 511-519.
19. Hoover, W. G., Canonical dynamics: Equilibrium phase-space distributions. *Physical Review A* **1985,** *31* (3), 1695-1697.
20. Choi, P., Molecular dynamics studies of the thermodynamics of HDPE/butene-based LLDPE blends. *Polymer* **2000,** *41* (24), 8741-8747.
21. Bristow, G. M.; Watson, W. F., Cohesive energy densities of polymers. 1. Cohesive energy densities of rubbers by swelling measurements. *Transactions of the Faraday Society* **1958,** *54* (11), 1731-1741.
22. Barton, A. F. M., *CRC handbook of solubility parameters and other cohesion parameters*. CRC Press: Boca Raton, 1991.
23. Zeng, Z. Y.; Xu, Y. Y.; Li, Y. W., Calculation of solubility parameter using perturbed-chain SAFT and cubic-plus-association equations of state. *Industrial & Engineering Chemistry Research* **2008,** *47* (23), 9663-9669.
24. Barton, A. F. M., *CRC handbook of polymer-liquid interaction parameters and solubility parameters*. CRC Press: Boca Raton, 1990.
25. Paricaud, P.; Galindo, A.; Jackson, G., Understanding liquid-liquid immiscibility and LCST behaviour in polymer solutions with a Wertheim TPT1 description. *Molecular Physics* **2003,** *101* (16), 2575-2600.
26. Nies, E.; Stroeks, A.; Simha, R.; Jain, R. K., LCST phase behavior according to the Simha-Somcynsky Theory: Application to the n-hexane polyethylene system. *Colloid and Polymer Science* **1990,** *268* (8), 731-743.
27. Darden, T.; York, D.; Pedersen, L., Particle mesh Ewald. An N.log(N) method for Ewald sums in large systems. *Journal of Chemical Physics* **1993,** *98* (12), 10089-10092.
28. Essmann, U.; Perera, L.; Berkowitz, M. L.; Darden, T.; Lee, H.; Pedersen, L. G., A smooth particle mesh Ewald method. *Journal of Chemical Physics* **1995,** *103* (19), 8577-8593.

5 Molecular Mechanics and Equation of State Modeling of Compressible Polyolefin Solutions: Impact of Pressure and Cut-off Radius of Intermolecular Potentials

5.1 Summary

This paper reports on the density of solutions of polyethylene (PE) in hexane using molecular dynamics (MD) simulations based upon the accurate OPLS-AA force field at high pressures and 425 K. The NPT-MD simulations are carried out at polymer concentration of 20 wt% in hexane in the pressure range from 100 to 3000 bar. For PE solutions of 10 and 20 wt% the pressure is varied from 100 to 1000 bar. Additionally, the PE solution densities are calculated based on the modified Sanchez-Lacombe (MSL) equation of state (EOS) model to examine the accuracy of the MD computations. The simulated densities increase monotonically with increasing external pressure and compare quite favorably with the experimental and EOS data. It is also revealed that the MSL EOS model produces identical mixture densities regardless of the type of the *b* parameter. The effect of cut-off radius to density is investigated and it is shown that the solution density increases as cut-off radius increases. A minimum cut-off radius of 1.1 nm is suggested for the intermolecular forces for accurate densities at pressures below 100 bar. For higher pressures density and non-bonded interactions display less sensitivity to cut-off distance. Analysis of the pair distribution function versus pressure is carried out where the height of the first peak increases and the radial distribution function shifts to shorter separations reflecting structural change of the condensed phase. The molecular modeling approach employed in this research provides a good insight into the polymer-polymer, polymer-solvent, and solvent-solvent interactions. The implemented methodology using the OPLS-

AA force field and constant pressure/temperature algorithms compare well with the literature data, suggesting the validity of the proposed method.

5.2 Introduction

Polyethylene (PE), one of the most widely used plastic materials occupying a crucial position in the polyolefin market, is widely produced by the solution polymerization process. In solution polymerization, ethylene reacts under high pressures to produce PE while dissolved in an inert hydrocarbon solvent mixture (typically pentane to octane). Hexane and cyclohexane are commonly used as the main components of the inert hydrocarbon solution. In the production of linear low-density polyethylene (LLDPE) co-monomers are added during the polymerization to control the branching in the molecule. In subsequent processing steps, the solution undergoes a series of separations by depressurizing the reactor effluent to purify the PE product and recover the unreacted ethylene and the solvent for recycling. The pressure decrease also affects the density of the mixture, which consequently influences the phase equilibria and process design. As a result, a full characterization of the thermodynamic and physical properties of polymer solution including changes in pressure and mixture density is of great interest from a fundamental scientific point of view and also due to its importance in a wide variety of technological applications.[1-4] Although elevated pressures are involved in the solution polymerization process of PE, few experimental studies of the pressure dependence of thermodynamic properties such as density have been reported due to the difficulty of carrying out experiments at high pressures and temperatures.

Accordingly, within the last half century, numerous thermodynamic models have been proposed to predict phase equilibria of polymer solutions. Most of these models are revised forms of Flory-Huggins lattice theory where density is assumed constant. These models, therefore, cannot predict phase behavior of compressible systems especially where pressure and temperature changes are significant. Recently, to investigate the equilibrium thermodynamics of compressible polymer solutions, the well-known Sanchez-Lacombe (SL) equation of state (EOS)[5-7] and its modified version known as the modified Sanchez-Lacombe (MSL) EOS[8] have been extensively used. The SL EOS is a statistical mechanical model that is capable of describing phase behavior of polymer solutions. The speed and

accuracy of the MSL equation make it a powerful tool for modeling the polyolefin solutions. To apply the MSL equation for binary mixtures requires an accurate parameterization to obtain the pure component parameters and binary interaction parameters, determined by fitting of the experimental values with theoretical ones. The MSL parameters for the solvent are typically calculated using the parameterization based on molar masses, critical temperatures, critical pressures, and acentric factors. In case of PE, parameters may be obtained by manipulating the PE lattice energy to fit the liquid-liquid critical point and cloud point boundaries of different PE + hydrocarbon mixtures. The remaining parameters are found by minimizing the errors in the liquid density data of pure PE for the specified lattice energy.[9] Hence, although there is an abundance of well-established thermodynamic models to describe phase behavior of polymer solutions, in many cases difficulties arise mainly due to the lack of experimental data for the determination of model parameters. Moreover, the problem becomes complex in case of multicomponent mixtures, consistent with industrial polymer production. Thus, alternative methods are undoubtedly required to capture pressure dependence of physical properties of polyolefin solution systems without the need for costly and time-consuming experimental efforts.

Lately, the development of molecular modeling techniques has opened a new highway to a more detailed picture on the molecular-level information. Molecular modeling is a rapidly evolving discipline which has unquestionably benefited a lot from advances in computing. Mathematical models such as molecular mechanics and intensive ab initio electronic structure calculations may be applied to chemical problems, but each has practical limitations. For instance, since ab initio models are not parameterized they do not require experimental data for model development, but use of ab initio electronic structure procedures is computationally expensive and the model is restricted to small systems. In contrast to ab initio models, molecular mechanical models need to be parameterized but they enable us to handle large systems. Since the advent of today's powerful computers, molecular modeling simulations have been advanced to such a level to predict physical properties of polymeric systems. In particular, molecular mechanics in combination with molecular dynamics (MD) method have been applied in the past decade in simulation studies of polymer dynamics in melts and solutions.[10] These techniques have been found

effective methods to conduct studies of the structure and dynamics on the molecular-level, founded on reliable atomistic force fields.

However, the effect of high pressure on physical properties of polymer solutions based on a molecular perspective has not yet been accurately characterized. In relation to the characterization of pressure effects on thermophysical properties, a molecular perspective proves to be of great value in bringing some light on the changes in intra- and intermolecular interactions with pressure. In this regard, establishing a molecular-level characterization of density-pressure-composition relations in compressible polymer solutions is essential to thermodynamic processes and transport phenomena. To this end, we have revealed that the simulations performed in the NPT (constant mole number, pressure, and temperature) ensemble have the potential for accomplishing this objective. In previous work[11] we focused on developing a MD calculation platform under the isobaric-isothermal (NPT) ensemble to compute the effect of pressure on densities, structure (i.e. polymer radius of gyration and pair distribution functions), and cohesive energies of PE and hexane over a wide range of pressures from 100 up to 3000 bar by quantifying specific contributions of bonded/non-bonded interactions to gain a fundamental understanding of phase behavior in polymer solutions at high pressures. Furthermore, on the basis of the NPT-MD ensemble predictions of internal pressures were performed at elevated pressures and the knowledge of pressure dependence of solubility parameters and molar volumes was further utilized to build a molecular thermodynamic characterization of compressible PE solutions. In this regard, the Flory-Huggins binary interaction parameter, volume change upon mixing, and the chemical potential factor as functions of pressure were computed to predict miscibility and phase stability and to shed light on the pressure-induced phase separation mechanism in binary solutions of PE in hexane.[12]

The present work aims to contribute to the atomistic-level understanding of the pressure effects on binary solution density and structural properties of PE in hexane solutions at conditions of industrial interest, which have relevance to applied and fundamental polymer chemical physics based on MD simulations in the NPT ensemble. As established in previous work,[1] spinodals and binodals must be calculated by solving chemical and mechanical coupled balances, where the coupling involve compositional derivatives of pressure in addition to the usual compressibility. Furthermore, the kinetics of

compressible phase separation, denoted acousto-spinodal decomposition,[4] integrates total mass, a component mass and momentum through compositional derivatives of pressure. Moreover, the binary solution densities are calculated using the MSL EOS model (as detailed below) to verify the accuracy of the proposed molecular modeling methodology.

Since in most cases non-bonded interactions dominate MD computations for large systems such as mixtures of polymer-solvent and polymer blends, it is of utmost importance to reduce the calculation time of the non-bonded forces while maintaining the required accuracy. Hence, the secondary objective of the present paper is to investigate the effect of the cut-off radius on the intermolecular potentials and densities of PE in hexane solution. To the best of our knowledge, no such studies on the aforementioned topics have been made earlier for a PE in hydrocarbon solution based on a molecular modeling approach.

The organization of this paper is as follows. The methodology section presents the computational method and a detailed molecular mechanics model description for conducting NPT simulations. In the results and discussion section, part I evaluates the PE solution density as a function of pressure for several PE mass fractions using NPT-MD simulations together with MSL EOS modeling; part II investigates the effect of cut-off distance of non-bonded interactions on density and the total system energy, and part III characterizes the pressure effect on the structural properties of binary mixture of PE in hexane. The final section summarizes findings and gives some concluding remarks.

5.3 Computational Methods

5.3.1 Molecular Modeling

In the present work the standard computational tool GROMACS[13-16] version 4.5.4 has been employed with the OPLS-AA[17] force field parameters. The OPLS-AA was selected since it is widely applicable to hydrocarbon systems.[18] For all the simulation runs, we have used quad-core AMD processors, running under CentOS/Linux. The total system energy E_{total} is represented by the sum of bonded and non-bonded interactions:

$$E_{\text{total}} = E_b + E_\theta + E_\phi + E_{\text{vdW}} + E_{\text{electrostatics}} \qquad (5.1)$$

The molecular mechanics model incorporates the intramolecular interactions of covalent bond stretching (2-body), E_b, angle bending (3-body), E_θ, and dihedral angle (4-body), E_ϕ, which are based on a fixed list of atoms. The 2-body and 3-body interaction terms were expressed in harmonic form and dihedrals were treated by cosine series potentials. The intermolecular interactions which are computed on the basis of a list of non-bonded atoms within a certain radius between atoms separated by more than three bonds or those belong to different molecules, were modeled by pairwise additive 12-6 Lennard-Jones, E_{vdW}, and electrostatic, $E_{\text{electrostatics}}$, potential energies. A neighbor list with cut-off distance of 1.25 nm and update frequency of every 10 steps was used for calculating the non-bonded interactions. To alleviate the ill effect of plain cut-offs, non-bonded potentials were treated by a shift function,[19] which ensures that the truncated forces are continuous and have continuous derivatives at the group-based cut-off radius of 1 nm (unless stated otherwise).

The molecular architecture of PE chains and hexane were built and the geometry was optimized by minimizing the energy of the system. Subsequently four linear PE chains composed of 240 repeating units (4PE240) were placed in a low-density cubic simulation box with the 3-D periodic boundary conditions. After this, the long polymer chains were solvated to generate binary polymer solutions of 10, 20, and 30 wt%, corresponding to 2800, 1200, and 730 solvent molecules, for a total of 61,768, 29,768, and 20,368 atoms in the system, respectively (notation 4PE240-2800Hexane represents a PE solution composed of 4 polymer chains solvated in 2800 hexane molecules). The random overlaps were avoided by using the steepest descent algorithm to energy minimize the initial molecular structures. In the next step, solvent was allowed to relax by running a 500 ps MD simulation with position restraints applied on all the polymer atoms. The restraints were then removed from all atoms and a pressure-induced compression using the Berendsen barostat[20] algorithm was employed for 20 x 10^6 molecular dynamics steps of 1 fs (i.e. 20 ns of total time) to increase the gas density of the system close to the experimental density and to remove the unfavorable local minima with high energies.

On the basis of the fully relaxed models produced as described above, the isobaric-isothermal (NPT) simulations were conducted from the end of the previous relaxed 20 ns-

NPT simulation for 10 ns where time steps were set to 0.5 fs at external pressures over a broad range of 100 to 3000 bar to achieve the equilibrium densities. Parrinello-Rahman barostat[21] with time constant of 1 ps and temperature coupling using velocity rescaling[22] with a relaxation constant of 0.1 were applied throughout the simulations to maintain the system pressure and temperature at the target values. The equations of motion were solved using a leap-frog integration step and the coordinates and energy values were stored at every 100 steps for the confirmation of the equilibration and analysis. The total energy, pressure, and density were monitored to ensure equilibration of the system and ultimately, the last 1 ns of each simulation was analyzed and used to compute the physical properties of interest.

5.3.2 Equation of State Modeling

The MSL EOS is based on a compressible lattice fluid model and therefore, can describe the thermodynamics of compressible polymer solutions, especially for different molecular weights and polydisperse PE solutions. The model which is an extension of the SL EOS involves three pure component parameters: d_i, the number of lattice sites occupied by molecule type *i*, v_i, the volume occupied by molecule of type *i*, and ε_i, the interaction energy of component *i*. These parameters are determined for each pure component using *PVT* data.

The specific molar Helmholtz free energy of the solution, *A*, for the MSL EOS[8] is presented below from which other thermodynamic properties such as pressure can be derived:

$$\frac{A}{RT} = -\frac{a}{RT\upsilon} + \frac{d^2}{b}\left(\upsilon - \frac{b}{d}\right)\ln\left(\frac{\upsilon - b/d}{\upsilon}\right) + \sum_{i=1}^{N_c} x_i \ln\left(\frac{x_i d_i b}{d^2 \upsilon}\right) \qquad (5.2)$$

where υ is the solution molar volume, x_i the mole fraction of *i*th component, N_c the number of components and parameters *d*, *b*, and *a* are the concentration-dependent mixture parameters in the MSL EOS calculated using mixing rules:

$$d = \sum_{i=1}^{N_c} x_i d_i$$

$$b = \sum_{i=1}^{N_c}\sum_{j=1}^{N_c} x_i x_j b_{ij} = \sum_{i=1}^{N_c}\sum_{j=1}^{N_c} x_i x_j d_i d_j \frac{\left(\nu_i + \nu_j\right)}{2}$$

$$a = \sum_{i=1}^{N_c}\sum_{j=1}^{N_c} x_i x_j a_{ij} = \sum_{i=1}^{N_c}\sum_{j=1}^{N_c} x_i x_j b_{ij}\varepsilon_{ij} = \sum_{i=1}^{N_c}\sum_{j=1}^{N_c} x_i x_j d_i d_j \frac{\left(\nu_i + \nu_j\right)}{2}\varepsilon_{ij} \tag{5.3}$$

$$\varepsilon_{ij} = \left(1 - K_{ij}\right)\sqrt{\varepsilon_i \varepsilon_j}$$

ε_{ij}, denotes the attractive energy parameter between components of type *i* and the binary interaction parameter for the mixture is defined as:

$$K_{ij} = K_{ij}^a + K_{ij}^b T \tag{5.4}$$

where K_{ij}^a and K_{ij}^b are respectively the temperature-independent and temperature-dependent parts of the binary interaction parameter, and T is absolute temperature. The EOS relating the pressure, temperature, and molar volume of the polymer solution which can be found by differentiating the free energy $P = -\left(\frac{\partial A}{\partial \upsilon}\right)_{T,n} = \rho^2\left(\frac{\partial A}{\partial \rho}\right)_{T,n}$, reads:

$$\frac{P}{RT} = -\frac{a}{RT\upsilon^2} - \frac{d^2}{b}\ln\left(\frac{\upsilon - b/d}{\upsilon}\right) + \frac{1-d}{\upsilon} \tag{5.5}$$

The free energy per unit mass can be found by defining the mass fraction-based model parameters as indicated below:

$$d_m = \sum_{i=1}^{N_c} \omega_i \frac{d_i}{M_i} \tag{5.6}$$

$$b_m = \sum_{i=1}^{N_c}\sum_{j=1}^{N_c} \omega_i \omega_j \frac{d_i}{M_i}\frac{d_j}{M_j}\frac{\left(\nu_i + \nu_j\right)}{2}$$

$$a_m = \sum_{i=1}^{N_c}\sum_{j=1}^{N_c} \omega_i \omega_j \frac{d_i}{M_i}\frac{d_j}{M_j}\frac{\left(\nu_i + \nu_j\right)}{2}\varepsilon_{ij}$$

where M_i and ω_i indicate the molecular weight and mass fraction of component *i* and the equivalent mass-based parameters of *d*, *b*, and *a* were respectively obtained as: $d_m = \frac{d}{M}$, $b_m = \frac{b}{M^2}$, and $a_m = \frac{a}{M^2}$. By applying the mass fraction-based mixing rules the homogenous specific Helmholtz free energy per unit mass of polymer solution, MSL-type 1, and the density derivative of the free energy, pressure, can be expressed as:

$$\frac{A_m}{RT} = -\frac{\rho a_m}{RT} + \frac{{d_m}^2}{\rho b_m}\left(1-\rho\frac{b_m}{d_m}\right)\ln\left(1-\rho\frac{b_m}{d_m}\right) + \sum_{i=1}^{N_c}\frac{\omega_i}{M_i}\ln\left(\frac{\omega_i\frac{d_i}{M_i}b_m\rho}{{d_m}^2}\right) \qquad (5.7)$$

$$\frac{P}{RT} = -\frac{\rho^2 a_m}{RT} - \frac{{d_m}^2}{b_m}\ln\left(1-\rho\frac{b_m}{d_m}\right) + \frac{\rho}{M} - \rho d_m \qquad (5.8)$$

The MSL free energy and its derived EOS expression may also be presented in the following form with the new mixing rules:

$$\frac{A}{RT} = -\frac{a}{RT\upsilon} + \frac{d}{b}(\upsilon - b)\ln\left(\frac{\upsilon - b}{\upsilon}\right) + \sum_{i=1}^{N_c} x_i \ln\left(\frac{x_i d_i b}{d\upsilon}\right) \qquad (5.9)$$

$$\frac{P}{RT} = -\frac{a}{RT\upsilon^2} - \frac{d}{b}\ln\left(\frac{\upsilon - b}{\upsilon}\right) + \frac{1-d}{\upsilon} \qquad (5.10)$$

By applying the mass fraction-based parameters in the form of linear/quadratic mixing rules where $b_i = d_i v_i$, the homogenous specific Helmholtz free energy per unit mass of polymer solution, MSL-type 2, is presented as below:

$$d_m = \sum_{i=1}^{N_c} \omega_i \frac{d_i}{M_i}$$

$$b_m = \sum_{i=1}^{N_c} \omega_i \frac{b_i}{M_i} = \sum_{i=1}^{N_c} \omega_i \frac{d_i}{M_i} v_i \tag{5.11}$$

$$a_m = \sum_{i=1}^{N_c} \sum_{j=1}^{N_c} \omega_i \omega_j \frac{d_i}{M_i} \frac{d_j}{M_j} \frac{\left(v_i + v_j\right)}{2} \varepsilon_{ij}$$

$$\frac{A_m}{RT} = -\frac{\rho a_m}{RT} + \frac{d_m}{\rho b_m}\left(1-\rho b_m\right)\ln\left(1-\rho b_m\right) + \sum_{i=1}^{N_c} \frac{\omega_i}{M_i} \ln\left(\frac{\omega_i \frac{d_i}{M_i} b_m \rho}{d_m}\right) \tag{5.12}$$

The pure compound parameters[23-24] employed in the present paper are summarized in Table 5.1. The EOS is obtained by differentiation of the Helmholtz energy with respect to the molar volume based on the linear and quadratic rules for the mass fraction-based model parameters as given below:

$$\frac{P}{RT} = -\frac{\rho^2 a_m}{RT} - \frac{d_m}{b_m}\ln\left(1-\rho b_m\right) + \frac{\rho}{M} - \rho d_m \tag{5.13}$$

The EOS needs to be solved iteratively to capture the binary polymer solution density as a function of pressure for different polymer compositions.

Table 5.1. Modified SL EOS pure compound and interaction parameters.

Parameter	HDPE	Hexane
Number of occupied lattice sites d_i / M_i (mol/g)	0.08644	0.1122
Volume occupied per lattice site v_i (cm^3/mol)	8.181	12.55
Energy per lattice site ε_i (J/mol)	4280	3685
Binary interaction parameter: K_{ij}=-1.708 10^{-1}+3.35710^{-4}T		

5.4 Results and Discussion

5.4.1 Effect of Pressure on PE Solution Density

Isobaric-isothermal thermodynamic ensemble simulations were employed to investigate the pressure dependence of potential energy contributions and mixture density. Figure 5.1 shows the pressure and temperature fluctuations versus simulation time (ps) for the 4PE240-1200Hexane model where the target values are 100 and 3000 bar and 425 K (at 100 bar). The total system energy leveled off during the first few nanoseconds, indicating the equilibrium state has been achieved. The simulations were long enough for the densities to reach equilibrium where the system densities fluctuate around an average value.

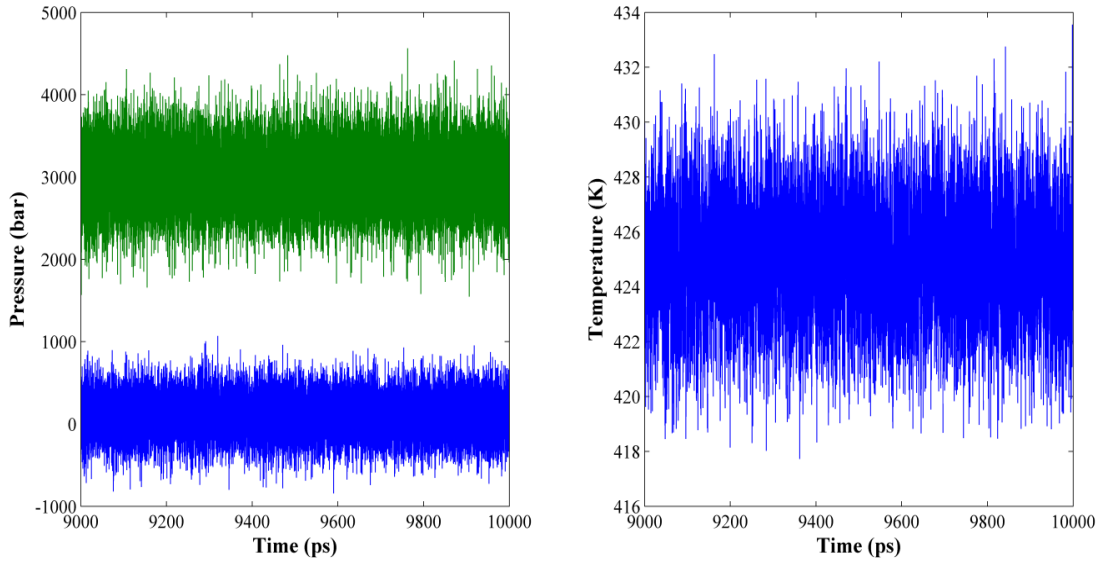

Figure 5.1. Pressure fluctuations (left) around target values of 100 and 3000 bar (425 K); Temperature fluctuation (right) around target temperature of 425 K (100 bar) for PE solution of 20 wt%.

Figure 5.2 illustrates the time evolution of density profiles for model systems of 4PE240-2800Hexane (10 wt%), 4PE240-1200Hexane (20 wt%), and 4PE240-730Hexane (30 wt%) where densities have reached an equilibrium value. The accuracy of the force field OPLS-AA was examined by comparing the equilibrated densities as a function of pressure for different polymer solution concentrations of 10-30 wt%. As depicted in Figure 5.3 simulated densities are in very good quantitative agreement with the experimental data. The simulation results are comparable with that of the previous experimental work done for 5.7 wt% solution of PE but of different molecular weight in pentane.[25] The density of PE solution models as a function of pressure are also compared with the densities modeled using the MSL EOS theoretical method and the model parameters summarized in Table 5.1. The NPT predicted densities show an increase with PE concentration from 10 to 30 wt%. However, the mixture density becomes less sensitive to PE concentration with raising pressure. In addition, densities indicate a monotonic increase as a result of pressure change from 100 to 1000/3000 bar for the three above mentioned models. This behavior is attributed to the absolute non-bonded interaction energies that increase with pressure, as discussed below (see Table 5.2). Astonishingly, the densities as a function of pressure may be described in the entire investigated pressure range by a power regression type with R-squared value of 1 (see Figure 5.4).

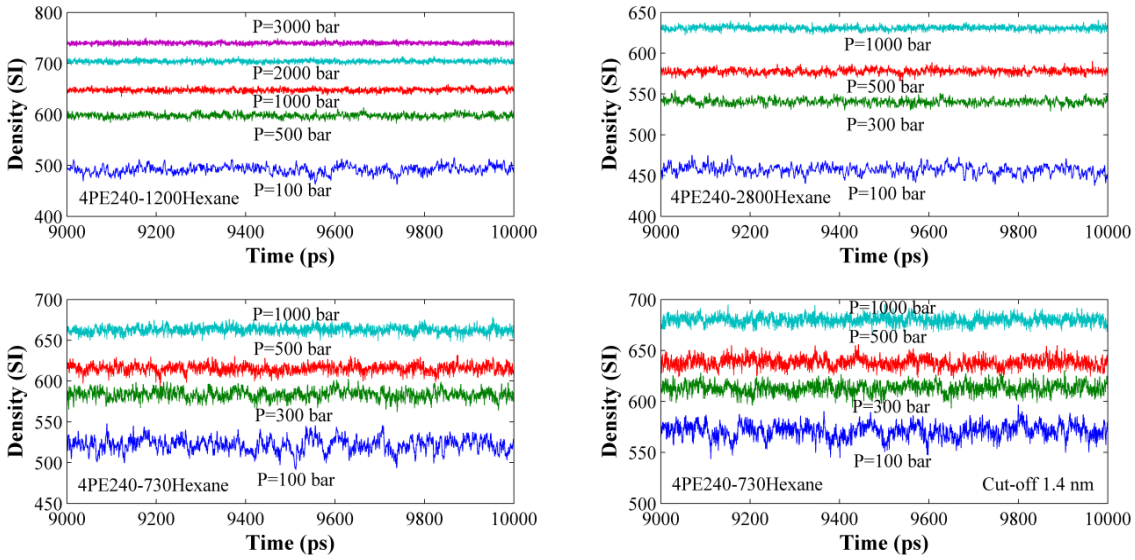

Figure 5.2. Time evolution of densities for PE solutions of 10 wt% (4PE240-2800Hexane), 20 wt% (4PE240-1200Hexane), 30 wt% (4PE240-730Hexane) obtained by NPT-MD simulations at different external pressures of 100, 300, 500, 1000, 2000, and 3000 bar.

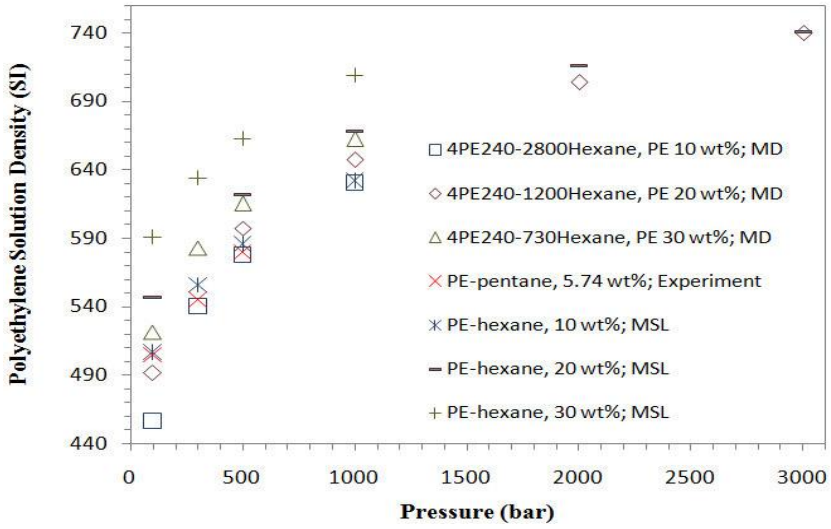

Figure 5.3. Variation of density with pressure for solutions of 10, 20, and 30 wt% PE in hexane using MD simulations and EOS modeling.

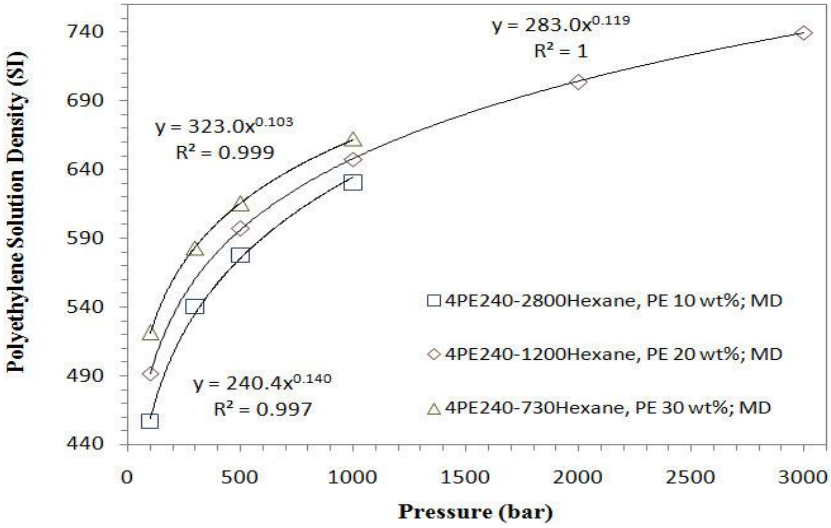

Figure 5.4. Variation of density with pressure for solutions of 10, 20, and 30 wt% PE in hexane based on constant pressure-constant temperature MD simulations.

It is noteworthy that the EOS predicted solution densities based upon the MSL-type 1 and 2 models produce identical densities with the provided model parameters. The averaged potential energies (listed in Table 5.2) were calculated at varied pressures for different model systems. As may be inferred from the total energy breakdown, the difference in total system energies is mainly due to the Lennard-Jones interactions and the remaining terms do not demonstrate significant pressure dependence. Consequently,

increase in the polymer solution density is due to the increase in Lennard-Jones attractive potential resulting in higher density and shorter separation.

Table 5.2. Computed values of energy components (kJ/mol) for PE in hexane models at 425 K.

Model System	P (bar)	Bonds	Angles	Torsions	Lennard-Jones	Electrostatics	Kinetic
	100	51309.1	78312.9	21662.3	-28449.2	11485.6	157783
	500	51172.9	78339	21668.1	-34793.8	11463.4	157783
4PE240-1200Hexane	1000	51062.8	78313.2	21650.8	-38279.9	11465.8	157783
Cut-off 1 nm	2000	50900.7	78322.4	21660.6	-42255.6	11441.2	157783
	3000	50800.6	78311.2	21707.3	-44657.1	11393.8	157783
	100	105838	160795	43026.3	-55289.3	23293.2	327401
4PE240-2800Hexane	300	105601	160820	43041.2	-65023.9	23273.6	327401
Cut-off 1 nm	500	105540	160809	43032.2	-70123.6	23266.9	327401
	1000	105355	160775	43036.2	-77763.8	23235.9	327401
	100	35292.1	54114.7	15436.2	-20542.2	7980.4	107960
4PE240-730Hexane	300	35229.8	54110.4	15388.7	-22997	7998.2	107960
Cut-off 1 nm	500	35207	54090.6	15414.9	-24408	7991.6	107960
	1000	35112.5	54105.9	15398.8	-26681.7	7986.8	107960

Figure 5.5 (right) illustrates the total van der Waals (vdW) energy fluctuations obtained from the last 1 ns of the MD simulations for 4PE240-730Hexane model at external pressures of 100, 300, 500, and 1000 bar where the vdW energy decreases with increasing pressure. To gain a better insight on the interaction energy terms that play major role in such pressure dependence, the breakdown of vdW energy were obtained. Figure 5.5 (left) indicates that the PE-hexane and hexane-hexane short range interaction energies are more sensitive to pressure changes and PE-PE binary interactions demonstrate less sensitivity to pressure.

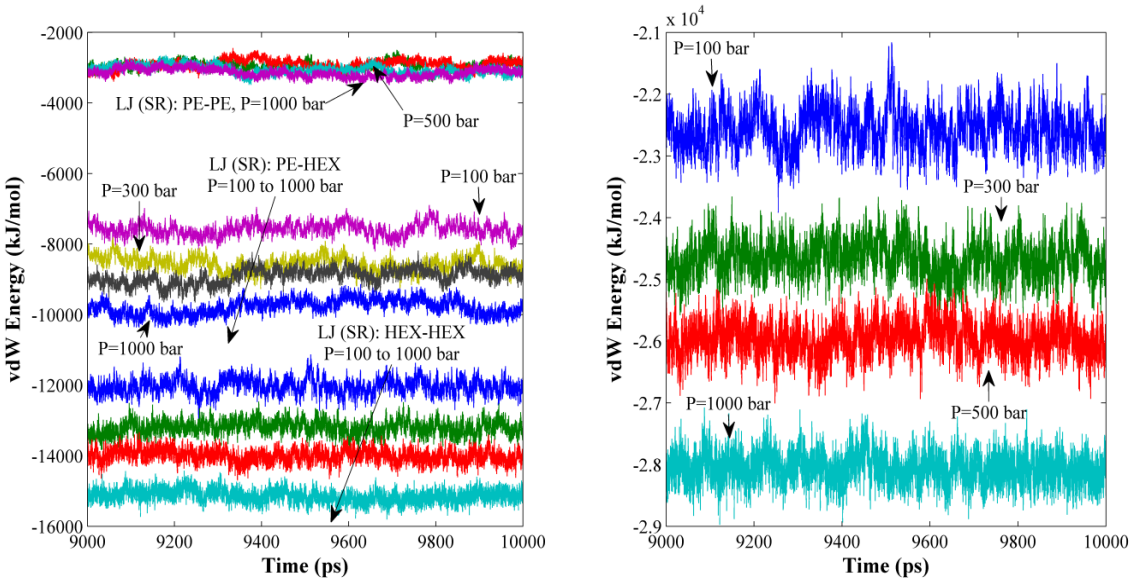

Figure 5.5. Time evolution of total (right) and breakdown (left) of vdW energy for 4PE240-730Hexane model (30 wt% PE solution) at pressures of 100, 300, 500, and 1000 bar.

5.4.2 Effect of Cut-off Radius on PE Solution Density

The effect of cut-off distance on polymer solution density has been also investigated. To achieve this, three neighbor lists with cut-off distance of 1.25, 1.35, and 1.65 nm and update frequency of every 10 steps was used for calculating the non-bonded interactions in the model system of 4PE240-730Hexane. The Lennard-Jones and electrostatic potentials are decreased over the range and the forces decay smoothly to zero between 0.9-1, 1-1.1, and 1.3-1.4 nm, respectively for the above mentioned neighbor search cut-offs of short range interactions. Table 5.3 shows the averaged potential energies with different cut-off radii. As can be seen in Figure 5.2 the 4PE240-730Hexane model with 1.4 nm cut-off (bottom-right) produces higher equilibrated densities compared to 4PE240-730Hexane with 1 nm cut-off (bottom-left). Figure 5.6 presents polymer solution densities versus system pressure for the aforementioned cut-offs. The MD results indicate that a better agreement with the MSL predictions may be achieved by increasing the cut-off distance from 1 to 1.4 nm. This agreement which is particularly noticeable at low pressures reduces the difference in predicted values at 100 bar from 11% in case of 1 nm cut-off to 6 and 3% for cut-off radii of 1.1 and 1.4 nm, respectively. For 300, 500, and 1000 bar a difference of 8, 7, 6% (cut-off 1 nm), 5, 5, 5% (cut-off 1.1 nm), and 3, 3, 4% (cut-off 1.4 nm) has been observed,

respectively, indicating that the effect of cut-off radius of intermolecular potentials decays with raising the external pressure, discussed below. Similar to the pressure study, as may be inferred from the total energy breakdown, the difference in total system energies as a result of change in cut-off distance is mainly due to the Lennard-Jones interactions not electrostatic energy contribution.

Table 5.3. Computed values of energy components (kJ/mol) for 4PE240-730Hexane models at 425 K.

Model System	P (bar)	Bonds	Angles	Torsions	Lennard-Jones	Electrostatics	Kinetic
	100	35292.1	54114.7	15436.2	-20542.2	7980.4	107960
4PE240-730Hexane	300	35229.8	54110.4	15388.7	-22997	7998.2	107960
Cut-off 1 nm	500	35207	54090.6	15414.9	-24408	7991.6	107960
	1000	35112.5	54105.9	15398.8	-26681.7	7986.8	107960
	100	35261.6	54136.4	15527.8	-22575.8	8905.7	107960
4PE240-730Hexane	300	35218.5	54102.5	15463.8	-24676.1	8896.8	107960
Cut-off 1.1 nm	500	35197.7	54112.8	15530.8	-25968	8834.6	107960
	1000	35118.7	54108.4	15521.2	-28063.7	8797.1	107960
	100	35236.2	54113.9	15507.8	-24769.4	9380.8	107960
4PE240-730Hexane	300	35195.1	54125	15465.4	-26728.8	9383.8	107960
Cut-off 1.4 nm	500	35161.7	54140.2	15501.9	-28020.2	9346.9	107960
	1000	35080.6	54113.4	15454.5	-30229.5	9338.3	107960

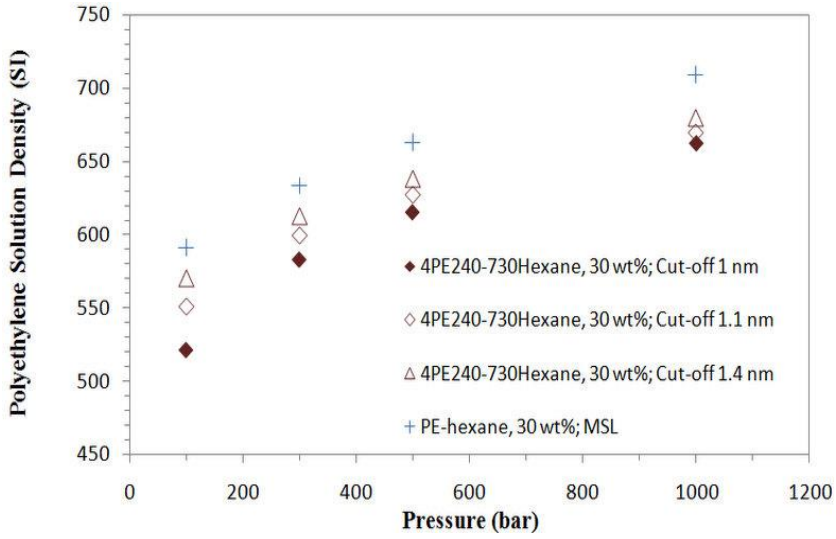

Figure 5.6. Impact of cut-off radius of intermolecular potential energy on the mixture density in the pressure range of 100-1000 bar at 425 K.

Figure 5.7 (right) illustrates the total vdW energy fluctuations obtained from the last 1 ns of the MD simulations for three 4PE240-730Hexane models where cut-off radii is set to 1, 1.1, and 1.4 nm for external pressure of 100 bar. It may be concluded that the vdW energy decreases as cut-off radius increases. The breakdown of this energy contribution

(left) shows that the PE-hexane and hexane-hexane short range interaction energies are more sensitive to cut-off radius.

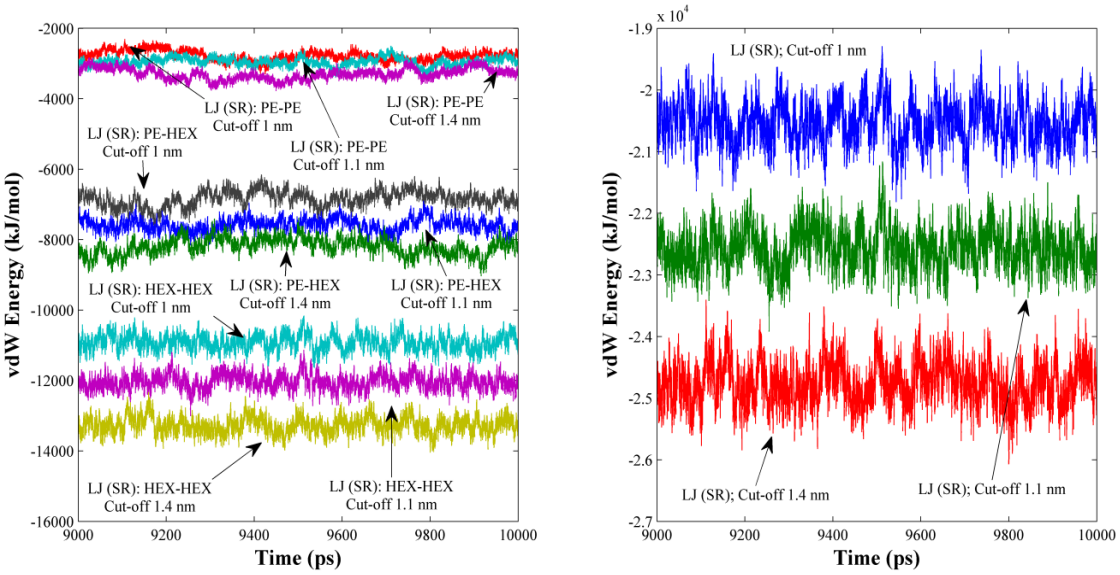

Figure 5.7. Time evolution of total (right) and breakdown (left) of vdW energy for 4PE240-730Hexane model (30 wt% PE solution) with cut-off radius of 1, 1.1, and 1.4 nm at 100 bar.

It is worth noting that the equilibrated densities corresponding to pressures above 100 bar display less dependence on the implemented cut-offs (see Table 5.4). At 100 bar, equilibrated density varies in the range of 522–571 which correspond to nearly 9% increase in the magnitude of solution density for a cut-off change from 1 to 1.4 nm. At 300 bar, an increase of 5% in density and for higher pressures nearly 3% increase in the magnitude of density for such a cut-off change is estimated. Additionally, at 100 bar, the computed density increases by 5% as a result of cut-off change from 1.1 to 1.4 nm and for higher pressures less than 2% increase in density is predicted. This suggests that for pressures below 100 bar, though reasonable densities can be predicted when the cut-off radius is set to 1 nm, a minimum cut-off of 1.1 nm is required for more accurate data.

Table 5.4. Densities obtained via NPT-MD simulations for varied cut-offs at 425 K.

Model System/ Cut-off	Density (SI)/MD versus MSL Error%			
	100 (bar)	**300 (bar)**	**500 (bar)**	**1000 (bar)**
4PE240-730Hexane/ 1 nm	522 (11%)	583 (8%)	615 (7%)	663 (6%)
4PE240-730Hexane/ 1.1 nm	551 (6%)	600 (5%)	627 (5%)	670 (5%)
4PE240-730Hexane/ 1.4 nm	571 (3%)	613 (3%)	638 (3%)	680 (4%)

5.4.3 Structural Analysis

Besides the influence of pressure and cut-offs on the binary polymer solution densities, the radius of gyration and end-to-end distance of polymer chains in the solution have been calculated and also the effect of external pressure (P=100, 500, 1000, 2000, and 3000 bar) on the radial distribution functions (RDFs) has been investigated. The structural stability was achieved in the first few nanoseconds; however, trajectories were analyzed in the last 1 ns of the runs to ensure that the structures are stabilized. Figure 5.8 reveals the radius of gyration of polymer at different external pressures and the end-to-end distance of four PE chains in the solution of 20 wt% at 3000 bar where an average end-to-end distance value of 8 nm has been observed. To examine the structure around a molecule the RDF is calculated and it is noticed that as pressure increases, the height of the first peak which occurs at a radius of nearly 0.5 nm, increases and the distribution function is shifted to the left, as illustrated in Figure 5.9 and Figure 5.10. This shift of the RDF as a result of pressure change is due to the increased local order upon increase in the intermolecular contribution (particularly dispersion forces) and subsequently density, as reported in Table 5.5. A magnified indication of the increased compactness of the structure at high pressure is noticed at a radius of 0.8-1 nm in the RDF for all carbon atoms (C-C) in PE and hexane system as well as PE-hexane carbons. A similar behavior has been observed for pure PE and hexane in liquid state.[11]

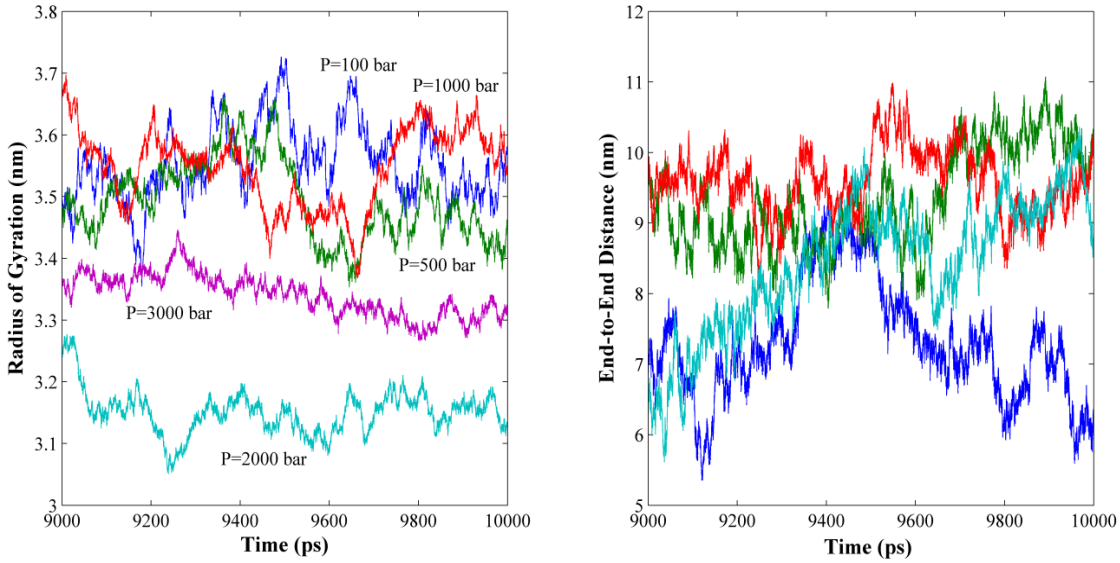

Figure 5.8. Radius of gyration (left) of PE at different external pressures of 100, 500, 1000, 2000, and 3000 bar. End-to-end distance (right) of PE chains for 4PE240-1200Hexane model at 3000 bar and 425 K.

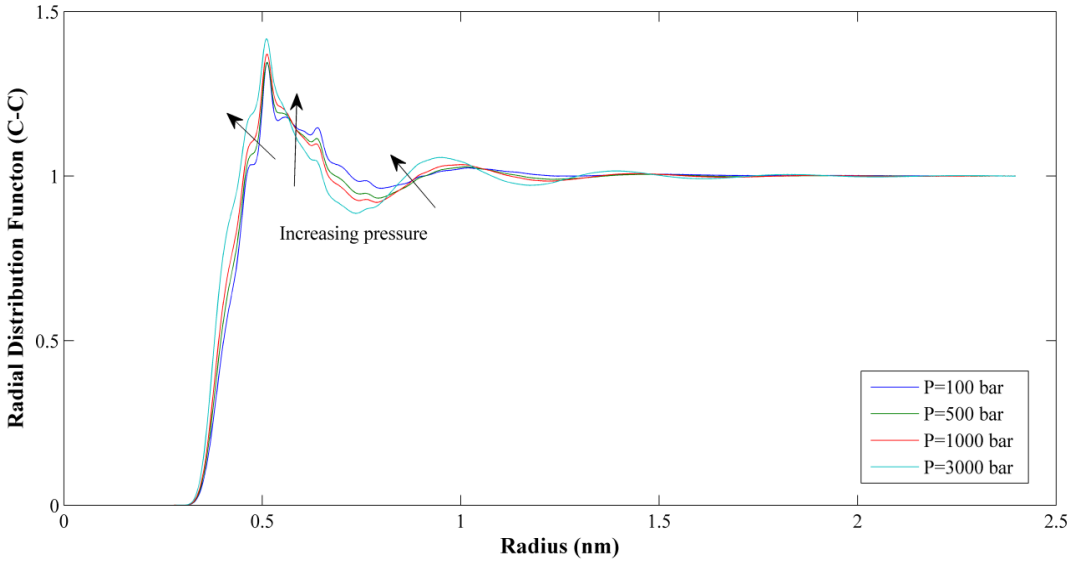

Figure 5.9. RDF for binary PE solution (all carbons) at different external pressures of 100, 500, 1000, 2000, and 3000 bar.

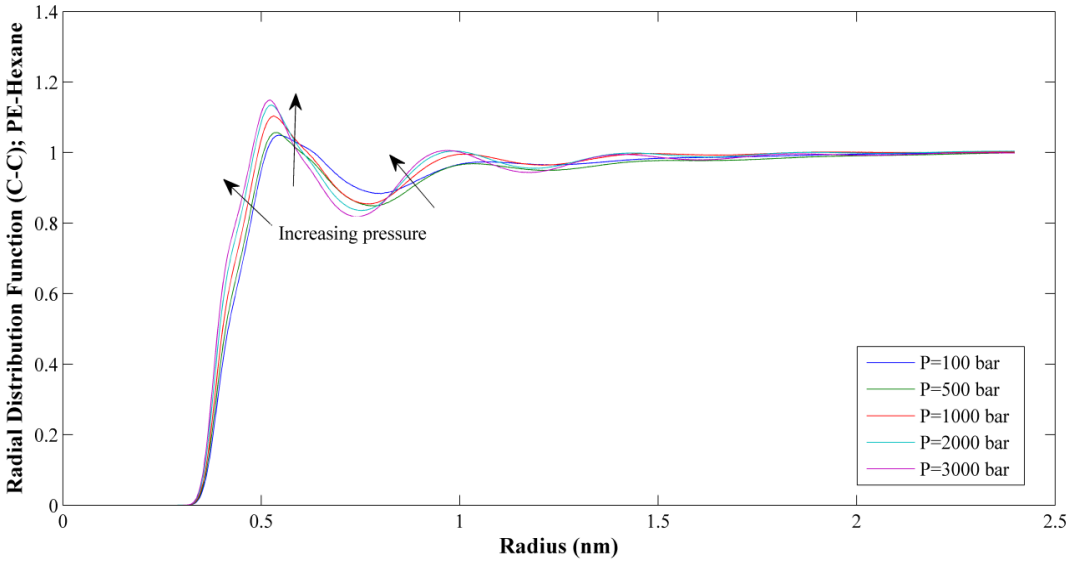

Figure 5.10. RDF for PE-hexane (PE carbons-hexane carbons) at different external pressures of 100, 500, 1000, 2000, and 3000 bar.

Table 5.5. PE solution densities computed by NPT-MD simulations at 425 K.

Model System/ Cut-off	Density (SI)				
	100 (bar)	300 (bar)	500 (bar)	1000 (bar)	2000, 3000 (bar)
4PE240-2800Hexane/ 1 nm	457	540	578	631	-
4PE240-1200Hexane/ 1 nm	492	-	597	647	704, 740
4PE240-730Hexane/ 1 nm	522	583	615	663	-

5.5 Conclusions

The potential energy and density of HDPE in hexane were computed by changing the pressure and cut-off radius for several model systems via MD technique on the basis of the OPLS-AA force field. It was shown that the solution density increases monotonically with increasing pressure for all model systems due to increase in the magnitude of Lennard-Jones interactive potential. Polymer solution densities were found to increase with polymer mass fraction; however, both pressure and concentration dependence of density tend to vanish with raising pressure. The electrostatic energy revealed no sensitivity to pressure variation indicating that the differences in densities versus pressure are essentially due to Lennard-Jones interaction energies not pressure-independent intramolecular or electrostatic energy contributions. PE solution densities were also calculated based on the MSL EOS

and it was revealed that the model produces identical mixture densities regardless of the type of the *b* parameter.

To investigate the cut-off radius effect, several group-based cut-off of 1, 1.1, and 1.4 nm were applied to evaluate the non-bonded interactions. The comparison of MD results with the MSL model predictions indicated that the estimated error may be lowered by increasing the cut-off radius. The NPT predicted densities have been found to be reasonable when the cut-off radius is larger than 1 nm; however, a more accurate representation of thermodynamic properties may be attained for a minimum cut-off of 1.1 nm while maintaining an affordable computational speed. The densities obtained by molecular simulations for 1 nm cut-off were slightly lower than the larger cut-off values since the magnitude of attractive vdW interactions increase with increasing cut-off radius. Nevertheless, our results predicted that the mixture density is relatively insensitive to the choice of cut-off beyond 1.1 nm especially for pressures beyond 100 bar. It should also be remarked that the molecular perspective provided by the employed MD technique is of great value in fundamental understanding of the changes in intra- and intermolecular interactions with pressure. The breakdown of vdW energy showed that the polymer-solvent and solvent-solvent short range interaction energies are more sensitive to pressure and cut-off radius than electrostatic potential energies.

Structural analysis of PE-solvent mixture revealed noticeable difference in the RDF (C-C atoms) where the height of the first peak increases and the pair distribution function shifts to shorter separations upon increasing pressure owing to increase in the positional compactness. This increase in the local order may be deduced from a increase of densities at high pressures which in turn stems from non-bonded interaction energies. There is a good agreement between simulated, theoretical EOS, and experimental density values, suggesting that molecular simulation strategy based upon the OPLS-AA force field adopted in this investigation provides reliable estimates of polyolefin solution densities at elevated pressures.

5.6 References

1. Ghiass, M.; Rey, A. D., Interfacial thermodynamics of compressible polymer solutions. *Journal of Chemical Physics* **2008,** *128* (7), 0711021-0711025.

2. Ghiass, M.; Rey, A. D., Interfacial properties of compressible polymer solutions. *Journal of Polymer Science Part B: Polymer Physics* **2009,** *47* (6), 640-654.
3. Ghiass, M.; Rey, A. D., Thermodynamic modeling of polymer solution interface. *Macromolecular Theory and Simulations* **2009,** *18* (2), 127-137.
4. Rasouli, G.; Rey, A. D., Acousto-spinodal decomposition of compressible polymer solutions: Early stage analysis. *Journal of Chemical Physics* **2011,** *134* (18), 1849011-18490119.
5. Sanchez, I. C.; Lacombe, R. H., An elementary molecular theory of classical fluids. Pure fluids. *Journal of Physical Chemistry* **1976,** *80* (21), 2352-2362.
6. Lacombe, R. H.; Sanchez, I. C., Statistical thermodynamics of fluid mixtures. *Journal of Physical Chemistry* **1976,** *80* (23), 2568-2580.
7. Sanchez, I. C.; Lacombe, R. H., Statistical thermodynamics of polymer solutions. *Macromolecules* **1978,** *11* (6), 1145-1156.
8. Koak, N.; Heidemann, R. A., Polymer-solvent phase behavior near the solvent vapor pressure. *Industrial & Engineering Chemistry Research* **1996,** *35* (11), 4301-4309.
9. Krenz, R. A.; Laursen, T.; Heidemann, R. A., The modified Sanchez-Lacombe equation of state applied to polydisperse polyethylene solutions. *Industrial & Engineering Chemistry Research* **2009,** *48* (23), 10664-10681.
10. Maranas, J. K.; Kumar, S. K.; Debenedetti, P. G.; Graessley, W. W.; Mondello, M.; Grest, G. S., Liquid structure, thermodynamics, and mixing behavior of saturated hydrocarbon polymers. 2. Pair distribution functions and the regularity of mixing. *Macromolecules* **1998,** *31* (20), 6998-7002.
11. Shahamat, M.; Rey, A. D., Characterization of pressure effects on the cohesive properties and structure of hexane and polyethylene using molecular dynamics simulations. *Macromolecular Theory and Simulations* **2012,** *21* (8), 535-543.
12. Shahamat, M.; Rey, A. D., High pressure miscibility predictions of polyethylene in hexane solutions based on molecular dynamics. *European Polymer Journal* **2013,** *49* (2), 471-481.
13. Berendsen, H. J. C.; van der Spoel, D.; van Drunen, R., Gromacs: A message-passing parallel molecular dynamics implementation. *Computer Physics Communications* **1995,** *91* (1-3), 43-56.
14. Lindahl, E.; Hess, B.; van der Spoel, D., GROMACS 3.0: A package for molecular simulation and trajectory analysis. *Journal of Molecular Modeling* **2001,** *7* (8), 306-317.
15. van der Spoel, D.; Lindahl, E.; Hess, B.; Groenhof, G.; Mark, A. E.; Berendsen, H. J. C., GROMACS: Fast, flexible, and free. *Journal of Computational Chemistry* **2005,** *26* (16), 1701-1718.
16. Hess, B.; Kutzner, C.; van der Spoel, D.; Lindahl, E., GROMACS 4: Algorithms for highly efficient, load-balanced, and scalable molecular simulation. *Journal of Chemical Theory and Computation* **2008,** *4* (3), 435-447.
17. Jorgensen, W. L.; Madura, J. D.; Swenson, C. J., Optimized intermolecular potential functions for liquid hydrocarbons. *Journal of the American Chemical Society* **1984,** *106* (22), 6638-6646.
18. Shahamat, M.; Rey, A. D., Molecular thermodynamic characterization of LCST fluid phase behavior and exploring electrostatic algorithms to compute polymer/solvent solubility parameters in the canonical ensemble. *Polymer* **2013,** *54* (18), 4997-5004.

19. van der Spoel, D.; van Maaren, P. J., The origin of layer structure artifacts in simulations of liquid water. *Journal of Chemical Theory and Computation* **2006,** *2* (1), 1-11.
20. Berendsen, H. J. C.; Postma, J. P. M.; van Gunsteren, W. F.; Dinola, A.; Haak, J. R., Molecular dynamics with coupling to an external bath. *Journal of Chemical Physics* **1984,** *81* (8), 3684-3690.
21. Parrinello, M.; Rahman, A., Polymorphic transitions in single crystals: A new molecular dynamics method. *Journal of Applied Physics* **1981,** *52* (12), 7182-7190.
22. Bussi, G.; Donadio, D.; Parrinello, M., Canonical sampling through velocity rescaling. *Journal of Chemical Physics* **2007,** *126* (1), 014101.
23. Nagy, I.; de Loos, T. W.; Krenz, R. A.; Heidemann, R. A., High pressure phase equilibria in the systems linear low density polyethylene + n-hexane and linear low density polyethylene + n-hexane + ethylene: Experimental results and modelling with the Sanchez-Lacombe equation of state. *Journal of Supercritical Fluids* **2006,** *37* (1), 115-124.
24. Krenz, R. A.; Heidemann, R. A., Modelling the fluid phase behaviour of polydisperse polyethylene blends in hydrocarbons using the modified Sanchez-Lacombe equation of state. *Fluid Phase Equilibria* **2007,** *262* (1-2), 217-226.
25. Dindar, C.; Kiran, E., High-pressure viscosity and density of polymer solutions at the critical polymer concentration in near-critical and supercritical fluids. *Industrial & Engineering Chemistry Research* **2002,** *41* (25), 6354-6362.

6 Equation of State Modeling and Force Field-Based Molecular Dynamics Simulations of Supercritical Polyethylene + Hexane + Ethylene Systems

6.1 Summary

Understanding of polymer solution thermodynamics and characterization of pressure effects on fundamental polymer physics of macromolecular systems is significant in the manufacturing of polyolefins. Consequently, numerous experimental and theoretical efforts have been made towards understanding phase behavior of polymer solutions at elevated pressures. Despite this progress, only limited efforts are directed towards understanding the underlying phenomena behind the influence of high pressure upon the thermophysical properties of ternary polymer solutions at a molecular level. The present paper, therefore, reports on the influence of supercritical ethylene, the unreacted monomer in the solution polymerization process used in PE manufacturing, on the density of PE + hydrocarbon solvent system by exploring ternary mixtures of PE + hexane + ethylene for ethylene concentrations up to 10 wt% at varied temperatures and in a pressure range from 100 to 1000 bar via fully-atomistic molecular dynamics (MD) simulations. Additionally, the modified Sanchez-Lacombe equation of state (EOS) model is iteratively solved to capture the pressure, concentration, and temperature dependence of ternary PE solution density. It is shown that the small amounts of ethylene dissolved in the liquid mixtures of PE + hexane decreases significantly the polymer solution density. Nonetheless, pressure, solvent composition, and temperature dependence of density display less sensitivity as pressure increases. In relation to the characterization of the impact of addition of ethylene an atomistic-level insight is provided, which proves to be of great value in revealing intermolecular interactions in the binary subsystems of polymer/solvent/monomer. The MD

computations are shown to be in excellent agreement with the theoretical EOS model, confirming the validity of the proposed methodology. Furthermore, the OPLS-AA has been found a reliable atomistic force field, which provides detailed molecular information on the thermophysical properties of polyolefin in hydrocarbon solutions. Ultimately, it is demonstrated that the MD simulations complement parametric EOS predictions and costly experimental approaches.

6.2 Introduction

The phase behavior and thermodynamics of polymer solutions have been topics of great academic and commercial interest within the last several decades owing to the fact that the design of a large number of industrial chemical processes is associated with separation and equilibrium thermodynamics of polymer-solvent systems. As an example, in the industrial solution polymerization of polyethylene (PE) it is of great importance that the solution remains homogeneous during the actual polymerization to avoid poor flow characteristic and high-viscosity issues as a result of forming a viscous polymer within one of the phases. In addition, solvent and unreacted ethylene are recovered as vapors by reducing the pressure to bring the one-phase mixture into the vapor-liquid or vapor-liquid-liquid region. Moreover, data on thermodynamic and physical properties of multicomponent mixtures are critically important to the development and operation of the separation process.

It has been recognized that the addition of a small amount of ethylene, which is a monomer in the polymerization reaction for PE, to PE + hexane mixture is more representative of an industrial solution polymerization process. The presence of unreacted monomer significantly influences the phase equilibria, which consequently affects all subsequent processing of the polymer solution. Considerable research has for this reason been performed on the phase equilibria of PE solutions, which involve costly and time-consuming experimental work. Thus, a great deal of effort has been expended to develop alternatives to experimental methods for correlating and predicting the solubility in such polymer-solvent mixtures; e.g. various equations of state have been proposed and modified to predict polymer-solvent phase behaviour. These models have become important tools in process design and development because they are accurate and easy to implement. A few of

the more common are the Sanchez-Lacombe[1-3] (SL) and the modified SL[4] (MSL) equation of state (EOS) models, which provide a good fit of the experimental data, despite of their relative computational simplicity. Nevertheless, application of these equations of state for mixtures requires the accurate value of several model parameters (e.g. interaction parameter), which involves fitting the model to the difficult to access experimental data. Hence, estimation of the characteristic parameters, appearing in the EOS model, is a problem of profound importance for the thermodynamic analysis of chemical processes. Furthermore, to our knowledge those investigations were never directed towards molecular-level understanding of the pressure effects on thermophysical properties of ternary mixtures of PE in hydrocarbons.

With the fast progress of computer hardware and calculation algorithms, computer simulations of molecular systems, which enable computing macroscopic phenomena based on microscopic interactions, have significantly grown during the past decade.[5-7] The force field methods, which ignore the details of electron-electron and electron-nucleon interactions, utilize a set of empirical formulas to mimic the interatomic interactions. When dealing with large molecular systems and molecules in condensed phases, the empirical force-fields have an incomparable advantage over ab initio methods owing to the fact that force fields are several order of magnitude faster than ab initio calculations.

The present paper aims to explore the impact of high pressure on density of ternary mixture of PE + hexane + ethylene based on the isobaric-isothermal (NPT) force field-molecular dynamics (MD) computations and the modified SL EOS model. The adopted molecular simulation methodology enables understanding of the influence of adding supercritical ethylene to the binary solution of PE in hexane based on a molecular perspective, which has not yet been precisely characterized.

The organization of this paper is as follows. The methodology section presents the computational modeling methods and a detailed model description for conducting NPT simulations. The results and discussion section investigates the impact of pressure and temperature upon the density of supercritical PE + hexane + ethylene system for several ethylene mass fractions based on NPT-MD simulations together with the EOS modeling. Furthermore, the impact of unreacted monomer ethylene on the PE solution density is discussed. The final section summarizes findings and gives some concluding remarks.

6.3 System Set-up and Computational Method

6.3.1 Molecular Mechanics Model

In the present work the GROMACS,[8-11] molecular dynamics program version 4.5.4 has been employed with the force field OPLS-AA[12] parameters, which is appropriate for liquid hydrocarbon systems. For all the simulation runs, we have used quad-core AMD processors, running under CentOS/Linux. The total system energy was represented by the sum of bonded and non-bonded interactions. The molecular mechanics model incorporated the intramolecular interactions of covalent bond stretching (2-body), angle bending (3-body), and dihedral angle (4-body), which are based on a fixed list of atoms. The bond stretching and valence angle bending were described by harmonic forces and the energy due to twisting of the dihedral angle was treated by cosine series potentials. The non-bonded van der Waals (vdW) type of interaction was modeled by pairwise additive 12-6 Lennard-Jones and the electrostatic energy was evaluated based on charge groups to reduce the cut-off artifacts of coulomb interactions. A neighbor list, used for calculating the non-bonded vdW and electrostatic interactions, was kept to 13.5 A˚ and updated every 10 steps. The non-bonded interactions were treated by a shift function[13] with a group-based cut-off radius of 11 A˚ where potential functions were switched smoothly to zero over the region 10–11 A˚.

6.3.2 Molecular Dynamics Simulation Methodology

The molecular architecture of PE chains, hexane, and ethylene were built and the geometry was optimized by minimizing the energy of the structure. Subsequently four linear PE chains composed of 240 repeating units (4PE240) were placed in a low-density cubic simulation box with the 3-D periodic boundary conditions. Subsequently, the long polymer chains were solvated to generate ternary polymer solutions of 30 wt% PE/60 wt% hexane/10 wt% ethylene, 30 wt% PE/65 wt% hexane/5 wt% ethylene, and 30 wt% PE/67 wt% hexane/3 wt% ethylene, corresponding to 620/320, 670/170, and 700/100 hexane/ethylene molecules, respectively. These ternary model systems correspond to a total of 20,088, 20,188, and 20,368 atoms, respectively (notation 4PE240-620Hexane-320Ethylene represents a PE solution composed of 4 polymer chains solvated in 620 hexane and 320 ethylene molecules). Random overlaps were avoided by using the steepest

descent algorithm to energy minimize the initial molecular structures. In the next step, solvent molecules were allowed to relax by running a 500 ps MD simulation with position restraints applied on all the polymer atoms. The restraints were then removed from all atoms and a pressure-induced compression using the Berendsen barostat[14] algorithm was employed for 10 x 10^6 molecular dynamics steps of 1 fs (i.e. 10 ns of total time) to increase the gas density of the system close to the experimental density and to remove the unfavorable local minima with high energies.

On the basis of the fully relaxed models produced as described above, the isobaric-isothermal (NPT) simulations were conducted from the end of the previous relaxed 10 ns-NPT simulation for 5 ns where time steps were set to 0.5 fs at external pressures over a broad range of 100 to 1000 bar to achieve the equilibrium densities. Parrinello-Rahman barostat[15] with time constant of 1 ps and temperature coupling using velocity rescaling[16] with a relaxation constant of 0.1 were applied throughout the simulations to maintain the system pressure and temperature at the target values. The equations of motion were solved using a leap-frog integration step and the coordinates and energy values were stored at every 100 steps for the confirmation of the equilibration and analysis. The total energy, pressure, and density were monitored to ensure equilibration of the system and ultimately, the last 1 ns of each simulation was analyzed and used to explore the supercritical mixture.

6.3.3 Equation of State Model (modified SL)

The modified SL EOS is based on a compressible lattice-fluid model and therefore, it can describe the thermodynamics of compressible polymer solutions, especially for different molecular weights and polydisperse PE solutions. The model which is an extension of the SL EOS, involves three pure component parameters: d_i, the number of lattice sites occupied by molecule type *i*; v_i, the volume occupied by molecule of type *i*, and ε_i, the interaction energy of component *i*. These parameters are determined for each pure component using *PVT* data.

By applying the mass fraction-based parameters in the form of linear/quadratic mixing rules where $b_i = d_i v_i$, the homogenous specific Helmholtz free energy per unit mass of polymer solution is:

$$\frac{A_m}{RT} = -\frac{\rho a_m}{RT} + \frac{d_m}{\rho b_m}(1-\rho b_m)\ln(1-\rho b_m) + \sum_{i=1}^{N_c}\frac{\omega_i}{M_i}\ln\left(\frac{\omega_i \frac{d_i}{M_i} b_m \rho}{d_m}\right) \tag{6.1}$$

$$\begin{aligned} d_m &= \sum_{i=1}^{N_c} \omega_i \frac{d_i}{M_i} \\ b_m &= \sum_{i=1}^{N_c} \omega_i \frac{b_i}{M_i} = \sum_{i=1}^{N_c} \omega_i \frac{d_i}{M_i} \nu_i \\ a_m &= \sum_{i=1}^{N_c}\sum_{j=1}^{N_c} \omega_i \omega_j \frac{d_i}{M_i}\frac{d_j}{M_j}\frac{(\nu_i + \nu_j)}{2}\varepsilon_{ij} \\ \varepsilon_{ij} &= (1-K_{ij})\sqrt{\varepsilon_i \varepsilon_j} \end{aligned} \tag{6.2}$$

where N_c denotes the number of components, M_i and ω_i indicate the molecular weight and mass fraction of component *i*, and the equivalent mass-based parameters of *d*, *b*, and *a* were respectively obtained as: $d_m = \frac{d}{M}$, $b_m = \frac{b}{M^2}$, and $a_m = \frac{a}{M^2}$. ε_{ij}, denotes the attractive energy parameter between components of type *i* and the binary interaction parameter for the mixture is:

$$K_{ij} = K_{ij}^a + K_{ij}^b T \tag{6.3}$$

where K_{ij}^a and K_{ij}^b are respectively the temperature-independent and temperature-dependent parts of the binary interaction parameter, and *T* is absolute temperature.

The pure compound parameters[17-18] for PE, hexane, and ethylene are summarized in Table 6.1. The EOS is obtained by differentiation of the Helmholtz energy with respect to the molar volume based on the linear and quadratic rules for the mass fraction-based model parameters as given below:

$$\frac{P}{RT} = -\frac{\rho^2 a_m}{RT} - \frac{d_m}{b_m}\ln\left(1-\rho b_m\right) + \frac{\rho}{M} - \rho d_m \qquad (6.4)$$

The EOS needs to be solved iteratively to describe the ternary polymer solution density as a function of pressure for different polymer mass fractions.

Table 6.1. Modified SL EOS pure compound and interaction parameters.

Parameter	HDPE	Hexane	Ethylene
Number of occupied lattice sites d_i/M_i (mol/g)	0.08644	0.1122	0.2271
Volume occupied per lattice site v_i (cm^3/mol)	8.181	12.55	7.471
Energy per lattice site ε_i (J/mol)	4280	3685	2288
Binary interaction parameters: K_{ij}=-1.708x10^{-1}+3.357x10^{-4}T(PE-hexane); K_{ij}=-5.453x10^{-2}+2.05x10^{-4}T (PE-ethylene) K_{ij}=-1.52x10^{-1}+4.405x10^{-4}T(hexane-ethylene)			

6.4 Results and Discussion

Isobaric-isothermal thermodynamic ensemble simulations were employed to investigate the pressure dependence of potential energy contributions and densities. Figure 6.1 (top-left) illustrates the time evolution of density profile for ternary polymer solutions of 30 wt% PE in 55 wt% hexane/15 wt% ethylene, 60 wt% hexane/10 wt% ethylene, and 65 wt% hexane/5 wt% ethylene where pressure coupling was used to increase the ternary mixture density close to the experimental values. The time evolution of density fluctuations are illustrated in Figure 6.1 for 30 wt% ternary PE solutions containing 5, 10, and 15 wt% ethylene obtained from the last 1 ns of the MD production runs. The density of ternary PE solution models as a function of pressure are also calculated using the MSL EOS theoretical method to examine the accuracy of the MD results for different ethylene concentrations at 425 K (see Table 6.2). The MD and EOS predicted densities, presented in Figure 6.2, suggest that the addition of co-solvent ethylene to the binary solution of PE in hexane produces lower mixture density as compared to the binary solutions with the same polymer mass fraction; nevertheless, the mixture density becomes less sensitive to ethylene concentration as external pressure increases. In addition, densities indicate a monotonic increase as a result of pressure change from 100 to 1000 bar. This behavior is attributed to the absolute non-bonded interaction energies that increase with pressure, discussed below.

As illustrated in Figure 6.3 the ternary solution density as a function of pressure may be described in the entire investigated pressure range by a power regression type with R-squared value of 1.

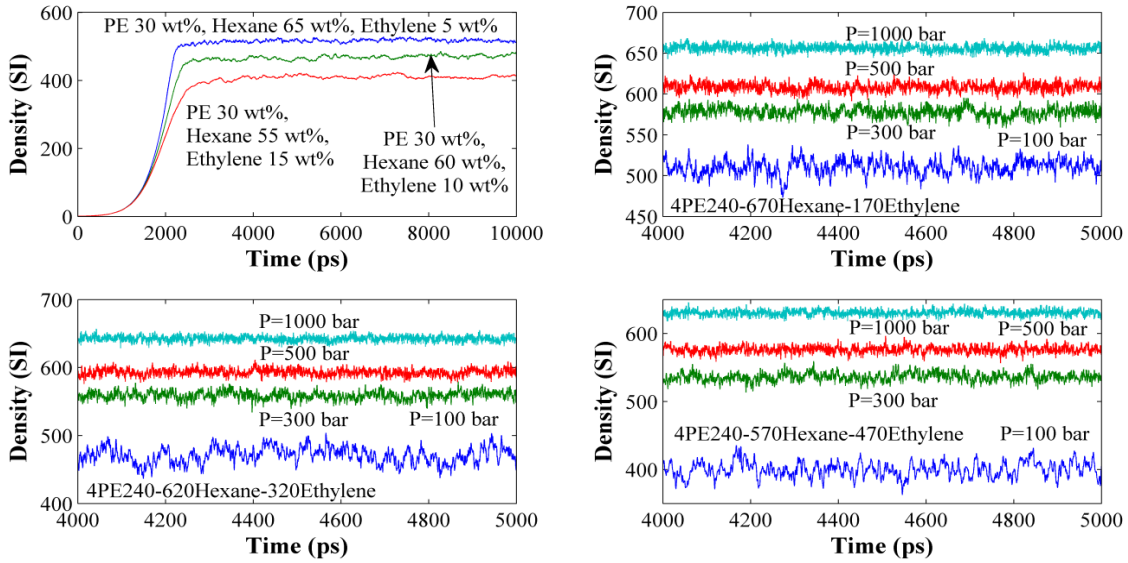

Figure 6.1. Density profiles during compression to equilibrate the polymer solution and to achieve the experimental density (top-left). Time evolution of densities for PE-hexane-ethylene solutions of respectively 30/65/5 wt% (4PE240-670Hexane-170Ethylene), 30/60/10 wt% (4PE240-620Hexane-320Ethylene), 30/55/15 wt% (4PE240-570Hexane-470Ethylene) obtained by NPT-MD simulations at different external pressures of 100, 300, 500, and 1000 bar.

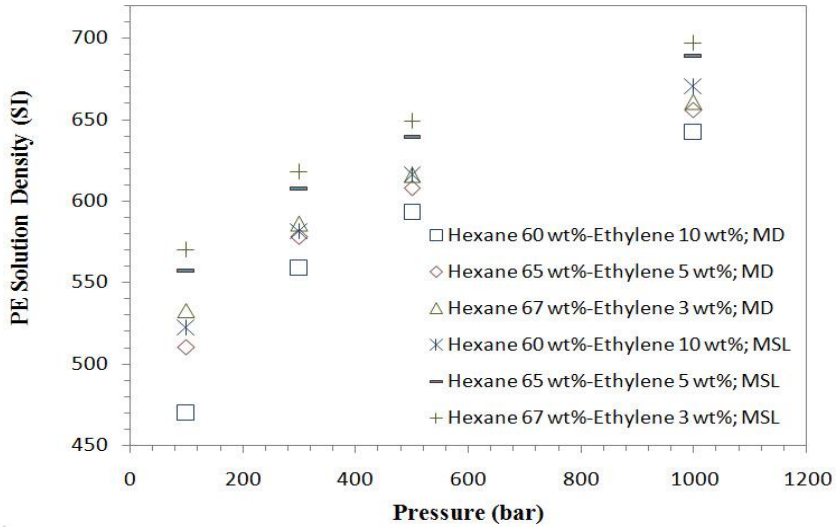

Figure 6.2. Variation of density with pressure for ternary solutions of PE (30 wt%)/ethylene (10, 5, 3 wt%). The squares, diamonds, and triangles represent simulation data at 425 K. The asterisk, dash, and cross symbols represent densities predicted by the MSL EOS.

Table 6.2. Densities computed via NPT-MD simulations for ternary PE solutions at 425 K.

Ternary Model System/Ethylene Content	Density (SI)/MD vs. MSL Error%			
	100 (bar)	**300 (bar)**	**500 (bar)**	**1000 (bar)**
4PE240-620Hexane-320Ethylene (10%)	470 (10%)	559 (3%)	593 (3%)	642 (4%)
4PE240-670Hexane-170Ethylene (5%)	510 (8%)	578 (4%)	608 (4%)	656 (4%)
4PE240-700Hexane-100Ethylene (3%)	533 (6%)	586 (5%)	616 (5%)	661 (5%)

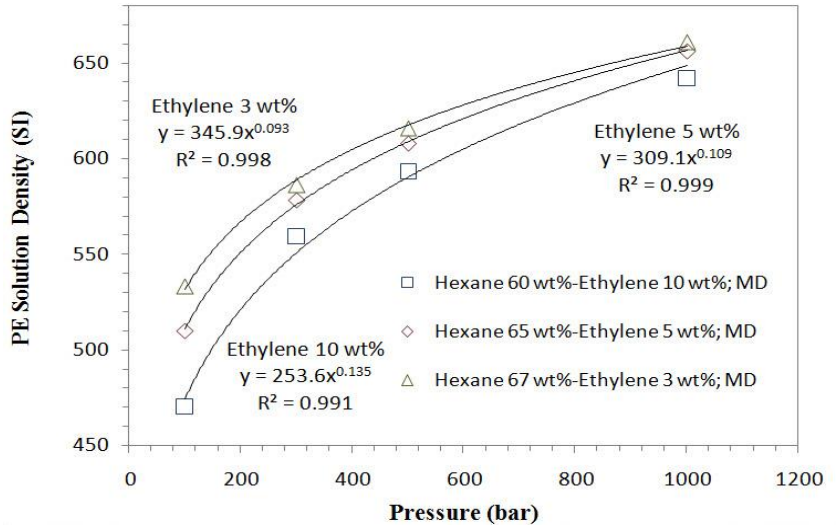

Figure 6.3. Pressure dependence of ternary PE + hexane + ethylene solution densities shown in power equation for ethylene (co-solvent) concentrations of 10, 5, and 3 wt% at constant PE mass fraction of 0.3.

Figure 6.4 illustrates the fluctuation profiles in the total vdW and electrostatic energies during MD simulations for 4PE240-620Hexane-320Ethylene model corresponding to a ternary polymer solution of PE (30 wt%)/hexane (60 wt%)/ethylene (10 wt%) at the external pressures of 100, 300, 500, and 1000 bar. It is found that the difference in the non-bonded energies as a result of pressure variation is mainly due to the Lennard-Jones interactions while the electrostatic energy reveals no sensitivity. To gain a better insight into the vdW interactions that play major role in such pressure dependence, the breakdown of total vdW energy is provided. As depicted in Figure 6.5, which shows the time evolution of breakdown of vdW energy for the ternary PE solution of PE (30 wt%)/hexane (60 wt%)/ethylene (10 wt%), the PE-PE and ethylene-ethylene binary interactions are the pressure independent contributions. Thus, it may be concluded that the differences in densities of PE + hexane + ethylene system are essentially due to PE-solvent, hexane-hexane/ethylene Lennard-Jones interaction energies. Also none of the binary electrostatic energy terms contribute to variations of mixture volume upon changing pressure as shown in Figure 6.6.

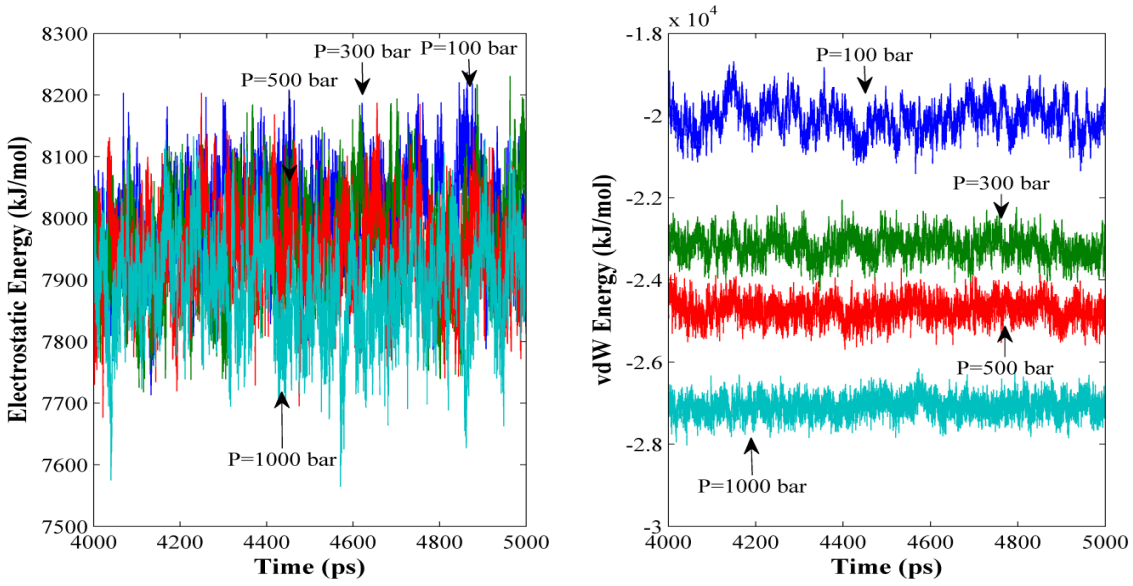

Figure 6.4. Time evolution of total electrostatic (left) and vdW energy (right) for 4PE240-620Hexane-320Ethylene model corresponding to ternary PE solution of PE (30 wt%)/hexane (60 wt%)/ethylene (10 wt%) at pressures of 100, 300, 500, and 1000 bar.

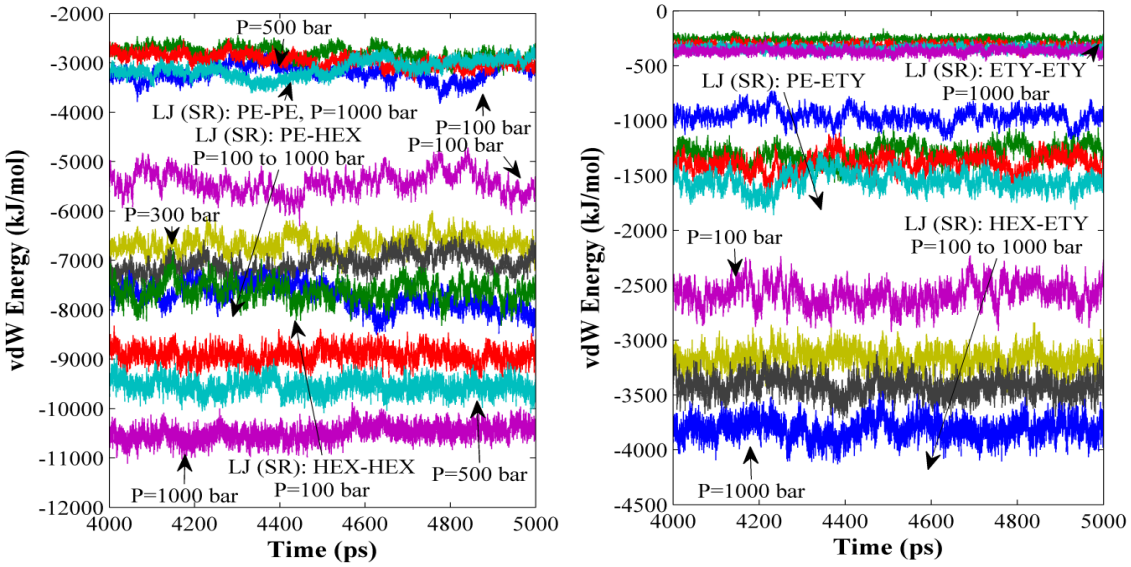

Figure 6.5. Time evolution of breakdown of vdW energy for 4PE240-620Hexane-320Ethylene model corresponding to ternary PE solution of PE (30 wt%)/hexane (60 wt%)/ethylene (10 wt%) at pressures of 100, 300, 500, and 1000 bar.

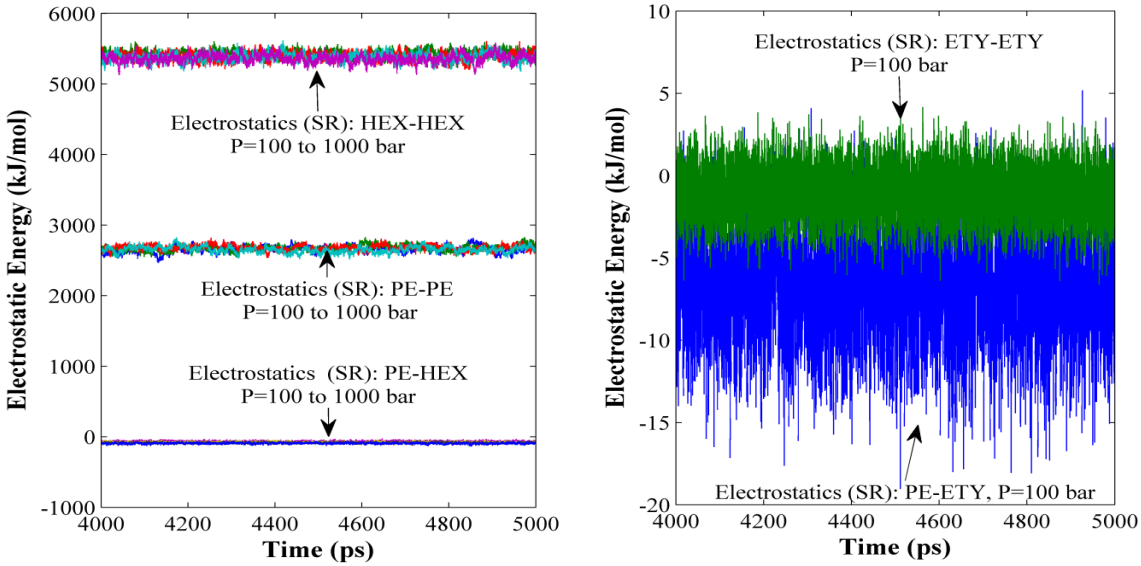

Figure 6.6. Time evolution of breakdown of electrostatic energy for 4PE240-620Hexane-320Ethylene model corresponding to ternary PE solution of PE (30 wt%)/hexane (60 wt%)/ethylene (10 wt%) at pressures of 100, 300, 500, and 1000 bar.

Table 6.3 reports on the change in the binary solution density due to unreacted monomer ethylene at varied pressures and mass fractions. This volume change upon

dissolving supercritical ethylene is particularly noticeable at lower pressures. At 100 bar, the computed binary solution density decreases by 7 and 15%, as a result of adding 5 and 10 wt% ethylene. This significant density reduction, consequently, influences design and operation of the liquid-liquid phase separator in manufacturing of PE via solution polymerization. For 300, 500, and 1000 bar a volume decrease of 7, 5, and 4% has been observed due to 10 wt% ethylene added, respectively, indicating that the impact of unreacted monomer in polyolefin solution decays with raising the external pressure.

Table 6.3. Density change due to adding co-solvent ethylene to PE + hexane binary mixture at 425 K.

Added Ethylene in wt%	**Density Change%**			
	100 (bar)	**300 (bar)**	**500 (bar)**	**1000 (bar)**
10%	15%	7%	5%	4%
5%	7%	4%	3%	2%
3%	3%	2%	2%	1%
0%- Binary Density (SI)	551	600	627	670

In Figure 6.7 and Figure 6.8 the results of MD calculations along with the MSL model at various temperatures for ethylene concentrations of 10 and 3 wt% are plotted. The system pressure varies between 100 and 1000 bar. The full, dotted, and dashed curves are the results of the MD simulations at 425, 450, and 475 K, respectively. It is clearly seen that the mixture density decreases with increasing temperature and the effect of temperature decays as pressure increases. These figures illustrate that the quality of the fits are very good and that the MD simulations give a very good predictions of the influence of temperature on the ternary system density.

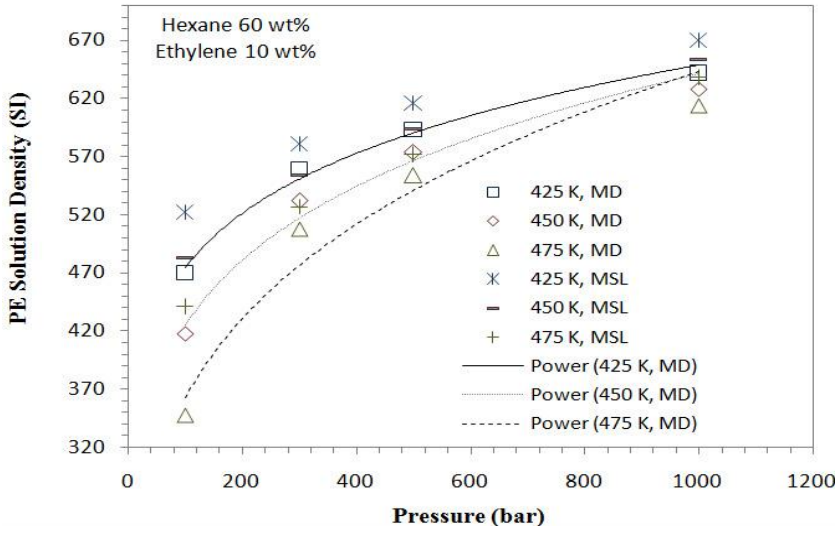

Figure 6.7. Pressure and temperature dependence of ternary PE + hexane + ethylene solution densities shown in power equation for ethylene (co-solvent) concentration of 10 wt% and PE mass fraction of 0.3.

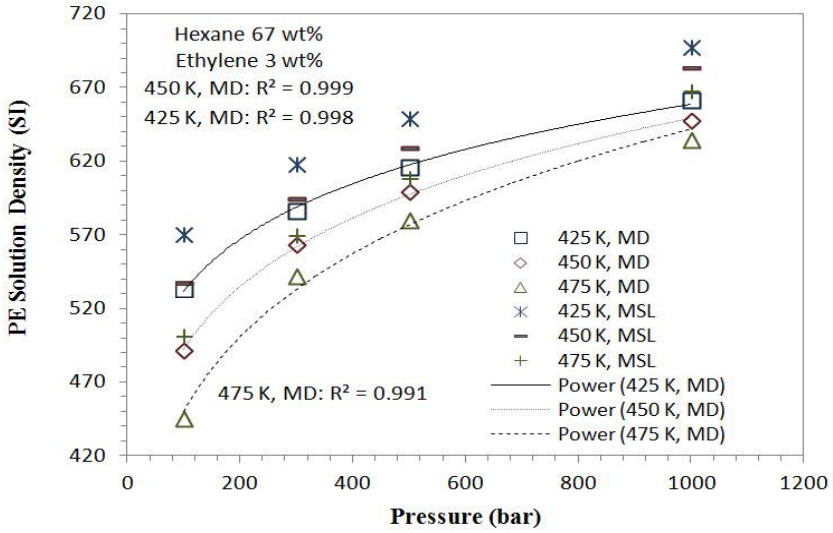

Figure 6.8. Pressure and temperature dependence of ternary PE + hexane + ethylene solution densities shown in power equation for ethylene (co-solvent) concentration of 3 wt% and PE mass fraction of 0.3.

6.5 Conclusions

The potential energy and density of PE in hexane + ethylene solution were computed by changing the pressure for several model systems via all-atom MD calculations. It was shown that the ternary solution density increases monotonically with raising pressure for all model systems due to an increase in Lennard-Jones interactive forces. The MD predicted

densities of ternary polymer solutions of PE + hexane + ethylene of different solvent compositions were compared with those of binary mixtures of PE in hexane to understand the effect of adding the unreacted monomer on mixture densities in the solution polymerization process. The presence of unreacted monomer was found to decrease the PE solution density. In addition, it was demonstrated that the polymer solution density decreases as temperature increases. However, pressure, solvent composition, and temperature dependence of density tend to vanish with increasing pressure. The correctness of MD simulations was verified by iteratively solving the MSL EOS using the pure compound and interaction parameters. The simulated data were found to be in quantitative accordance with the EOS model.

It should also be remarked that the implemented molecular modeling methodology provides a fundamental understanding of the changes in intra- and intermolecular interactions versus pressure. From the breakdown of non-bonded energies it may be inferred that the magnitude of vdW potential energy increases with raising pressure, whereas the electrostatic term displays no sensitivity to pressure changes.

Ultimately, the NPT-MD simulation results based upon the OPLS-AA model provide thermophysical properties of ternary PE + hexane + ethylene mixtures across a wide range of pressures, temperatures, and compositions to high degree of accuracy, required for phase behavior predictions in polyolefin synthesis and processing. The presented methodology can be extended to characterization and processing of material systems where piezo-thermodynamics is the dominant phenomenon.

6.6 References

1. Sanchez, I. C.; Lacombe, R. H., An elementary molecular theory of classical fluids. Pure fluids. *Journal of Physical Chemistry* **1976,** *80* (21), 2352-2362.
2. Lacombe, R. H.; Sanchez, I. C., Statistical thermodynamics of fluid mixtures. *Journal of Physical Chemistry* **1976,** *80* (23), 2568-2580.
3. Sanchez, I. C.; Lacombe, R. H., Statistical thermodynamics of polymer solutions. *Macromolecules* **1978,** *11* (6), 1145-1156.
4. Koak, N.; Heidemann, R. A., Polymer-solvent phase behavior near the solvent vapor pressure. *Industrial & Engineering Chemistry Research* **1996,** *35* (11), 4301-4309.
5. Shahamat, M.; Rey, A. D., Characterization of pressure effects on the cohesive properties and structure of hexane and polyethylene using molecular dynamics simulations. *Macromolecular Theory and Simulations* **2012,** *21* (8), 535-543.

6. Shahamat, M.; Rey, A. D., High pressure miscibility predictions of polyethylene in hexane solutions based on molecular dynamics. *European Polymer Journal* **2013,** *49* (2), 471-481.
7. Shahamat, M.; Rey, A. D., Molecular thermodynamic characterization of LCST fluid phase behavior and exploring electrostatic algorithms to compute polymer/solvent solubility parameters in the canonical ensemble. *Polymer* **2013,** *54* (18), 4997-5004.
8. Berendsen, H. J. C.; van der Spoel, D.; van Drunen, R., Gromacs: A message-passing parallel molecular dynamics implementation. *Computer Physics Communications* **1995,** *91* (1-3), 43-56.
9. Lindahl, E.; Hess, B.; van der Spoel, D., GROMACS 3.0: A package for molecular simulation and trajectory analysis. *Journal of Molecular Modeling* **2001,** *7* (8), 306-317.
10. van der Spoel, D.; Lindahl, E.; Hess, B.; Groenhof, G.; Mark, A. E.; Berendsen, H. J. C., GROMACS: Fast, flexible, and free. *Journal of Computational Chemistry* **2005,** *26* (16), 1701-1718.
11. Hess, B.; Kutzner, C.; van der Spoel, D.; Lindahl, E., GROMACS 4: Algorithms for highly efficient, load-balanced, and scalable molecular simulation. *Journal of Chemical Theory and Computation* **2008,** *4* (3), 435-447.
12. Jorgensen, W. L.; Madura, J. D.; Swenson, C. J., Optimized intermolecular potential functions for liquid hydrocarbons. *Journal of the American Chemical Society* **1984,** *106* (22), 6638-6646.
13. van der Spoel, D.; van Maaren, P. J., The origin of layer structure artifacts in simulations of liquid water. *Journal of Chemical Theory and Computation* **2006,** *2* (1), 1-11.
14. Berendsen, H. J. C.; Postma, J. P. M.; van Gunsteren, W. F.; Dinola, A.; Haak, J. R., Molecular dynamics with coupling to an external bath. *Journal of Chemical Physics* **1984,** *81* (8), 3684-3690.
15. Parrinello, M.; Rahman, A., Polymorphic transitions in single crystals: A new molecular dynamics method. *Journal of Applied Physics* **1981,** *52* (12), 7182-7190.
16. Bussi, G.; Donadio, D.; Parrinello, M., Canonical sampling through velocity rescaling. *Journal of Chemical Physics* **2007,** *126* (1), 014101.
17. Nagy, I.; de Loos, T. W.; Krenz, R. A.; Heidemann, R. A., High pressure phase equilibria in the systems linear low density polyethylene + n-hexane and linear low density polyethylene + n-hexane + ethylene: Experimental results and modelling with the Sanchez-Lacombe equation of state. *Journal of Supercritical Fluids* **2006,** *37* (1), 115-124.
18. Krenz, R. A.; Heidemann, R. A., Modelling the fluid phase behaviour of polydisperse polyethylene blends in hydrocarbons using the modified Sanchez-Lacombe equation of state. *Fluid Phase Equilibria* **2007,** *262* (1-2), 217-226.

7 Computing Equation of State Characteristic Parameters via the Optimized Potentials for Liquid Simulations All-Atom Force Field under Isobaric-Isothermal Thermodynamic Ensemble

7.1 Summary

The phase behavior of polymer-solvent systems, which exhibit pressure-induced phase separation has significant applications in industry for the production and processing of many kinds of polyolefin materials. There are several methods available in the literature that can be used to estimate the parameters associated with the thermodynamic models, relevant to the synthesis, processing, and characterization of polyolefins. The present paper evaluates the effectiveness of the optimized potentials for liquid simulations all-atom (OPLS-AA) force field in predicting the thermodynamic and physical properties relating to polyolefin solution processes. Molecular dynamics (MD) simulations are adopted to calculate the Sanchez-Lacombe equation of state (i.e. SL EOS) characteristic parameters of P^*, T^*, and ρ^* for hexane and high-density polyethylene (HDPE) without experimental effort based upon the physical meaning of the parameters. The calculated T^* is a function of the temperature, as found in the literature. To solve this problem, a Boltzmann fitting of the data is used to obtain T^* at the high-temperature limit. The OPLS-AA force field has been found to be a promising alternative to predict the EOS characteristic parameters and eliminates the need for difficult to obtain experimental phase equilibrium data as well as the least-squares fitting of thermodynamic data.

7.2 Introduction

A full characterization of phase behavior of polymer solutions is a very important aspect in the manufacturing, processing, and formulation of polymers. Accordingly, detailed high-pressure experimental and theoretical knowledge of the phase equilibria is of great fundamental and theoretical interest. Numerous thermodynamic models have been proposed to predict phase equilibria of such systems, which are mostly revised forms of Flory-Huggins lattice theory. Nonetheless, the Flory-Huggins equation does not consider the polymer chain conformation, chain stiffness, and free volume. Moreover, since this theory in its simplest form is on the basis of a rigid lattice, it fails to describe thermodynamic behavior of compressible systems. There have been a number of modifications to the Flory-Huggins model. The essential difference in the revised forms of the lattice models results from how compressibility and thermal expansion are treated. For instance, to describe thermodynamics of pure and mixed fluids a molecular theory founded on a statistical mechanical model known as Sanchez-Lacombe (SL) lattice-fluid model[1-2] was proposed, which soon after was applied to polymer-solvent systems.[3] This model accounts for compressibility and density changes by introducing vacant sites in the lattice. The ability of lattice models to describe the mixtures with large size differences makes them particularly applicable in the modeling of polymer solutions. To compute phase equilibria, chemical potentials and the equation of state (EOS) are derived from the Helmholtz free energy, which is in turn obtained from the partition function. In this theory pure fluids are completely characterized by three molecular parameters and the characterization of a binary mixture requires pure fluid parameters and a binary interaction energy. To predict the phase behavior of compressible polymer solutions especially where pressure and temperature changes are significant, the SL EOS and its modified version known as the modified SL (MSL)[4] EOS have been extensively used. These theories have been developed as useful tools enabling the predictions of thermodynamic properties, surface tension, and phase stability of polymer solutions and blends. The reduced SL EOS, derived from the free energy function, reads:

$$\tilde{\rho}^2 + \tilde{P} + \tilde{T}\left[\ln(1-\tilde{\rho}) + \left(1-\frac{1}{r}\right)\tilde{\rho}\right] = 0 \qquad (7.1)$$

where $\tilde{P}=P/P^*$, $\tilde{T}=T/T^*$, and $\tilde{v}=1/\tilde{\rho}=V/V^*=\rho^*/\rho$ are the respective reduced pressure, temperature, and volume of a pure component. The characteristic variables of the pure component which are related to state variables are defined as $P^*=\varepsilon^*/v^*$, $T^*=\varepsilon^*/k$, and $V^*=Nrv^*$, respectively, in which the pure component parameter v^* is the close-packed volume of segment that contains the molecule, ε^* the interaction energy of lattice per site (mer), i.e. the required energy to generate a hole of the lattice, *k* the Boltzmann constant, r the number of segments in a polymer molecule (*r*-mer), and *N* is the number of *r*-mers (no holes).

The free energy function and phase behavior of the polymer-solvent system is very sensitive to accurate determination of model parameters. The values of the parameters of a pure component are usually obtained by fitting the model to the available experimental *PVT* data. In general, alternative methods that predict the EOS model parameters are of great practical value due to the fact that these parameters are extremely difficult to experimentally determine. This situation is exacerbated in multicomponent mixtures and especially in the high-pressure and high-temperature systems. Furthermore, it is of utmost importance to achieve a detailed insight on the molecular-level information that directly govern the fundamental aspects of materials science.

Recent advances in computing power have opened new highways for research in molecular modeling simulations such as Monte Carlo, molecular mechanics, and molecular dynamics (MD), which has made it feasible to treat polymers with several thousand atoms in full atomistic simulations. Force field-based molecular simulation methods can in principle be applied to make quantitative predictions of thermodynamic and physical properties. Nevertheless, molecular modeling efforts that focus on the thermodynamic properties of polyolefin solutions are few.[5-7]

The significance of this research is that molecular mechanics (empirical force field methods) are to be applied for computing SL EOS model parameters of hexane and PE, which can be further applied to develop phase equilibria in such systems. To achieve this, isobaric-isothermal (NPT) MD simulations are carried out to calculate the characteristic parameters of P^*, T^*, and ρ^*, and to report on the applicability and effectiveness of the OPLS-AA force field in predicting these parameters.

The organization of this paper is as follows. The methodology section presents the computational method and a detailed model description for conducting NPT simulations. The results and discussion section provides the MD results to capture the SL model parameters of P^*, T^*, and ρ^* for hexane and PE. The final section summarizes findings and gives some concluding remarks.

7.3 System Set-up and Computational Details

7.3.1 Molecular Mechanics Model

In the present work the GROMACS,[8-11] molecular dynamics program version 4.5.4 has been employed with the force field OPLS-AA[12] parameters, which is appropriate for liquid hydrocarbon systems. For all the simulation runs, we have used quad-core AMD processors, running under CentOS/Linux. The total system energy E_{total} was represented by the sum of bonded and non-bonded interactions:

$$E_{\text{total}} = E_b + E_\theta + E_\phi + E_{\text{vdW}} + E_{\text{electrostatics}} \tag{7.2}$$

The molecular mechanics model incorporated the intramolecular interactions of covalent bond stretching (2-body), E_b, angle bending (3-body), E_θ, and dihedral angle (4-body), E_ϕ, which are based on a fixed list of atoms. The 2-body and 3-body interaction terms were expressed in harmonic form and dihedrals were treated by cosine series potentials. The intermolecular interactions which were computed on the basis of a list of non-bonded atoms within a certain radius between atoms separated by more than three bonds or those belong to different molecules, were modeled by pairwise additive 12-6 Lennard-Jones, E_{vdW}, and electrostatic, $E_{\text{electrostatics}}$, potential energies. A neighbor list, used for calculating the non-bonded vdW and electrostatic interactions, was kept to 13.5 A˚ and updated every 10 steps. The non-bonded interactions were treated by a shift function[13] with a group-based cut-off radius of 11 A˚ where potential functions were switched smoothly to zero over the region 10–11 A˚.

7.3.2 Simulation Details

The initial cell structures were relaxed to avoid the overlaps between atoms using the steepest descent algorithm. The model systems, built with 3-D periodicity, were used to carry out equilibration and production runs under constant pressure and temperature ensemble (NPT) at several different temperatures based on leap-frog integration algorithm with a time step of 1 fs. A series of NPT-MD simulations over a temperature range from 50 up to 525 K with an interval of 25/50 K were conducted and the total energy was monitored to ensure equilibration. The pressure was controlled by Berendsen barostat[14] with time constant of 1 ps and the temperature coupling algorithm of velocity rescaling[15] with time constant of 0.1 ps was employed to maintain the temperature at the target values. Model systems were subjected to 10 ns dynamics with the trajectories and energies being saved every 0.1 ps for the confirmation of the equilibration and analysis. Upon equilibrating the model systems during a period of 10 ns, the last nanosecond (ns) of this period for each run was analyzed to compute physical properties of interest.

7.4 Results and Discussion

A series of densities for hexane and PE at several different temperatures and 1 bar were obtained via NPT runs. Figure 7.1 illustrates the time evolution of density profiles for hexane and PE where densities have reached an equilibrium value. In the original SL lattice-fluid theory the EOS characteristic parameter ρ^* corresponds to the close-packed density at 0 K. As a result, extrapolating from the density data plotted against temperature results in ρ^*. Figure 7.2 and Figure 7.3 show the equilibrium densities for hexane and PE, respectively, where the correctness of the force field OPLS-AA is verified by comparing the simulated densities as a function of temperature with the corresponding experimental[16] and theoretical data.[17] The simulated densities are smaller than those from experiments and theoretical data at the same temperature for hexane and PE, respectively. However, the error decreases with decreasing temperature, indicating an acceptable agreement between the simulated and literature data.

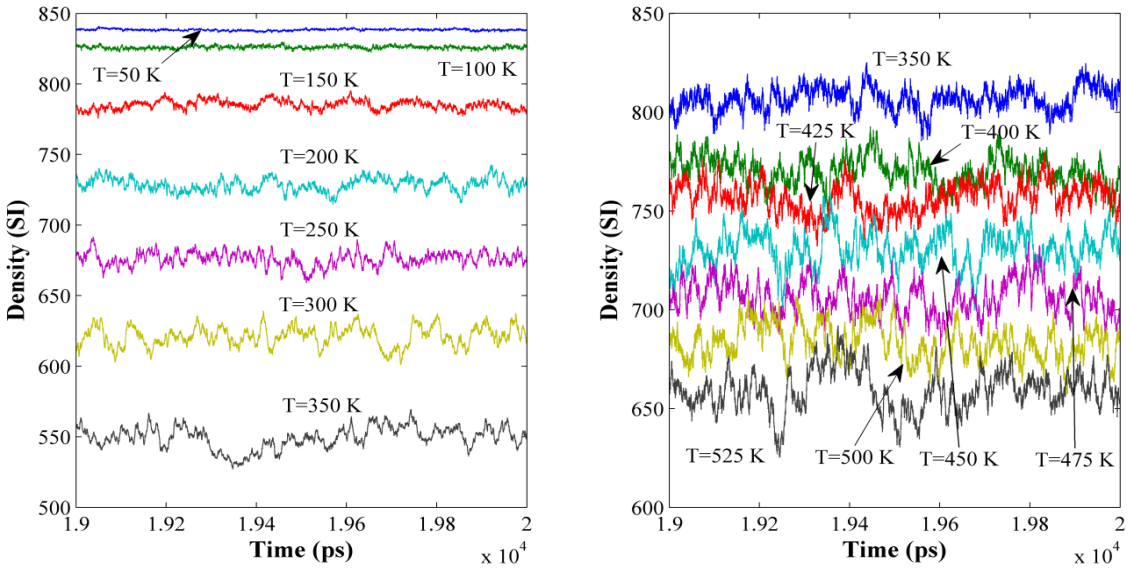

Figure 7.1. Time evolution of densities for hexane (left) and PE (right) obtained by NPT-MD simulations at different temperatures.

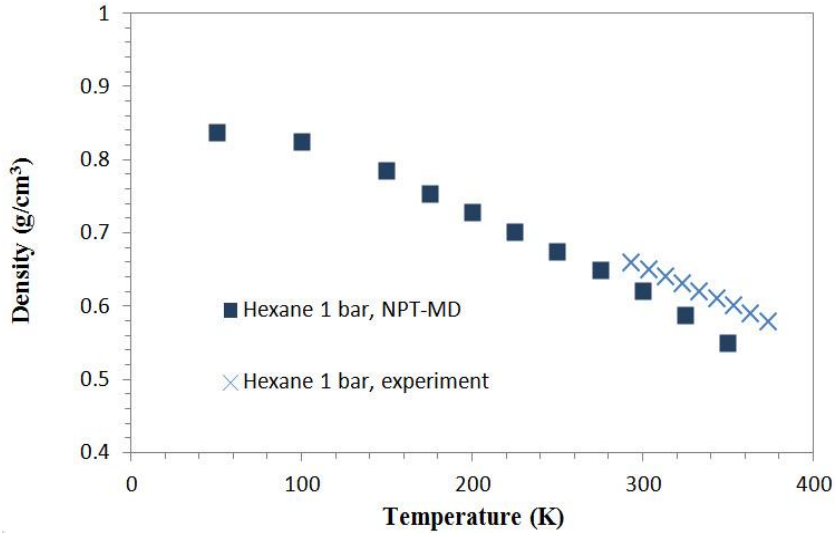

Figure 7.2. Temperature dependence of hexane density calculated via MD.

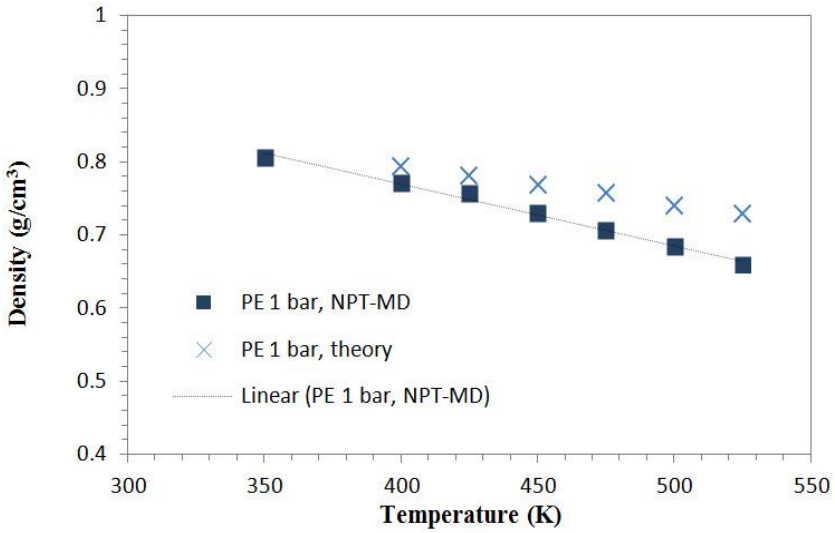

Figure 7.3. Temperature dependence of PE density calculated via MD.

The characteristic parameter P^* corresponds to the cohesive energy density (CED) at 0 K. The CED is defined as the ratio of the cohesive energy (CE) and the molar volume V at the temperature and pressure that vaporization occurs. The CE is the increase in the internal energy per mol as a result of eliminating all intermolecular forces. In molecular simulations this quantity may be computed from the internal energy of the periodic simulation cell at bulk state, U_{bulk} and the sum of the internal energies of the isolated molecules in vacuum, $U_{\text{i,isolated}}$ (absence of intermolecular interactions) averaged over a certain number of samples via the NPT runs:

$$CE(P,T) = \left\langle \sum_{i=1}^{n} U_{\text{i,isolated}}(T) - U_{\text{bulk}}(P,T) \right\rangle_{NPT} \tag{7.3}$$

The calculated CEDs versus temperature are shown in Figure 7.4 and Figure 7.5 for hexane and PE, respectively.

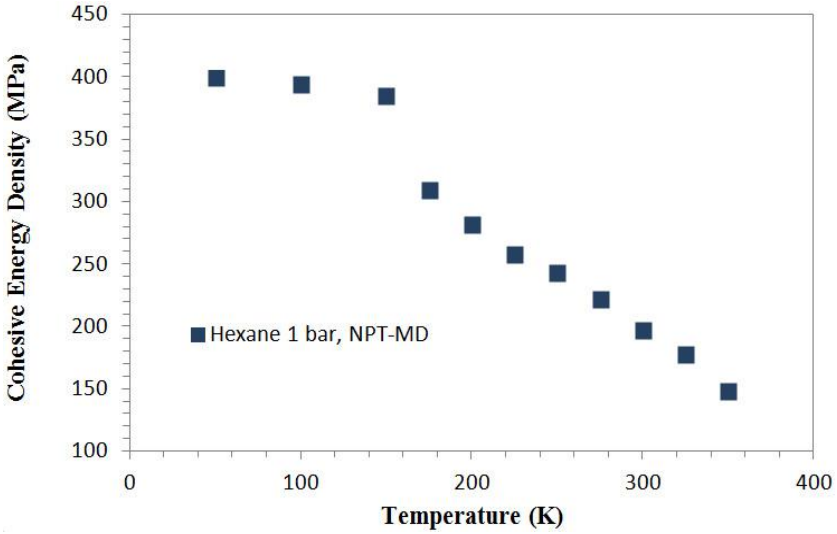

Figure 7.4. Temperature dependence of hexane cohesive energy density calculated via MD.

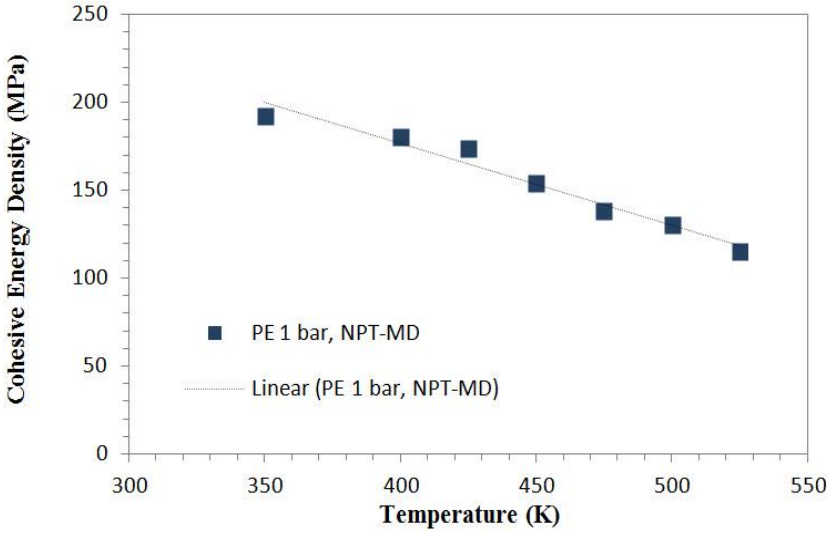

Figure 7.5. Temperature dependence of PE cohesive energy density calculated via MD.

The characteristic parameter T^* was obtained by inserting the corresponding ρ^*, P^*, and the NPT-MD predicted densities versus temperature into the SL EOS model, presented above. The calculated T^* at different temperatures for hexane and PE is shown in Figure 7.6 and Figure 7.7, respectively. A non-linear fitting scheme using Boltzmann function was employed to fit the data, where T_1, T_2, T_3, and T_4 are the fitting constants. The proposed

fitting function, which successfully describes the data and enables us to predict T^* at high temperatures has the following form:

$$T^* = T_2 + \frac{T_1 - T_2}{1 + \exp[(T - T_4)/T_3]} \tag{7.4}$$

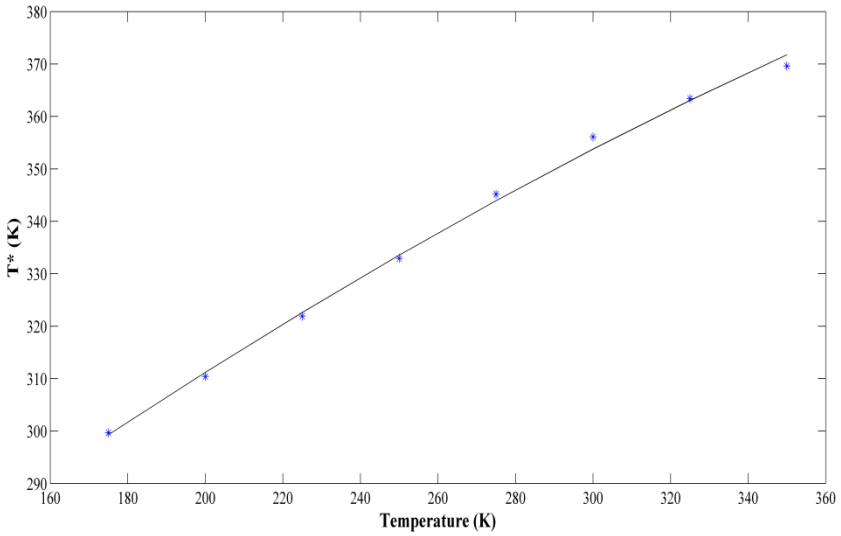

Figure 7.6. Temperature dependence of the SL parameter T^* for hexane. The asterisk points represent the calculated T^* and the solid line represents the Boltzmann fitting curve.

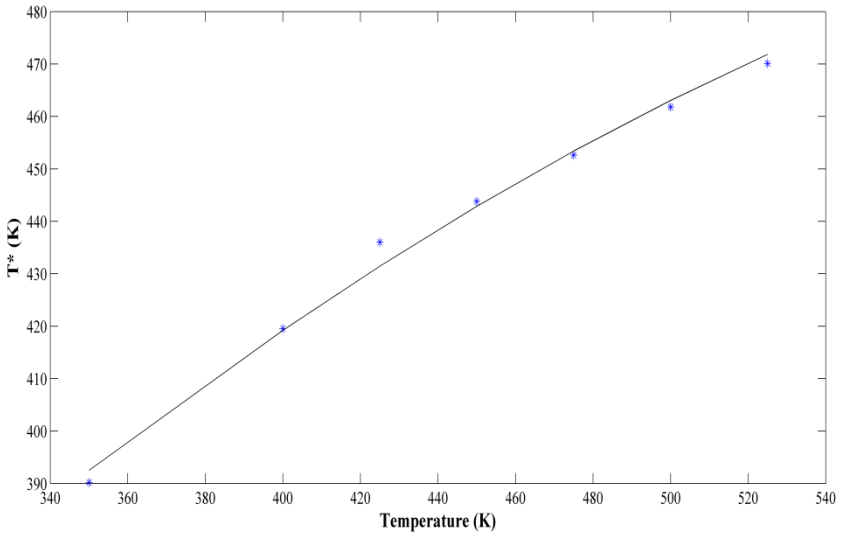

Figure 7.7. Temperature dependence of the SL parameter T^* for PE. The asterisk points represent the calculated T^* and the solid line represents the Boltzmann fitting curve.

The EOS parameters computed with MD simulations are listed in Table 7.1 where we note a good quantitative agreement with the experimental data suggesting that the OPLS-AA force field has been successful in predicting the SL model parameters.

Table 7.1. Computed values of SL EOS characteristic parameters via MD.

Model System	MD/Validation	ρ^* (g/cm^3)	P^* (MPa)	T^* (K)
Hexane	MD Simulation	0.85	403	466
	Experiment[1]	0.78	298	476
PE	MD Simulation	1	354	537
	Experiment[18-19]	0.9	359	521/650[20]

7.5 Conclusions

Understanding the thermodynamic properties of PE in hydrocarbon solvents is significant for industrial production of PE systems. A combined MD simulation-EOS algorithm was adopted to calculate the thermodynamic properties from which the SL EOS parameters for hexane and PE are obtained. A Boltzmann fitting function was used to describe the temperature dependence of T^*, which enables us to obtain this parameter in the high-temperature limit. The results produced by MD are in quantitative accordance with the reported experimental data, indicating that the OPLS-AA force field provides reliable estimates of the SL model characteristic parameters and eliminates the need for tedious non-linear parameter estimation methods. Lastly, the undertaken force field-based molecular dynamics methodology emphasizes the effectiveness of the force field methods in the prediction of properties of large molecular systems and molecules in the condensed phase wherein the most important interaction terms are the non-bonded (in particular dispersion) forces, which are extremely difficult to describe using ab initio methods.

7.6 References

1. Sanchez, I. C.; Lacombe, R. H., An elementary molecular theory of classical fluids. Pure fluids. *Journal of Physical Chemistry* **1976,** *80* (21), 2352-2362.
2. Lacombe, R. H.; Sanchez, I. C., Statistical thermodynamics of fluid mixtures. *Journal of Physical Chemistry* **1976,** *80* (23), 2568-2580.
3. Sanchez, I. C.; Lacombe, R. H., Statistical thermodynamics of polymer solutions. *Macromolecules* **1978,** *11* (6), 1145-1156.
4. Koak, N.; Heidemann, R. A., Polymer-solvent phase behavior near the solvent vapor pressure. *Industrial & Engineering Chemistry Research* **1996,** *35* (11), 4301-4309.

5. Shahamat, M.; Rey, A. D., Characterization of pressure effects on the cohesive properties and structure of hexane and polyethylene using molecular dynamics simulations. *Macromolecular Theory and Simulations* **2012,** *21* (8), 535-543.
6. Shahamat, M.; Rey, A. D., High pressure miscibility predictions of polyethylene in hexane solutions based on molecular dynamics. *European Polymer Journal* **2013,** *49* (2), 471-481.
7. Shahamat, M.; Rey, A. D., Molecular thermodynamic characterization of LCST fluid phase behavior and exploring electrostatic algorithms to compute polymer/solvent solubility parameters in the canonical ensemble. *Polymer* **2013,** *54* (18), 4997-5004.
8. Berendsen, H. J. C.; van der Spoel, D.; van Drunen, R., Gromacs: A message-passing parallel molecular dynamics implementation. *Computer Physics Communications* **1995,** *91* (1-3), 43-56.
9. Lindahl, E.; Hess, B.; van der Spoel, D., GROMACS 3.0: A package for molecular simulation and trajectory analysis. *Journal of Molecular Modeling* **2001,** *7* (8), 306-317.
10. van der Spoel, D.; Lindahl, E.; Hess, B.; Groenhof, G.; Mark, A. E.; Berendsen, H. J. C., GROMACS: Fast, flexible, and free. *Journal of Computational Chemistry* **2005,** *26* (16), 1701-1718.
11. Hess, B.; Kutzner, C.; van der Spoel, D.; Lindahl, E., GROMACS 4: Algorithms for highly efficient, load-balanced, and scalable molecular simulation. *Journal of Chemical Theory and Computation* **2008,** *4* (3), 435-447.
12. Jorgensen, W. L.; Madura, J. D.; Swenson, C. J., Optimized intermolecular potential functions for liquid hydrocarbons. *Journal of the American Chemical Society* **1984,** *106* (22), 6638-6646.
13. van der Spoel, D.; van Maaren, P. J., The origin of layer structure artifacts in simulations of liquid water. *Journal of Chemical Theory and Computation* **2006,** *2* (1), 1-11.
14. Berendsen, H. J. C.; Postma, J. P. M.; van Gunsteren, W. F.; Dinola, A.; Haak, J. R., Molecular dynamics with coupling to an external bath. *Journal of Chemical Physics* **1984,** *81* (8), 3684-3690.
15. Bussi, G.; Donadio, D.; Parrinello, M., Canonical sampling through velocity rescaling. *Journal of Chemical Physics* **2007,** *126* (1), 014101.
16. Daridon, J. L.; Lagourette, B.; Grolier, J. P. E., Experimental measurements of the speed of sound in n-hexane from 293 to 373 K and up to 150 MPa. *International Journal of Thermophysics* **1998,** *19* (1), 145-160.
17. Maloney, D. P.; Prausnitz, J. M., Thermodynamic properties of liquid polyethylene. *Journal of Applied Polymer Science* **1974,** *18* (9), 2703-2710.
18. Haruki, M.; Takakura, Y.; Sugiura, H.; Kihara, S.; Takishima, S., Phase behavior for the supercritical ethylene + hexane + polyethylene systems. *Journal of Supercritical Fluids* **2008,** *44* (3), 284-293.
19. Haruki, M.; Sato, K.; Kihara, S.; Takishima, S., High pressure phase behavior for the supercritical ethylene + cyclohexane + hexane + polyethylene systems. *Journal of Supercritical Fluids* **2009,** *49* (2), 125-134.
20. Kiran, E.; Xiong, Y.; Zhuang, W. H., Modeling polyethylene solutions in near and supercritical fluids using the Sanchez-Lacombe model. *Journal of Supercritical Fluids* **1993,** *6* (4), 193-203.

8 Conclusions and Accomplishments

8.1 General Conclusions

8.1.1 Introduction

The industrial solution polymerization process for producing PE requires a detailed fundamental understanding of thermodynamic and physical properties of the solution at high pressure and temperature. The present thesis is the first important step forward in this direction, wherein molecular modeling calculation platforms are developed, implemented, and validated to acquire a quantitative understanding of atomistic-level details that directly impact phase behavior. The key findings and conclusions of the undertaken modeling and simulation thesis work are summarized in the following subsections.

8.1.2 Chapter 2-3: Molecular Thermodynamic Characterization of PIPS Mechanism

Atomistic MD simulations in the isobaric-isothermal (NPT) thermodynamics ensemble using accurate OPLS-AA force field are conducted to compute solubility parameters, liquid phase densities, structure, and internal pressures of HDPE and hexane over a broad range of pressures. Using the knowledge of pressure dependence of solubility parameters, a relation is established for the dependence of the Flory-Huggins interaction parameter on pressure. It is found that the polymer-solvent interaction parameter decreases upon increasing the pressure, which indicates that the miscibility of the PE/hexane system may be improved by raising the pressure, in agreement with the experimental and theoretical predictions; however, miscibility displays weaker sensitivity to changes in pressure beyond a certain pressure. The undertaken modeling methodology assists to achieve a molecular-level understanding of the pressure effects upon phase stability, wherein the breakdown of the total system energy reveals that vdW interactions are the

only non-bonded potential energy contributions that govern variations in CED versus pressure. It is also found that the molecular mechanics model that incorporates the electrostatic energy contribution predicts more accurately the miscibility of PE in hexane as a result of a larger chemical potential factor particularly at lower pressures. Another significant finding concerns the relationship between CED and internal pressure. For non-polar monomeric liquids it is found that CED may be well approximated by internal pressure; nevertheless, for polymer it is shown that internal pressure is larger than CED for the entire range of pressures investigated. The results indicate that the ratio of π/CED for PE approaches unity with increasing pressure.

8.1.3 Chapter 4: Molecular Thermodynamic Characterization of LCST Fluid Phase Behavior

The Hildebrand solubility parameters for HDPE and hexane are computed as a function of temperature at high pressure using the MD technique in the NVT ensemble. The results reveal that the solubility parameter values decrease monotonically with increasing temperature for force field models with and without electrostatic forces. Although, the analysis of the non-bonded interactive energy indicates that vdW interaction is of greater importance compared to electrostatic forces in a PE-hexane solution, the electrostatic energy has been found to contribute significantly to the total non-bonded interactions, suggesting that inclusion of this term is representative of a more realistic model. The binary interaction parameters increase upon increasing the temperature, indicating that the phase stability of the PE/hexane solution may be lowered by raising the temperature, a result that is consistent with the LCST-type phase behavior. An increase in temperature or a reduction in pressure reduces abruptly the density of the solvent while the polymer tends to remain in the liquid state. This difference in compressibility between polymer and the solvent induces phase separation. Additionally, a series of simulations in the canonical ensemble are conducted to compare performance of the shift function and PME electrostatic algorithms. The total potential energy of liquid phase used to calculate the cohesive energy is found to be insensitive with respect to these electrostatic schemes. This investigation also reveals that the PME algorithm can be accelerated considerably by increasing grid spacing from 0.12 up to 0.25 nm without significant loss of accuracy.

8.1.4 Chapter 5: Molecular Mechanics and EOS Modeling of Compressible PE Solutions

The pressure and concentration dependence of solution density of HDPE in hexane are calculated on the basis of the OPLS-AA force field together with MSL model over a broad range of pressures. It is shown that the density increases monotonically as pressure increases for all investigated polymer weight fractions due to increase in Lennard-Jones interactions. PE solution densities increase with polymer composition; however, the simulation results reveal that pressure and concentration dependence of density tend to vanish as pressure increases. It is found that the mixture density increases with increasing the cut-off radius. Moreover, a minimum cut-off radius is suggested to evaluate the intermolecular forces and to gain accurate densities that have a better agreement with MSL predictions, while maintaining an affordable computational speed. The increase in the solution density as a result of cut-off change is attributed to the magnitude of attractive vdW interactions that increase upon increasing the cut-off radius. The atomistic-level structural analysis of the PE-solvent reveals that as pressure raises the height of the first peak in the pair distribution function increases and the curve shifts to shorter separations which imply structural change of the condensed phase.

8.1.5 Chapter 6: Multiscale Modeling of Supercritical PE + Hexane + Ethylene System

The isobaric-isothermal molecular dynamic simulations together with the MSL EOS model are implemented to capture the impact of pressure and temperature on the ternary solution densities of PE + hexane + ethylene and also to explore the influence of adding supercritical ethylene to the PE in hydrocarbon solution. It is revealed that the ternary solution density increases monotonically as pressure increases owing to increase in the magnitude of Lennard-Jones potential energy. The ternary solution densities decrease upon increasing the ethylene content and temperature; nevertheless, it is found that the effect of pressure, solvent composition, and temperature on the ternary polymer solution density tend to vanish with increasing pressure. Based on the verifications of the simulated densities with the ternary MSL EOS it can be concluded that the OPLS-AA force field is a

promising alternative to the difficult to access experimental data and non-linear parameter estimation methods involved in EOS modeling methods.

8.1.6 Chapter 7: Calculating the EOS Characteristic Parameters via the OPLS-AA Force Field

Combining the SL theory and molecular dynamics the characteristic parameters of the EOS are determined based on the physical meaning of the parameters. To this end, fully-atomistic simulations are adopted to compute the thermodynamic properties of PE and hexane, from which the characteristic parameters of the SL EOS are numerically evaluated. The simulated SL model parameters based upon the OPLS-AA force field have excellent agreement with the experimental data. The undertaken methodology, which does not require fitting to experimental phase equilibrium data, suggests an alternative way to construct the phase diagrams that are associated with tedious experiments and also to calculate surface tension, and density profiles at surface.

8.2 Original Contributions to Knowledge

- Force field-based calculations are used to perform a molecular thermodynamic characterization of compressible PE solutions at high pressures in the PIPS mechanism and LCST-type phase behavior. The molecular details of the interactions in liquid PE and hexane as a function of pressure and temperature, which influence the cohesive energy density and hence the high pressure miscibility of PE-hexane and are difficult to access experimentally, are revealed.
- The root cause behind the change in the positional compactness of PE and hexane in the condensed phase as a result of pressure change is revealed.
- For the first time, fully-atomistic simulations are employed to comprehend the ratio of internal pressure to cohesive energy of PE as a function of pressure up to 3000 bar; a result that is useful given the scarcity of experimental data.
- Electrostatic algorithms employed in the OPLS-AA force field are evaluated and a series of molecular dynamics simulations in the canonical ensemble are performed to ameliorate the computational efficiency.

- Accuracy of the widely used OPLS-AA force field in calculating the structural and thermodynamic properties of polyolefins and hydrocarbons at high pressures is tested and validated.
- A molecular-level characterization of density-pressure-composition relations in compressible PE solutions, essential in solving phase equilibria and kinetics of compressible phase separation, is established for the first time.
- The force field-based calculations along with the EOS modeling performed in this thesis capture high-pressure thermophysical properties of binary (polymer/solvent) and ternary (polymer/solvent/co-solvent) compressible polyolefin solutions, difficult to access experimentally but crucial to polyolefin synthesis and processing.
- The molecular mechanics model developed and validated to describe the compressible solutions of polyolefin in hydrocarbons at elevated pressures is optimized by investigating the impact of cut-off distance of intermolecular potential energies on thermophysical properties to increase the efficiency of future molecular dynamics computations.
- Using a combined EOS-molecular simulation method, the characteristic model parameters of the SL EOS are calculated to high degree of accuracy, which eliminates the need for rigorous experimental phase equilibrium data and tedious least-sqaures fitting of thermodynamic data.
- The implemented thermodynamics-molecular simulation methodology complements and serves as a reliable alternative to parametric EOS and experimental approaches.

8.3 Recommendations for Future Work

- The present thesis investigates the high-pressure phase stability of PE in hydrocarbon solvents at a molecular-level. Nevertheless, the implemented lattice-based thermodynamic formalism incorporates only the interactional energies of the constituting substances. It is recommended that the fully-atomistic simulations performed in this thesis be used to incorporate the concentration dependence of interaction parameter.
- Another aspect that deserves further consideration concerns the development of the present force field molecular dynamics approach, which can capture large-sized polymer

systems, to shed light into the dynamics of phase separation and formation of the co-existing phases in polyolefin solutions (i.e. equilibrium thermodynamics).

- In view of the fact that the force field-based molecular modeling methods enable performing large scale simulations, the present approach can be extended to capture the effect of pressure on interfacial properties, e.g. interfacial concentration and density between the equilibrated polymer-rich and polymer-lean phases, by running molecular dynamics in the isobaric-isothermal ensemble.
- The present atomistic force field approach can be extended to calculate the structure factor as a function of pressure to understand the underlying structure of a polyolefin solution.

Appendix A Molecular Modeling Methods

A.1 Introduction

Modeling is a method of describing a complex system or process. Molecular modeling is therefore concerned with theoretical and computational methods used to mimic the behavior of molecules in the fields of computational chemistry, drug design, and materials science. Computational chemistry uses the principles of theoretical chemistry in combination with computer-based methods to provide insights into the behavior of molecular systems. Molecular modeling continuously improves by the development of these theoretical methods and computational techniques to explain experimental observations and make new predictions. Since the advent of today's powerful computer hardware and software, it is no longer necessary for molecular modeling practitioners to write their own computer programs. In many cases, the problems to be tackled in molecular modeling involve three phases. First, an appropriate model is selected to describe the intra- and intermolecular interactions. To this end, numerous molecular structural models have been used as a foundation to calculate the structures and properties of molecules. Quantum mechanics and molecular mechanics are the two most common models that are used in molecular modeling. These models determine how the system energy evolves in time as the positions of the atoms and molecules change. The second phase is the computation, e.g. an energy minimization, a conformational search, or other methods to generate statistically faithful ensembles such as molecular dynamics and Monte Carlo simulation. When a starting configuration is very far from equilibrium, forces become unacceptably large at one time step, which can result in extremely large changes in position and velocity when going to the next time step. These large forces cause the simulation to fail, and for this reason it is necessary to start with an energy minimization of the starting structure prior to the

simulation to remove unrealistic interactions. Ultimately, computation/simulation is analyzed to calculate the properties of interest, and to check whether it has been performed properly. The present thesis deals with modeling various aspects of the thermodynamic, physical, and structural properties of polyolefins and hydrocarbons, which provide a useful basis for high-pressure miscibility predictions in these polymer-solvent mixtures. The necessary and sufficient details of modeling and simulation method are given in the respective chapters of the present thesis; however, since atomistic-level modeling is an integral part of this thesis, a detailed overview of the molecular modeling methods used in this thesis is provided in the following subsections.

A.2 Molecular Mechanics: Empirical Force Field Models

Since quantum mechanical methods deal with electrons in a system, treatment of systems containing large number of particles is time-consuming and expensive. Force field method (also known as molecular mechanics) is one of the most widely used techniques for reasons of computational efficiency when large numbers of compounds are to be investigated. Force field calculations ignore motions of electrons and calculate the electronic energy of the system as a parametric function of nuclear coordinates only. Unlike quantum mechanical methods, that consider electrons as individual particles, in force fields, the "building blocks" are atoms, and molecules are described by a "ball & spring" model. The basis of molecular mechanics is that molecular properties and structure can be estimated by taking into account the forces between atoms, calculated based on a mechanical approach. As an example, bonded atoms are taken to behave as mechanical springs with a parameter that defines the strength of the spring. The force field energy is expressed as a sum of potential energy functions, each describing a contribution to the total potential energy of system U_{FF}:

$$U_{FF} = U_{stretching} + U_{bending} + U_{torsion} + U_{vdW} + U_{electrostatics} + U_{cross} \qquad \text{(A.1)}$$

The first three terms describe bonding interactions. $U_{stretching}$ denotes the bond stretching contribution, $U_{bending}$ represents the angle bending contribution and $U_{torsion}$ is the torsional

energy for rotation around a bond. Non-bonding interactions include U_{vdW}, the van der Waals (vdW) energy term and $U_{electrostatics}$, the electrostatic energy. Depending on how sophisticated the force field model is, cross terms U_{cross} maybe incorporated, which describe the coupling between the first three terms. Figure A.1 illustrates the basic energy terms involved in calculating the force field energy.

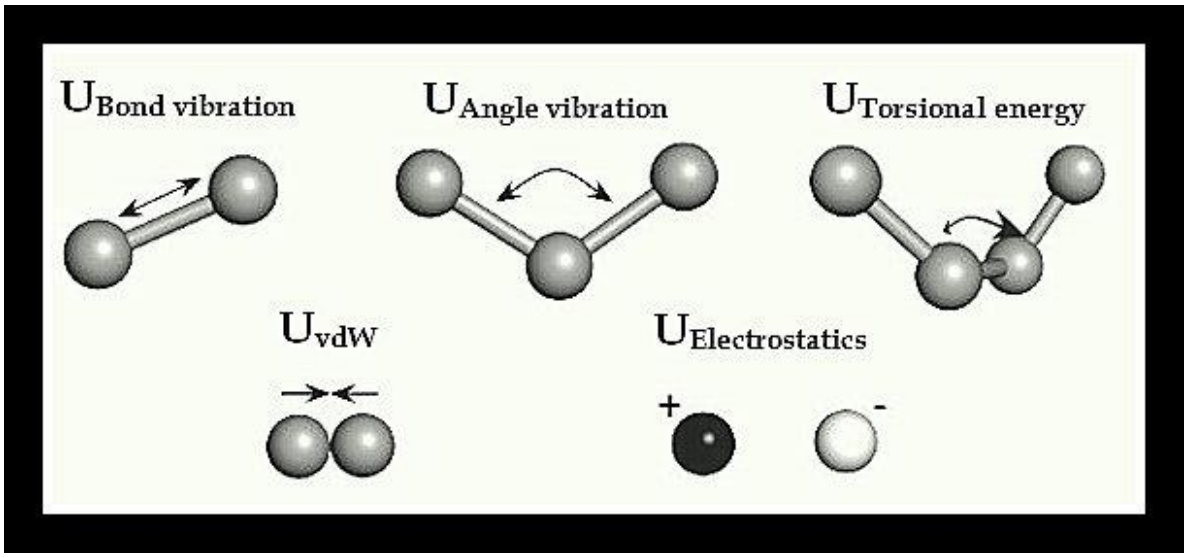

Figure A.1. Potential energy terms in molecular mechanics.

The individual potential energy terms are expressed in simple functions. Stable geometries, which correspond to minima on potential energy surface can be obtained by minimizing the total potential energy U_{FF} as a function of geometry. When a chemical bond is pulled the bond will be stretched or strained. This change in the bond length causes the energy of the bond to rise. The associated increase in bond energy is called bond strain energy. $U_{stretching}$, the potential energy function for stretching a bond between two atoms, has a simple harmonic form as:

$$U_{stretching} = \sum_{bonds} \frac{k_i}{2}\left(l_i - l_{i,0}\right)^2 \qquad \text{(A.2)}$$

Here, bonds are modeled as springs with force constants k_i that obey Hooke's law formula, i.e. the bond energy varies with the square of displacement from the reference bond length $l_{i,0}$ (also known as the natural bond length or strain-free value). The stiffness of the springs and natural bond distances are determined empirically and vary from force field to force field. Similar to bond stretching contribution, deviation of angles from reference values can be modeled using harmonic potential as:

$$U_{bending} = \sum_{angles} \frac{k_i}{2}\left(\theta_i - \theta_{i,0}\right)^2 \qquad \text{(A.3)}$$

Angle bending contribution is characterized by a force constant and a reference value, as in the bond deformation energy. Since less energy is involved in distorting an angle from its reference value than to stretch or compress a bond, angle bending force constants are rather smaller than those of bond deformation.

In case of flexible molecules the major changes in conformation arise from rotations around bonds. Torsional term can not be modeled in the same fashion as bond stretching and angle bending terms since a periodic function in torsion angle ω is needed to describe the torsional potential energy (i.e. bond rotation of 360° should return the same energy value). Most torsional potentials are expressed as a cosine series expansion to encompass the periodicity as:

$$U_{torsion} = \sum_{torsions} C_n\left(1+\cos\left(n\omega\right)\right) \qquad \text{(A.4)}$$

in which C_n is the barrier height to rotation about the torsion angle, n is the periodicity (also referred to as multiplicity). Cross terms describe coupling between bonding interactions. Most cross terms cover coupling between stretch-stretch, stretch-bend, stretch-torsion, and bend-bend terms and in some cases cross terms involving bend-bend-torsion have been considered. A typical model describing stretch-stretch cross term can be expressed as:

$$U_{stretch-stretch} = \frac{k_{i,j}}{2}\left(l_i - l_{i,0}\right)\left(l_j - l_{j,0}\right) \tag{A.5}$$

The vdW energy describes attractive and repulsive forces between atoms. At large (infinite) distances the energy is negligible and at short separation distances repulsive forces are dominant due to the overlap of electron clouds; however, at intermediate distances there is a slight attraction between electron clouds arising from dipole-dipole interactions. The well-known Lennard-Jones 12-6 potential function describes very well the vdW interaction. The function contains two parameters; the collision diameter σ, which is defined as the separation distance at which energy is zero and the well depth ε_{ij}:

$$U_{vdW} = \sum_{i>j} 4\varepsilon_{ij}\left(\left(\frac{\sigma_{ij}}{r_{ij}}\right)^{12} - \left(\frac{\sigma_{ij}}{r_{ij}}\right)^{6}\right) \tag{A.6}$$

The other contribution of non-bonding interaction arises from electrostatic interactions between two molecules (or between point charges on the same molecule). The electrostatic interaction is given by the Coulomb potential with ε being a dielectric constant:

$$U_{electrostatics} = \sum_{i=1}^{N_A}\sum_{j=1}^{N_B}\frac{q_i q_j}{\varepsilon r_{ij}} \tag{A.7}$$

It should be borne in mind that to define a force field it is not sufficient to specify only a set of potential energy functions but also the parameters must be specified. Two force fields may have identical functional terms but different parameters. The parameters which appear in the potential functions are adjustable parameters of a force field model and are chosen to reproduce the electronic structure calculation data and experimental data. Combination of these molecular mechanics interactions and the dynamical equation describes the time evolution of the system, discussed below. Atomistic molecular dynamics simulations based on classical force fields have contributed considerably to the

understanding of complex biological macromolecules such as protein-ligand aggregates, lipid bilayer, membrane proteins, and polymers.

A.3 Molecular Dynamics Simulation Method

Devised in the late 1950s, molecular dynamics simulations have been widely used in the design of novel materials with desirable properties. The evolution of computing resources and the development of novel algorithms implemented in molecular dynamics engines have substantially increased the achievable length and time scales during the last decades. Molecular dynamics computes the time evolution of positions, velocities, and orientations of molecules based upon the intermolecular forces determined by the empirical force fields and a set of initial conditions. The intermolecular potential energy on each particle as a function of coordinates of all the atoms in the system can be obtained by adding up the isolated pair interactions (pairwise additivity) as:

$$U = \sum_{i=1} \sum_{j=1} u\left(r_{ij}\right) \tag{A.8}$$

Here, $u\left(r_{ij}\right)$ is the pair potential energy function between molecules *i* and *j*. Fundamentally, the mass and velocity of particles determine the exact mathematical form of the dynamical equation. As nuclei of atoms are heavy enough to be treated classically (classical mechanics states that force equals mass times acceleration), the dynamics of atoms may be simulated by solving the Newton's second law of motion; i.e. quantum aspects of motions of nuclei are ignored. The resultant force arising from forces of all other molecules acting on molecule *i* is given by:

$$F_i = -\frac{\partial U\left(r^N\right)}{\partial r_i} = m\frac{d^2 r_i}{dt^2} \tag{A.9}$$

wherein r^N is a shorthand for the set of position vectors. By solving the dynamical equation, which includes time and space derivatives, the position and velocity of particles

can be predicted at later or earlier small time steps. The positions at a small time step Δt later are given by a Taylor expansion as:

$$r_{i+1} = r_i + \frac{\partial r_i}{\partial t}(\Delta t) + \frac{1}{2}\frac{\partial^2 r_i}{\partial t^2}(\Delta t)^2 + \ldots \qquad \text{(A.10)}$$

The updated coordinates are then used to evaluate the potential energy for the next step. The changes in coordinates and velocities with time lead to potential energy trajectories. The integration is performed using specific algorithms such as Verlet or some of its variants, which assume that the force on every atom is constant during the small time steps typically of 1 or 2 fs. For time-independent phenomena, the problem will be confined to finding the geometries with the energy minima on the potential energy surface. For the energy minimization, the steepest descent algorithm slightly moves the atomic positions in the direction of decreasing energy. In order to perform a molecular dynamics simulation numerous parameters need to be defined depending on the objective of the simulation itself. A number of them are listed below:

- **Unit cell of simulation:** Classical simulation cells are cubic or rectangular; however, to optimize the size of the system octahedron or dodecahedron boxes are also commonly employed.
- **Periodic boundary condition:** To avoid surface artifacts caused by the unrealistic walls of the simulation cell, periodic boundary conditions are applied; i.e. replicas of the simulation box are infinitely copied in three dimensions.
- **Energy minimization:** Prior to the production run, it is necessary to energy minimize the system to avoid unrealistic interactions, which can cause the simulation to fail or distort the structure. This can be accomplished using the steepest descent algorithm that simply moves each atom a short distance optimizing the interatomic interactions and the total potential energy of the system.
- **Initial velocities:** Molecular dynamics describes the movement of atoms in the system by solving numerically the Newton's equations of motion, which require an initial set of the atomic coordinates and velocities. The initial velocities of every atom are usually

randomly assigned under the restriction that the generated velocities follow a Maxwell distribution corresponding to the temperature at which the simulation will be performed.

- **Time step:** It is noteworthy that the selection of the time step is of great importance in a molecular dynamics run since it determines both the stability and the speed at which the simulation is performed. Time step for integration is limited by two extremes. A large time step gives instabilities (trajectory blow up) due to errors that may arise in the integration algorithm; reversely, a very small time step makes the simulation inefficient due to a long calculation time. With a proper time step, the phase space is sampled efficiently (i.e. a reasonable proportion of the phase space is covered) and collisions occur smoothly. The largest time step needs to be an order of magnitude smaller than that of the smallest oscillation period that can be found in the simulated system. Since hydrogen atoms are by far the lightest atoms, the largest vibrational frequency mostly originates from the fast atomic motions of C-H, which is about 10 femtoseconds (fs). These high frequency bond vibrations limit the time steps to a few femtoseconds.
- **Cut-off:** Simple cut-offs can be used for Lennard-Jones interactions that decay very rapidly, and as a result, only the contribution of the atoms contained within the cut-off radius is significant (Lennard-Jones is a short range interaction). However, for electrostatic interactions a sudden cut-off can lead to large errors owing to the fact that this energy contribution has important effects even at long molecularscale distances. To circumvent this, shift function or particle mesh Ewald (PME) algorithms can be used. PME calculates the infinite electrostatic interactions by splitting the summation into short- and long-range parts. For PME, the cut-off radius only determines the balance between these two parts.
- **Thermodynamic ensemble:** A number of algorithms are employed to perform the simulation under a particular thermodynamic ensemble. The most common of these algorithms are thermostats (temperature coupling) and barostats (pressure coupling), which correct the velocities and scale the simulation box size to maintain the system temperature and pressure, respectively, at the target values.
- **Trajectory analysis:** During the production simulation, atomic coordinates, velocities, and/or forces of all the atoms, the temperature, pressure, density, and energy contributions, are stored for further analysis. The output files are usually very large due

to the number of particles involved. Thus, the period at which data are stored in the trajectory file is typically 100-1000 integration steps.

The details of the implemented algorithms and a number of selected parameters are provided in the respective chapters. The following subsection presents the input parameters as well as the calculated energies and performance statistics written at the end of the output file for simulations of compressible PE solutions.

A.4 Input Parameters and Output for the Simulation of Compressible PE Solution in the NPT Ensemble

```
integrator          = md
nsteps              = 20000000
init_step           = 0
ns_type             = Grid
nstlist             = 10
ndelta              = 2
nstcomm             = 100
comm_mode           = Linear
nstlog              = 1000
nstxout             = 100
nstvout             = 0
nstfout             = 0
nstcalcenergy       = 10
nstenergy           = 100
nstxtcout           = 1000
init_t              = 0
delta_t             = 0.0005
xtcprec             = 1000
nkx                 = 0
nky                 = 0
nkz                 = 0
pme_order           = 4
```

ewald_rtol = 1e-05
ewald_geometry = 0
epsilon_surface = 0
optimize_fft = FALSE
ePBC = xyz
bPeriodicMols = FALSE
bContinuation = FALSE
bShakeSOR = FALSE
etc = V-rescale
nsttcouple = 10
epc = Parrinello-Rahman
epctype = Isotropic
nstpcouple = 10
tau_p = 1
ref_p (3x3):
ref_p[0]={ 3.00000e+02, 0.00000e+00, 0.00000e+00}
ref_p[1]={ 0.00000e+00, 3.00000e+02, 0.00000e+00}
ref_p[2]={ 0.00000e+00, 0.00000e+00, 3.00000e+02}
compress (3x3):
compress[0]={ 3.50000e-05, 0.00000e+00, 0.00000e+00}
compress[1]={ 0.00000e+00, 3.50000e-05, 0.00000e+00}
compress[2]={ 0.00000e+00, 0.00000e+00, 3.50000e-05}
refcoord_scaling = No
posres_com (3):
posres_com[0]= 0.00000e+00
posres_com[1]= 0.00000e+00
posres_com[2]= 0.00000e+00
posres_comB (3):
posres_comB[0]= 0.00000e+00
posres_comB[1]= 0.00000e+00
posres_comB[2]= 0.00000e+00

andersen_seed = 815131
rlist = 1.35
rlistlong = 1.35
rtpi = 0.05
coulombtype = Shift
rcoulomb_switch = 1
rcoulomb = 1.1
vdwtype = Shift
rvdw_switch = 1
rvdw = 1.1
epsilon_r = 1
epsilon_rf = 1
tabext = 1
implicit_solvent = No
gb_algorithm = Still
gb_epsilon_solvent = 80
nstgbradii = 1
rgbradii = 1
gb_saltconc = 0
gb_obc_alpha = 1
gb_obc_beta = 0.8
gb_obc_gamma = 4.85
gb_dielectric_offset = 0.009
sa_algorithm = Ace-approximation
sa_surface_tension = 2.05016
DispCorr = No
free_energy = no
init_lambda = 0
delta_lambda = 0
n_foreign_lambda = 0
sc_alpha = 0.5

sc_power = 1
sc_sigma = 0.3
sc_sigma_min = 0.3
nstdhdl = 10
separate_dhdl_file = yes
dhdl_derivatives = yes
dh_hist_size = 0
dh_hist_spacing = 0.1
nwall = 0
wall_type = 9-3
wall_atomtype[0] = -1
wall_atomtype[1] = -1
wall_density[0] = 0
wall_density[1] = 0
wall_ewald_zfac = 3
pull = no
disre = No
disre_weighting = Conservative
disre_mixed = FALSE
dr_fc = 1000
dr_tau = 0
nstdisreout = 100
orires_fc = 0
orires_tau = 0
nstorireout = 100
dihre-fc = 1000
em_stepsize = 0.01
em_tol = 10
niter = 20
fc_stepsize = 0
nstcgsteep = 1000

```
   nbfgscorr              = 10
   ConstAlg               = Lincs
   shake_tol              = 0.0001
   lincs_order            = 4
   lincs_warnangle        = 30
   lincs_iter             = 1
   bd_fric                = 0
   ld_seed                = 1993
   cos_accel              = 0
   deform (3x3):
      deform[    0]={ 0.00000e+00,  0.00000e+00,  0.00000e+00}
      deform[    1]={ 0.00000e+00,  0.00000e+00,  0.00000e+00}
      deform[    2]={ 0.00000e+00,  0.00000e+00,  0.00000e+00}
   userint1               = 0
   userint2               = 0
   userint3               = 0
   userint4               = 0
   userreal1              = 0
   userreal2              = 0
   userreal3              = 0
   userreal4              = 0
grpopts:
   nrdf:       61101
   ref_t:        425
   tau_t:        0.1
anneal:          No
ann_npoints:           0
   acc:            0          0          0
   nfreeze:           N          N          N
   energygrp_flags[  0]: 0 0
   energygrp_flags[  1]: 0 0
```

```
  efield-x:
    n = 0
  efield-xt:
    n = 0
  efield-y:
    n = 0
  efield-yt:
    n = 0
  efield-z:
    n = 0
  efield-zt:
    n = 0
  bQMMM              = FALSE
  QMconstraints      = 0
  QMMMscheme         = 0
  scalefactor        = 1
qm_opts:
  ngQM               = 0

Initializing Domain Decomposition on 8 nodes
Dynamic load balancing: auto
Will sort the charge groups at every domain (re)decomposition
Initial maximum inter charge-group distances:
    two-body bonded interactions: 0.486 nm, LJ-14, atoms 1858 1867
  multi-body bonded interactions: 0.486 nm, Ryckaert-Bell., atoms 1858 1867
Minimum cell size due to bonded interactions: 0.534 nm
Scaling the initial minimum size with 1/0.8 (option -dds) = 1.25
Optimizing the DD grid for 8 cells with a minimum initial size of 0.668 nm
The maximum allowed number of cells is: X 9 Y 9 Z 9
Domain decomposition grid 2 x 2 x 2, separate PME nodes 0
Domain decomposition nodeid 0, coordinates 0 0 0
```

Table routines are used for coulomb: TRUE

Table routines are used for vdw: TRUE

Using shifted Lennard-Jones, switch between 1 and 1.1 nm

Cut-off's: NS: 1.35 Coulomb: 1.1 LJ: 1.1

System total charge: -0.000

Generated table with 1175 data points for Shift.

Tabscale = 500 points/nm

Generated table with 1175 data points for LJ6Shift.

Tabscale = 500 points/nm

Generated table with 1175 data points for LJ12Shift.

Tabscale = 500 points/nm

Generated table with 1175 data points for 1-4 COUL.

Tabscale = 500 points/nm

Generated table with 1175 data points for 1-4 LJ6.

Tabscale = 500 points/nm

Generated table with 1175 data points for 1-4 LJ12.

Tabscale = 500 points/nm

Configuring nonbonded kernels...

Configuring standard C nonbonded kernels...

Testing x86_64 SSE2 support... present.

Removing pbc first time

Linking all bonded interactions to atoms

The initial number of communication pulses is: X 1 Y 1 Z 1

The initial domain decomposition cell size is: X 3.29 nm Y 3.29 nm Z 3.29 nm

The maximum allowed distance for charge groups involved in interactions is:

non-bonded interactions 1.350 nm

(the following are initial values, they could change due to box deformation)

two-body bonded interactions (-rdd) 1.350 nm

multi-body bonded interactions (-rdd) 1.350 nm

When dynamic load balancing gets turned on, these settings will change to:

The maximum number of communication pulses is: X 1 Y 1 Z 1

The minimum size for domain decomposition cells is 1.350 nm

The requested allowed shrink of DD cells (option -dds) is: 0.80

The allowed shrink of domain decomposition cells is: X 0.41 Y 0.41 Z 0.41

The maximum allowed distance for charge groups involved in interactions is:

non-bonded interactions 1.350 nm

two-body bonded interactions (-rdd) 1.350 nm

multi-body bonded interactions (-rdd) 1.350 nm

Making 3D domain decomposition grid 2 x 2 x 2, home cell index 0 0 0

Center of mass motion removal mode is Linear

We have the following groups for center of mass motion removal:

0: rest

++++ PLEASE READ AND CITE THE FOLLOWING REFERENCE ++++

G. Bussi, D. Donadio and M. Parrinello

Canonical sampling through velocity rescaling

J. Chem. Phys. 126 (2007) pp. 014101

-------- -------- --- Thank You --- -------- --------

There are: 20368 Atoms

Charge group distribution at step 0: 786 747 864 773 828 759 789 754

Grid: 6 x 6 x 6 cells

Initial temperature: 418.032 K

Step	Time	Lambda
0	0.00000	0.00000

Energies (kJ/mol)

Bond	Angle	Ryckaert-Bell.	LJ-14	Coulomb-14
3.54366e+04	5.38374e+04	1.54933e+04	7.05039e+03	-1.85918e+03

LJ (SR)	Coulomb (SR)	Potential	Kinetic En.	Total Energy
-2.14593e+04	9.06084e+03	9.75600e+04	1.04896e+05	2.02456e+05

Temperature	Pressure (bar)
4.12957e+02	8.08223e+02

DD step 9 load imb.: force 13.5%

At step 10 the performance loss due to force load imbalance is 9.3 %

NOTE: Turning on dynamic load balancing

DD step 999 vol min/aver 0.833 load imb.: force 0.3%

Step	Time	Lambda
1000	0.50000	0.00000

Energies (kJ/mol)

Bond	Angle	Ryckaert-Bell.	LJ-14	Coulomb-14
3.53662e+04	5.34227e+04	1.54155e+04	6.82070e+03	-1.81025e+03

LJ (SR)	Coulomb (SR)	Potential	Kinetic En.	Total Energy
-2.20188e+04	8.91643e+03	9.61125e+04	1.07963e+05	2.04075e+05

Temperature	Pressure (bar)
4.25030e+02	-7.63809e+01

DD step 1999 vol min/aver 0.837 load imb.: force 0.4%

Step	Time	Lambda
2000	1.00000	0.00000

Energies (kJ/mol)

Bond	Angle	Ryckaert-Bell.	LJ-14	Coulomb-14
3.47843e+04	5.39332e+04	1.55290e+04	6.89527e+03	-1.88255e+03

LJ (SR)	Coulomb (SR)	Potential	Kinetic En.	Total Energy
-2.29459e+04	8.98704e+03	9.53003e+04	1.07970e+05	2.03271e+05

Temperature	Pressure (bar)
4.25060e+02	4.20081e+02

DD step 2999 vol min/aver 0.849 load imb.: force 0.7%

Step	Time	Lambda
3000	1.50000	0.00000

Energies (kJ/mol)

Bond	Angle	Ryckaert-Bell.	LJ-14	Coulomb-14
3.49586e+04	5.38191e+04	1.56098e+04	6.93928e+03	-1.87175e+03

LJ (SR)	Coulomb (SR)	Potential	Kinetic En.	Total Energy
-2.30049e+04	9.00187e+03	9.54520e+04	1.07299e+05	2.02750e+05

Temperature	Pressure (bar)
4.22414e+02	-7.25451e+01

DD step 3999 vol min/aver 0.869 load imb.: force 0.4%

Step	Time	Lambda
4000	2.00000	0.00000

Energies (kJ/mol)

Bond	Angle	Ryckaert-Bell.	LJ-14	Coulomb-14
3.46267e+04	5.34983e+04	1.55775e+04	6.93743e+03	-1.89705e+03

LJ (SR)	Coulomb (SR)	Potential	Kinetic En.	Total Energy
-2.36837e+04	9.01677e+03	9.40759e+04	1.08582e+05	2.02658e+05

Temperature	Pressure (bar)
4.27466e+02	5.08803e+02

DD step 4999 vol min/aver 0.914 load imb.: force 0.4%

Step	Time	Lambda
5000	2.50000	0.00000

Energies (kJ/mol)

Bond	Angle	Ryckaert-Bell.	LJ-14	Coulomb-14
3.44984e+04	5.33226e+04	1.60226e+04	6.98154e+03	-1.83830e+03

LJ (SR)	Coulomb (SR)	Potential	Kinetic En.	Total Energy
-2.35734e+04	8.92697e+03	9.43404e+04	1.07155e+05	2.01495e+05

Temperature	Pressure (bar)
4.21849e+02	6.20092e+02

DD step 5999 vol min/aver 0.931 load imb.: force 0.4%

Step	Time	Lambda
6000	3.00000	0.00000

Energies (kJ/mol)

Bond	Angle	Ryckaert-Bell.	LJ-14	Coulomb-14
3.47235e+04	5.31442e+04	1.57447e+04	6.96092e+03	-1.83247e+03

LJ (SR)	Coulomb (SR)	Potential	Kinetic En.	Total Energy
-2.36274e+04	8.89341e+03	9.40069e+04	1.07909e+05	2.01916e+05

Temperature	Pressure (bar)
4.24817e+02	3.07331e+02

DD step 6999 vol min/aver 0.916 load imb.: force 0.4%

Step Time Lambda

7000 3.50000 0.00000

Energies (kJ/mol)

Bond Angle Ryckaert-Bell. LJ-14 Coulomb-14

3.48273e+04 5.41555e+04 1.55086e+04 6.96376e+03 -1.82326e+03

LJ (SR) Coulomb (SR) Potential Kinetic En. Total Energy

-2.34230e+04 8.89405e+03 9.51029e+04 1.07923e+05 2.03026e+05

Temperature Pressure (bar)

4.24874e+02 -7.18650e+01

DD step 7999 vol min/aver 0.903 load imb.: force 0.3%

Step Time Lambda

8000 4.00000 0.00000

Energies (kJ/mol)

Bond Angle Ryckaert-Bell. LJ-14 Coulomb-14

3.45209e+04 5.35900e+04 1.55439e+04 7.02906e+03 -1.81737e+03

LJ (SR) Coulomb (SR) Potential Kinetic En. Total Energy

-2.38211e+04 8.87240e+03 9.39179e+04 1.08132e+05 2.02050e+05

Temperature Pressure (bar)

4.25695e+02 8.00982e+02

DD step 8999 vol min/aver 0.933 load imb.: force 0.7%

Step Time Lambda

9000 4.50000 0.00000

Energies (kJ/mol)

Bond Angle Ryckaert-Bell. LJ-14 Coulomb-14

3.50507e+04 5.39804e+04 1.59450e+04 7.15984e+03 -1.82690e+03

LJ (SR) Coulomb (SR) Potential Kinetic En. Total Energy

-2.39226e+04 8.86487e+03 9.52512e+04 1.07434e+05 2.02686e+05

Temperature Pressure (bar)

4.22949e+02 3.06533e+02

DD step 9999 vol min/aver 0.942 load imb.: force 0.4%

Step Time Lambda

10000 5.00000 0.00000

Energies (kJ/mol)

Bond Angle Ryckaert-Bell. LJ-14 Coulomb-14

3.49859e+04 5.34811e+04 1.61676e+04 6.94923e+03 -1.78979e+03

LJ (SR) Coulomb (SR) Potential Kinetic En. Total Energy

-2.38803e+04 8.82568e+03 9.47394e+04 1.07888e+05 2.02627e+05

Temperature Pressure (bar)

4.24735e+02 1.47920e+02

DD step 19997999 vol min/aver 0.900 load imb.: force 0.4%

Step Time Lambda

19998000 9999.00000 0.00000

Energies (kJ/mol)

Bond Angle Ryckaert-Bell. LJ-14 Coulomb-14

3.52187e+04 5.45840e+04 1.56497e+04 7.03632e+03 -1.79505e+03

LJ (SR) Coulomb (SR) Potential Kinetic En. Total Energy

-2.48868e+04 8.81165e+03 9.46186e+04 1.07237e+05 2.01855e+05

Temperature Pressure (bar)

4.22171e+02 4.49388e+02

DD step 19998999 vol min/aver 0.886 load imb.: force 0.5%

Step Time Lambda

19999000 9999.50000 0.00000

Energies (kJ/mol)

Bond Angle Ryckaert-Bell. LJ-14 Coulomb-14

3.53821e+04 5.48607e+04 1.55041e+04 6.90476e+03 -1.75687e+03

LJ (SR) Coulomb (SR) Potential Kinetic En. Total Energy

-2.47882e+04 8.76025e+03 9.48668e+04 1.08912e+05 2.03779e+05

Temperature Pressure (bar)

4.28766e+02 1.61543e+02

DD step 19999999 vol min/aver 0.870 load imb.: force 0.5%

Step Time Lambda

20000000 10000.00000 0.00000

<====== ############### ==>

<==== A V E R A G E S ====>

<== ############### ======>

Statistics over 20000001 steps using 2000001 frames

Energies (kJ/mol)

Bond	Angle	Ryckaert-Bell.	LJ-14	Coulomb-14
3.52152e+04	5.41111e+04	1.55023e+04	6.95230e+03	-1.83367e+03

LJ (SR)	Coulomb (SR)	Potential	Kinetic En.	Total Energy
-2.46739e+04	8.87908e+03	9.41524e+04	1.07955e+05	2.02108e+05

Temperature	Pressure (bar)
4.25000e+02	3.00110e+02

Box-X	Box-Y	Box-Z
6.29016e+00	6.29016e+00	6.29016e+00

Total Virial (kJ/mol)

3.37275e+04	-1.45342e+00	-1.21655e+00
-1.45338e+00	3.37412e+04	-6.34540e-01
-1.21648e+00	-6.34570e-01	3.37470e+04

Pressure (bar)

3.01623e+02	8.64594e-02	1.59870e-01
8.64535e-02	2.99818e+02	3.34428e-03
1.59862e-01	3.34829e-03	2.98890e+02

Total Dipole (D)

6.94706e-03	1.13409e-02	-2.76363e-03

Epot (kJ/mol)	Coul-SR	LJ-SR	Coul-14	LJ-14
PE-PE	2.67065e+03	-3.05475e+03	-1.11468e+03	2.76953e+03
PE-HEX	-1.08018e+02	-8.33293e+03	0.00000e+00	0.00000e+00
HEX-HEX	6.31645e+03	-1.32862e+04	-7.18990e+02	4.18277e+03

M E G A - F L O P S A C C O U N T I N G

RF=Reaction-Field FE=Free Energy SCFE=Soft-Core/Free Energy
T=Tabulated W3=SPC/TIP3p W4=TIP4p (single or pairs)
NF=No Forces

Computing:	M-Number	M-Flops	% Flops
Coul(T) + VdW(T)	169752540.173881	11543172731.824	95.0
Outer nonbonded loop	1014799.365997	10147993.660	0.1
1,4 nonbonded interactions	1001880.050094	90169204.508	0.7
NS-Pairs	4482029.321965	94122615.761	0.8
Reset In Box	12600.006300	37800.019	0.0
CG-CoM	40736.040736	122208.122	0.0
Bonds	392680.019634	23168121.158	0.2
Angles	756000.037800	127008006.350	1.0
RB-Dihedrals	1001880.050094	247464372.373	2.0
Virial	41456.020728	746208.373	0.0
Stop-CM	4073.620368	40736.204	0.0
Calc-Ekin	407360.040736	10998721.100	0.1
Total		12147198719.453	100.0

D O M A I N D E C O M P O S I T I O N S T A T I S T I C S

av. #atoms communicated per step for force: 2 x 38463.3

Average load imbalance: 3.5 %

Part of the total run time spent waiting due to load imbalance: 2.0 %

Steps where the load balancing was limited by -rdd, -rcon and/or -dds: X 0 % Y 0 % Z 0 %

R E A L C Y C L E A N D T I M E A C C O U N T I N G

Computing:	Nodes	Number	G-Cycles	Seconds	%
Domain decomp.	8	2000001	359157.513	189016.2	2.0
DD comm. load	8	2000000	17322.432	9116.4	0.1
DD comm. bounds	8	2000000	62038.202	32649.3	0.3
Comm. coord.	8	20000001	922937.007	485720.2	5.1
Neighbor search	8	2000001	857998.652	451544.7	4.8
Force	8	20000001	11603073.284	6106427.1	64.6
Wait + Comm. F	8	20000001	3861004.389	2031956.6	21.5
Write traj.	8	201180	13988.911	7362.0	0.1
Update	8	20000001	128323.124	67533.5	0.7
Comm. energies	8	2000002	78438.493	41280.4	0.4
Rest	8		53433.223	28120.7	0.3
Total	8		17957715.231	9450727.0	100.0

Parallel run - timing based on wallclock.

	NODE (s)	Real (s)	(%)
Time:	1181340.880	1181340.880	100.0
	13d16h09:00		

	(Mnbf/s)	(GFlops)	(ns/day)	(hour/ns)
Performance:	143.695	10.283	0.731	32.815